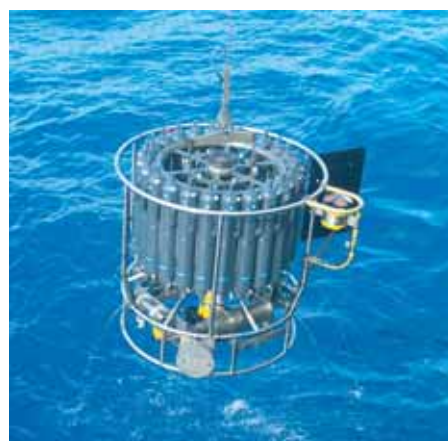MAX-PLANCK-GESELLSCHAFT

IMPRS

Pacific Decadal Variability: Internal Variability and Sensitivity to Subtropics

Daniela Mihaela Matei

Hinweis

Die Berichte zur Erdsytemforschung werden vom Max-Planck-Institut für Meteorologie in Hamburg in unregelmäßiger Abfolge heraus-gegeben.

Sie enthalten wissenschaftliche und technische Beiträge, inklusive Dissertationen.

Die Beiträge geben nicht notwendigerweise die Auffassung des Instituts wieder.

Die "Berichte zur Erdsystemforschung" führen die vorherigen Reihen "Reports" und "Examensarbeiten" weiter.

Notice

The Reports on Earth System Science are published by the Max Planck Institute for Meteorology in Hamburg. They appear in irregular intervals.

They contain scientific and technical contributions, including Ph. D. theses.

The Reports do not necessarily reflect the opinion of the Institute.

The "Reports on Earth System Science" continue the former "Reports" and "Examensarbeiten" of the Max Planck Institute.

Anschrift / Address

Max-Planck-Institut für Meteorologie
Bundesstrasse 53
20146 Hamburg
Deutschland

Tel.: +49-(0)40-4 11 73-0
Fax: +49-(0)40-4 11 73-298
Web: www.mpimet.mpg.de

Layout:

Bettina Diallo, PR & Grafik

Titelfotos:
vorne:
Christian Klepp - Jochem Marotzke - Christian Klepp
hinten:
Clotilde Dubois - Christian Klepp - Katsumasa Tanaka

Pacific Decadal Variability:
Internal Variability and Sensitivity to Subtropics

Dissertation zur Erlangung des Doktorgrades der Naturwissenschaften
im Departement Geowissenschaften der Universität Hamburg
vorgelegt von

Daniela Mihaela Matei
aus Bukarest, Rumänien

Hamburg 2007

Daniela Mihaela Matei
Max-Planck-Institut für Meteorologie
Bundesstrasse 53
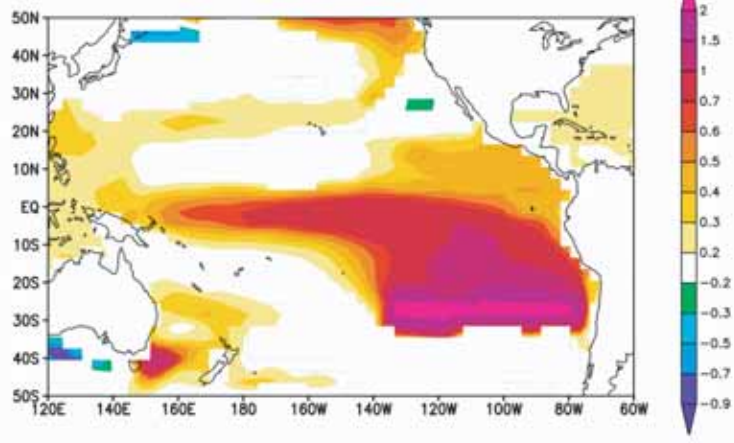20146 Hamburg
Germany

Pacific Decadal Variability:
Internal Variability and Sensitivity to Subtropics

Tropical Pacific SST response to subtropical thermal forcing

NPac +2°C
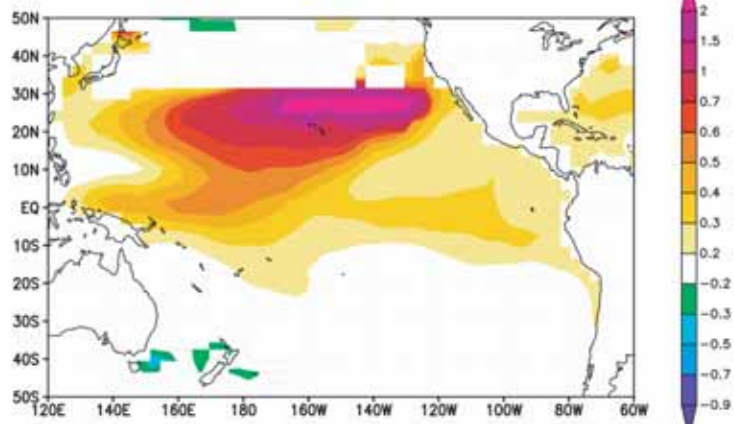
SPac +2°C

Daniela Mihaela Matei

Hamburg 2007

Outline

Abstract

Additional to the interannual variability, the Pacific region experiences climate fluctuations on decadal and longer time scales. It is not clear whether Tropical Pacific decadal variability is internal to Tropical Pacific, or whether the midlatitudes exhibit independent decadal variability that affects the tropics or ENSO variability. Available observational data are insufficient to determine the true causes of Tropical Pacific decadal variability. Internal and remote forcing from subtropics are investigated in this study. This is done with state of the art global circulation models (coupled and uncoupled).

The leading mode of Tropical Pacific decadal variability in the ECHAM5-MPIOM model, isolated in the tropical cells (TC) index by means of SSA, has a period of about 17 years. The associated SST spatial structure is characterized by a horseshoe-like pattern with maximum explained variance in the central-western equatorial Pacific and off the equator, therefore resembling the signature of the observed decadal climate variability in the tropical Pacific. The mechanism for decadal variability in the model involves coupled ocean-atmosphere processes over the western tropical South Pacific, in the region of the SPCZ. Strong positive TCs are associated with periods of increased ENSO variability and vice versa, contributing to the decadal modulation of ENSO activity.

The influence of the remote subtropical forcing was studied in more detail with tailored experiments performed with the ocean-atmosphere-sea ice coupled model ECHAM5/MPI-OM. In these sensitivity experiments, the coupled model is forced with idealized sea surface temperature anomalies (SSTA) and sea surface salinity anomalies (SSSA) in the subtropics of both hemispheres. Thus, the relative impact of the subtropical North and South Pacific Oceans on the tropical climate mean state and variability can be estimated.

The largest impact on tropical mean climate and variability was simulated in the SSTA experiments. Subtropical South Pacific thermal forcing had more impact on equatorial ocean sea surface temperature than the subtropical North Pacific. In response to a 2°C warming in the subtropical South Pacific, the equatorial Pacific SST increases by +0.58°C, being about 65% larger than the change in the North Pacific experiment. The results show that the subtropics affect equatorial SST mainly through the „atmospheric bridge" for the South Pacific experiments and through the„oceanic bridge" for the North Pacific experiments. This explains the different timescale of the response in the two experiments. Although the tropical

3

Pacific surface response to an enhanced warming/cooling in the subtropics is to first order linear, we found that the negative thermal forcing has a stronger impact on the equatorial thermocline.

Similar sensitivity experiments conducted with the AGCM ECHAM5 showed that both air-sea interactions and ocean dynamics are crucial for the generation of simulated tropical climate response to the subtropical surface warming/cooling.

We found that the statistics of ENSO exhibit significant changes in amplitude and frequency in response to a warming/cooling in the subtropical South Pacific: a 2°C subtropical South Pacific SST warming can reduce the mean ENSO standard deviation by 28%, while a 2°C subtropical South Pacific SST cooling can increase the mean ENSO standard deviation by 21%. The simulated changes in the equatorial zonal SST contrast between the eastern equatorial Pacific and the warm pool region are the main contributor to the modulation of ENSO variability in our South Pacific sensitivity experiments. The simulated intensification/weakening of the annual cycle in response to an enhanced warming/cooling in subtropical South Pacific may also lead to a weaker/stronger ENSO. The subtropical North Pacific thermal forcing did not change the statistical properties of ENSO.

The main results of this study suggest that subtropical South Pacific climate variations play a dominant role in tropical Pacific decadal variability and in the decadal modulation of ENSO activity.

1. Introduction

1.1 Motivation

Additional to the interannual changes, the Pacific region experiences climate fluctuations on decadal or longer time scales. After 1976 the tropical Pacific Ocean has been warmer than in preceding decades while the central and western North Pacific Ocean have been colder and atmospheric pressure has been lower over the midlatitude North and South Pacific Oceans. In the early 1940s the climate of the Pacific went through a shift in the opposite direction. These characteristics of Pacific Decadal Variability were described in several papers (Graham, 1994; Trenberth and Hurrel, 1994; Zhang et al., 1997; Mantua et al., 1997; Garreaud and Battisti, 1999).

Pacific decadal climate fluctuations have important consequences for the climate over the nearby continental regions. Mantua et al. (1997) have shown that when the tropical Pacific is warm (e.g. after 1976), winters are warm across most of North America, but cold in the southeastern United States. The winters are also drier than average over midlatitude North America, but wetter in the southwestern United States and Mexico. In the midlatitudes of the North Pacific, the changes are apparent not only in the sea surface temperature over virtually the entire North Pacific, but also in low frequency modulation of phytoplankton and fish population (Venrick et al., 1987; Mantua et al., 1997; Miller et al., 2003) as well as period of extended above normal/below normal rainfall over United States (Latif and Barnett, 1994, 1996). Interdecadal northeastern Australian rainfall anomalies were shown to be highly correlated to interdecadal fluctuations in the tropical Pacific (Latif et al., 1997b). In a recent study, Meehl et al. (2006) connected the megadroughts in the Indian Monsoon Region and Southwest North America to the decadal Pacific SST anomalies

Tropical Pacific variability associated with ENSO undergoes changes on decadal timescales as well. Using the entire instrumental record, many studies have pointed out a change in ENSO statistics over the past 100 years, including a decadal scale modulation in ENSO amplitude (Gu and Philander, 1997). As there were notable changes in ENSO statistics before and after 1976 climate transition (Fedorov and Philander, 2000), some studies suggest that the low-frequency modulation of ENSO and the interdecadal fluctuation may be linked.

Decadal variations of ENSO have also been associated with decadal variations in Australian climate (Power et al., 1999; Power et al., 2006) and the strength of the Indian monsoon (Kumar et al., 1999; Krishnamurthy and Goswani, 2000). However, more recent studies cast some doubts on the linkage (Deser et al., 2004; Yeh and Kirtman, 2004).

1.2 Mechanisms for Pacific decadal variability

Although the decadal ENSO-like pattern in the Tropical Pacific and its relation to the North Pacific decadal variability has been extensively studied using both observational and modeling data (Nitta and Yamada, 1989; Trenberth and Hurrel, 1994; Zhang et al., 1997; Barnett et al., 1999; Pierce et al., 2000; Deser et al., 2004; D'Arrigo et al., 2005), the physical mechanisms responsible for the decadal Pacific climate variability are still controversial. It is not clear whether the decadal variability is internal to Tropical Pacific, or whether the midlatitudes independently undergo decadal variability or affect ENSO variability.

One of the leading theories is represented by the connection between the subtropics/extratropics and tropics at decadal timescales. Various distinct hypotheses based on a hierarchy of models have been proposed to explain the subtropical-tropical connections, often with contradicting results.

On the one hand, the mean advection mechanism (Gu and Philander, 1997) assumes that the subtropical sea surface (SST) anomalies are first subducted into the thermocline. These are then advected to the equator within the subsurface branch of the subtropical cell (STC, McCreary and Lu, 1994), and finally upwelled to the surface in the eastern equatorial Pacific, where they affect the cold tongue. Recent studies, however, indicate that the temperature anomalies subducted into the pycnocline in the subtropical North Pacific may not reach the equator with any appreciable amplitude (Schneider et al., 1999; Nonaka and Xie, 2000). These anomalies, although important for generating subsurface variability in the subtropical gyre (Deser et al, 1996; Zhang et al., 2001), can either be strongly dissipated, dispersed in the form of planetary-scale oceanic waves, or become obscured by the wind-forced variations at low latitudes (Schneider et al., 1999a, 1999b; Nonaka and Xie, 2000).

On the other hand, the subtropical anomalies can induce changes in the overlying atmospheric circulations that could result in changes of the subtropical cells (STC) strength. The tropical climate can thus be changed due to the varying amount of the equatorward cold water transport. Using an intermediate coupled model, consisting of a 3-1/2 layer shallow water model coupled with a statistical atmospheric model, Kleeman et al. (1999) have shown

that decadal variations of tropical SSTs are primarily related to changes in wind stress and subduction rates in the subtropics (poleward of ~23°). Employing an OGCM forced by observed winds, Nonaka et al. (2002) found that equatorial winds (5°S-5°N) are as important as extraequatorial winds (poleward of 5°) for the decadal modulation of equatorial SSTs. The mechanism of tropical decadal variability proposed by Kleeman et al. (1999) was supported by the observational studies of McPhaden and Zhang (2002, 2004). They presented evidence that the warming and cooling events and mass transport anomalies seem to be related over the last 40-50yr.

In addition, Lysne et al. (1997) suggests a wave mechanism, in which the thermal anomalies propagate from the central North Pacific to the western boundary as long Rossby waves, southward along the coast as coastal Kelvin waves and westward along the equator as equatorial Kelvin waves. However, this wave mechanism does not exclude the ventilated thermocline dynamics as an important link between subtropics and tropics at decadal timescale.

The subtropical/midlatitude climate can also affect the tropics through the atmospheric teleconnections. Barnett et al. (1999), argued that anomalous winds related to a midlatitude decadal mode in the North Pacific may extend to the equatorial region and thus bring about low-frequency wind variations there that affect the equatorial thermocline and modulate ENSO. Pierce et al. 2000 also found that the strongest link between Tropics and midlatitudes on decadal timescales is communicated near-simultaneously via changes in surface wind stress.

In the last decade, the potential influence of North Pacific ocean-atmosphere processes on tropical Pacific decadal variability has dominated the literature, probably also due to the sparse observational data in South Pacific south of 30°S. More recently, a number of observational (Luo and Yamagata 2001, Giese et al. 2002, Bratcher and Giese 2002, Holland et al. 2006) and numerical modeling studies (Luo et al. 2003, Luo et al. 2005) have shown pronounced subsurface signals moving from South Pacific to the equatorial region. This is not surprising, since the South Pacific Ocean contributes about 70% to the water mass in the Equatorial Undercurrent (Lindstrom et al. 1987, McCreary and Lu 1994), and much of the water from the South Pacific can reach the equator through the interior pathways of the STC due to the absence of a potential vorticity barrier in the South Pacific. A potential vorticity barrier exists in the North Pacific being related to the Intertropical Convergence Zone (ITCZ).

Despite this rich variety of potential mechanisms the causes of tropical Pacific decadal variability are still unclear. Regardless of the quality of observational record, the data record

is too short to unambiguously determine the mechanisms responsible for Pacific decadal variability. Additionally, the increase in greenhouse gasses is making more difficult to distinguish between the natural climate variability from externally forced climate variability. Thus, long-term simulations performed with state-of-art fully coupled atmosphere-ocean models are essential tools for identifying the physics responsible for decadal variability in the climate system.

As described above, the research emphasis for decadal timescales has been on investigating the connections between the Tropical and North Pacific Ocean, with very few recent studies dealing with the interactions between South and Tropical Pacific. Hence, an important question to be address: What are the relative roles of North and South subtropical Pacific in the decadal modulation of tropical SSTs? Another important question emerges from literature and international research programs (e.g., CLIVAR): Does/Will anthropogenic climate change influence the characteristics of decadal Pacific climate variability?

1.3 Scientific objectives

In this study, we employ a state-of-art ocean-atmosphere coupled model to investigate how the projected changes in the subtropical Pacific climate mean state under global warming scenarios will affect the mechanisms responsible for decadal subtropical-tropical interactions in the Pacific Ocean. Furthermore, the relative contributions of North and South subtropical Pacific Ocean variations to the tropical Pacific climate and interannual variability will be estimated as well as the linearity of the response to the strength and sign of the forcing.

Therefore, several research questions will be addressed in the present study:

- What are the mechanisms governing the interaction between subtropical and tropical Pacific at decadal timescales?
- What is the climate response of the equatorial Pacific system to the variations in the subtropical surface climate?
- Are the subtropical-tropical interactions via the "atmospheric bridge" or via the "oceanic bridge"? What is the role of air-sea coupling and ocean dynamics in these interactions?
- Have the North and South subtropical Pacific climate variations a similar impact on the tropical Pacific mean state and interannual variability?

8

- Is the impact of subtropical climate variations linear in strength and sign?
- How do ENSO characteristics respond to enhanced Pacific subtropical warming/cooling?

1.4 Outline of the thesis

In this thesis, we will first investigate the mechanism responsible for the tropical Pacific decadal variability in an unforced integration of the new coupled ECHAM5/MPI-OM ocean-atmosphere-sea ice model. We then go to examine the connections between the subtropical and tropical Pacific on decadal timescales using specifically designed experiments. In these sensitivity experiments, the coupled model is forced with idealized sea surface temperature anomalies (SSTA) and sea surface salinity anomalies (SSSA) in the subtropics of both hemispheres. Thus, the relative impact of the subtropical North and South Pacific Oceans to the tropical climate mean state and variability can be estimated. Additionally, SSTA integrations with the stand-alone atmospheric model are performed with the purpose to separate between the role of ocean dynamics and ocean-atmospheric coupling in subtropical-tropical interactions. The experimental setup of the sensitivity experiments performed with the coupled ECHAM5/MPI-OM model and stand-alone ECHAM5 model are described at the beginning of Chapter 4.

The thesis is organized as follows: Chapter 2 gives a description of the coupled model ECHAM5/MPI-OM, together with a short presentation of tropical Pacific interannual variability in the model and of the SSA statistical method. Chapter 3 is focused on identifying the mechanism that causes internal tropical Pacific variability at decadal timescales in the model and its affect on ENSO activity. Chapter 4 is concentrated on the impact of subtropical thermal and salinity variations onto the mean state of tropical Pacific Ocean, while the modulation of ENSO variability by the subtropical Pacific thermal forcing is explored in Chapter 5. Conclusions and an outlook of future work are given in Chapter 6 and Chapter 7. Please note that the references of all chapters will be gather together in a references list at the end of the thesis.

2. Model description and statistical methods

2.1 ECHAM5/MPI-OM model description

The coupled atmosphere-ocean-sea ice model used in this study is the state-of-the-art ECHAM5/MPI-OM model developed at the Max Planck Institute for Meteorology (MPI). It consists of the atmosphere GCM model ECHAM5 (ECmwf HAMburg) and the ocean model MPI-OM (Max Planck Institute Ocean Model). A 1000-year control integration of the ECHAM5/MPI-OM model is used for the study of Pacific decadal variability in this thesis. The same model is also used to perform the sensitivity experiments described in chapter 4. This version of the ECHAM5/MPI-OM model was used to study the impact of the tropical Indian and Atlantic Oceans on ENSO (Dommenget et al., 2006) and of the tropical Pacific variability on the mean North Atlantic Thermohaline circulation (Semenov and Latif, 2006), while Bader and Latif (2005) analyzed the North Atlantic Oscillation response to anomalous Indian Ocean SST.

2.1.1 Atmosphere model - ECHAM5

The ECHAM model was adapted for climate application from the spectral weather prediction model of the European Center for Medium Range Weather Forecast (ECMWF). ECHAM5 is the latest version of the model. The main features of the model will be only briefly described, further details can be found in Roeckner et al. (2003) and in the special issue of Journal of Climate dedicated to the new ECHAM5/MPI-OM model (Roeckner et al., 2006; Wild and Roeckner, 2006).

The ECHAM5 model employs a spectral dynamical core, with vorticity, divergence, temperature and the logarithm of surface air pressure being represented in the horizontal by a truncated series of spherical harmonics. The model utilizes a semi-implicit leapfrog time-

differencing scheme. A hybrid sigma-pressure coordinate is used in the vertical direction. A flux-form semi-Lagrangian scheme (Lin and Rood, 1996) is used for passive tracer transport of water components (vapor, liquid, solid) and chemical substances. The cloud scheme consists of prognostics equations for the water phases, bulk cloud microphysics (Lohmann and Roeckner, 1996), and a statistical cloud cover scheme with prognostics equations for the distribution moments (Tompkins, 2002).

The ECHAM5 version we employ here is the tropospheric model resolving the atmosphere up to middle stratosphere (10 hPa). It has 19 irregularly distributed vertical levels, with the highest vertical resolution in the atmospheric boundary level. The horizontal spectral resolution is T31 (a triangular truncation at wave number 31), corresponding to approximately 3.75 degrees.

2.1.2 Ocean model – MPI-OM

The ocean model MPI-OM (Marsland et al., 2003) is a global version of the Hamburg Ocean Primitive Equations (HOPE) model (Wolf et al., 1997). The model is a z-coordinate global general circulation model with 40 unevenly spaced vertical levels (20 levels located in the upper 600m) and is based on the primitive equations for a hydrostatic Boussinesq fluid on a rotating sphere. It includes parameterizations of sub-grid scale mixing processes like isopycnal diffusion of the thermohaline fields, a Gent and McWillimas style eddy-induced tracer transport and a bottom boundary layer slope convection scheme. The model employs a free surface and the grid is based on an Arakawa C-grid (Arakawa and Lamb, 1977).

A dynamic, thermodynamic sea ice model is embedded in the ocean model (Legutke et al., 1997). The dynamics of sea ice are formulated using a viscous-plastic rheology (Hibler, 1979). The thermodynamics relate sea ice thickness changes to a balance of radiant, turbulent and oceanic heat fluxes.

An orthogonal curvilinear grid allows for an arbitrary placement of the model's poles. The configuration used in this study places the North Pole over Greenland (80°N, 30°W), while the South Pole is shifted to the center of Antarctic continent (80°S, 30°W) (Figure 2.1). This approach not only removes the numerical singularities associated with the convergence of the meridians at the geographical North Pole, but also results in higher resolution in the deep-water formation regions near Greenland and in the Weddell Sea. The horizontal resolution of this model version is about 3° on average and varies between a minimum of 20 km in the Arctic to a maximum of about 350 km in the Tropics.
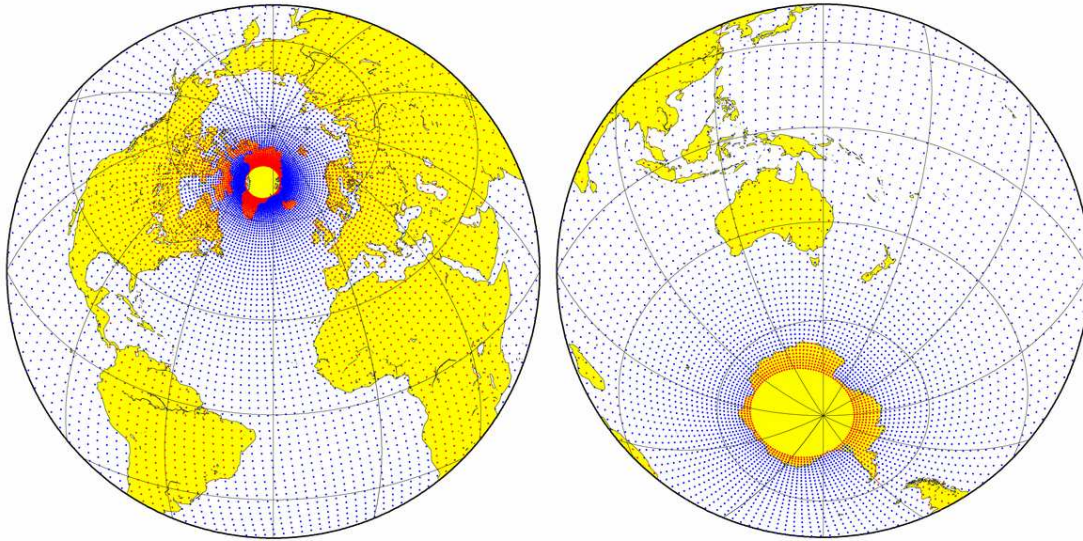
Figure 2.1 Grid of the ocean model MPI-OM.

2.1.3 OASIS – coupler

The atmosphere and ocean model are coupled by means of Ocean-Atmosphere-Sea Ice-Soil (OASIS) coupler (Valcke et al., 2003). The coupler exchanges the momentum, heat and freshwater fluxes from the atmosphere to the ocean and performs the interpolation onto the ocean model's grid. The ocean model passes the sea surface temperature, sea ice concentration, sea ice thickness, snow depth, and the ocean surface velocities to the atmospheric model. River runoff and glacier calving are treated interactively in the atmospheric model and the respective freshwater fluxes transferred to the ocean as part of the atmospheric freshwater flux field. The land hydrology model includes a river runoff scheme (Hagemann and Dümenil, 1998; Hagemann and Dümenil-Gates, 2003), but the mass balance of glacier ice sheets is not accounted for in the model. This climate model does not employ any flux adjustment.

2.2 Tropical Pacific interanual variability in ECHAM5/MPI-OM

The El Niño-Southern Oscillation (ENSO) phenomenon is the dominant mode of interannual climate variability in the tropical Pacific. ENSO is a coupled ocean-atmosphere

mode that influences almost all regions of the globe. In the following, we will give a brief description of the ENSO characteristics in our coupled model and compare them with the observed ENSO characteristics. The observational data used in this study are from Kaplan et al. (1998), and are a reconstruction of historical SST anomalies on a 5 ° X 5° grid for the period 1856-2003. Monthly mean sea surface temperature anomalies (SSTA) were computed with respect to the period 1950-1980.

The leading EOF (Empirical Orthogonal Function) of the monthly mean SSTA over the tropical Pacific for both the model and observations are shown in Figure 2.2a and b. Please note that the EOF spatial patterns are displayed in the standardized form: the units are degrees Kelvin per one standard deviation of the principal component (PC). The dominant simulated interannual signal has a spatial pattern that is broadly similar to the observed one. Nevertheless, there are several differences between the modeled and the observed ENSO. First, the simulated ENSO variability is larger than the observed one. For example, the monthly Niño3-SSTA index standard deviation is 1.6 °C compared to only 0.8°C for the observations. Niño3-SSTA index - a common measure of ENSO variability – is computed as an area averaged SSTA over the Niño-3 region (150°W-90°W, 5°N-5°S). Second, the modeled ENSO pattern is more equatorially confined and extends too far westward compared to the observations. The coupled model has a realistic ENSO period with maximum variance at a period of about 3 years (Figure 2.2c). However, in contrast to the observed broad spectral peak between 2-7 years, the model spectral peak is too sharp, indicating far too regular variability. The ENSO dynamics seem to be similar to the observed one, with a slow eastward propagation of heat content anomalies in the subsurface and a standing SST pattern (not shown).

The above-mentioned differences between the model and observed tropical Pacific interannual variability represent typical systematic errors of coupled models (Latif et al., 2001) also unflux corrected. Like many other coupled models, ECHAM5/MPI-OM suffers from a cold bias in the Tropics and a too westward extension of the equatorial cold tongue. Meehl et al. (2001) related the high ENSO amplitude simulated in the quasi-biennial band to the mean state of the model, with a shallow mean thermocline favoring large ENSO amplitude. Since the zonal mean of the equatorial thermocline depth is relatively shallow in the model (103m), this may be one explanation for the high ENSO variability in ECHAM5/MPI-OM.
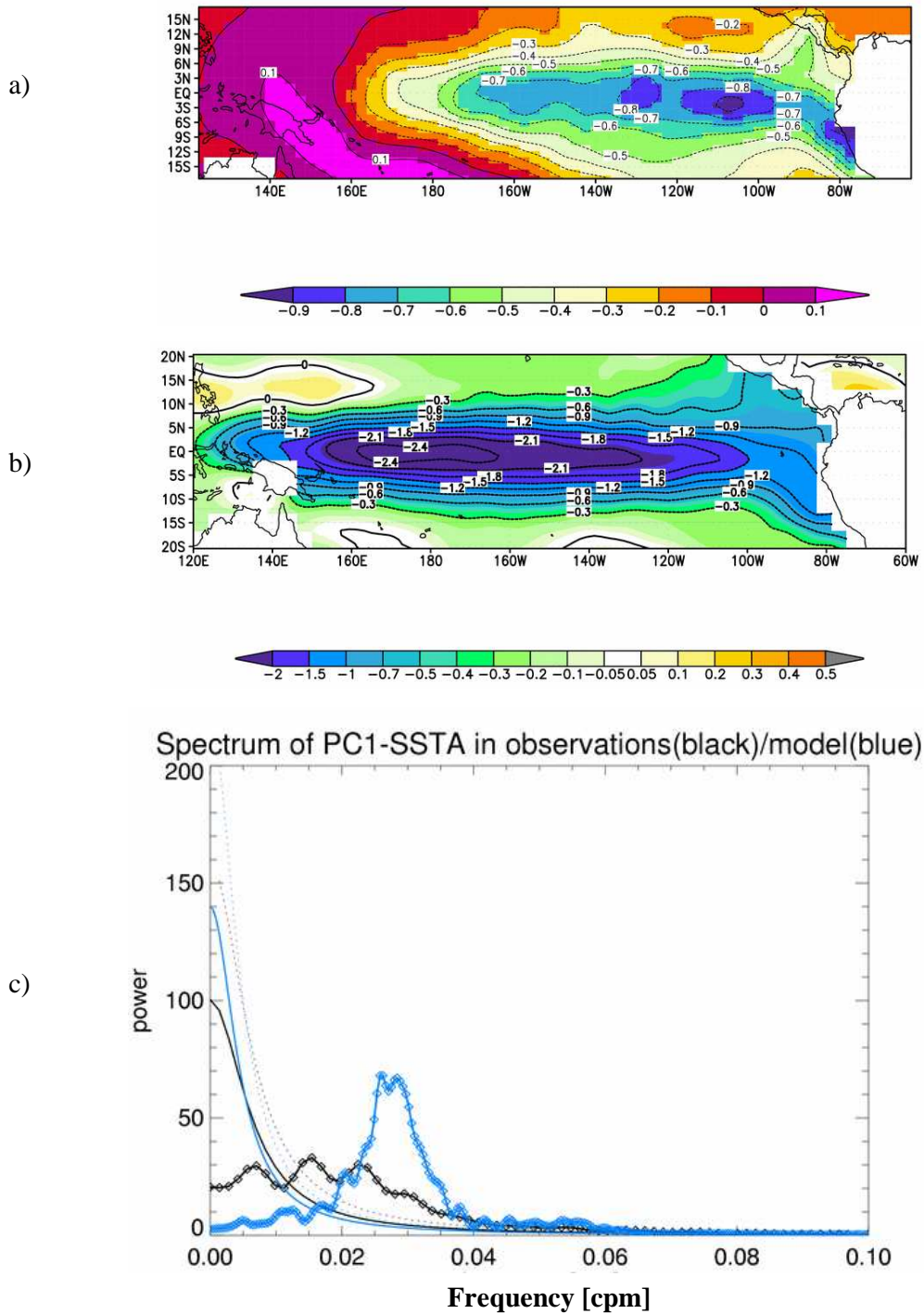
a)

b)

c)

Figure 2.2 Spatial pattern of the dominant EOF mode of sea surface temperature anomalies in the tropical Pacific basin for the observations **(a)** and for the ECHAM5/MPI-OM model **(b)**. Contour interval is 0.1 °C in **(a)** and 0.3 °C in **(b)**. **(c)** Power spectra of Niño3-SSTA for the observations (black line with diamonds), and ECHAM5/MPI-OM model (blue line with diamonds). The 95% confidence level (dotted line) is calculated based on the theoretical spectrum of an AR1 (red noise) process fitted to the data (thin solid line). The power spectrum is estimated using a Bartlett window.

2.3 Tropical Cells/Subtropical Cells in the model

The mainly wind-driven subtropical cells (STCs) are shallow meridional circulation cells in which water flows out of the tropics within the surface layer, subducts in the subtropics, flows equatorward within the thermocline, and upwells in the eastern equatorial ocean (McCreary and Lu, 1994; Liu et al., 1994). The equatorial upwelling is partly balanced by downwelling within the tropics forming the relatively narrow recirculation cells known as tropical cells (TC) (Lu et al., 1998).
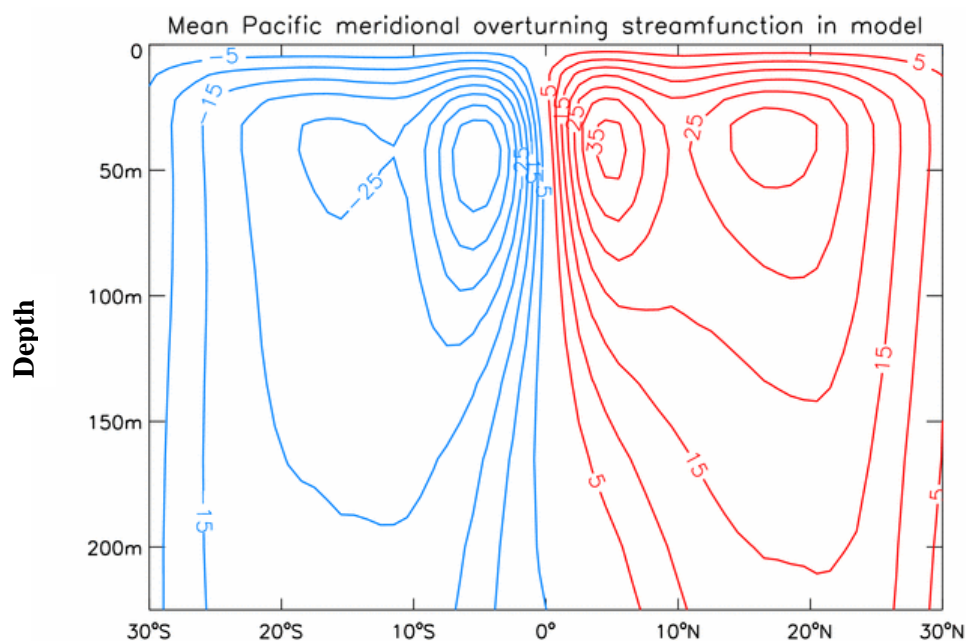
Figure 2.3 Mean Pacific meridional overturning streamfunction in the ECHAM5/MPI-OM model. Red (blue) lines represent clockwise (anticlockwise) flow. The contour interval is 5 Sv (1 Sv = 10^6 m^3/s).

Figure 2.3 shows the mean meridional overturning streamfunction for the upper subtropical-tropical Pacific in the ECHAM5/MPI-OM model. The strength of the cells in our model is 45 Sv (1Sv = 10^6 m^3) for the southern cell, respectively 35Sv for the northern cell. These values are comparable with those suggested from observations and other model integrations (Nonaka et al., 2002; McPhaden and Zhang, 2002; Capotondi et al., 2005). However, the meridional extension of the tropical cells is slightly greater than the observed

one, probably due to the coarser resolution of the ocean model. The tropical cells index is defined as psi_{max} (7.5°S-7.5°N, upper 250m) - psi_{min} (7.5°S-7.5°N, upper 250m), where psi is the Pacific meridional overturning streamfunction. Please note that the overturning is negative for the southern cell. The subtropical cells index is defined in a similar way by psi_{max} (10°N-30°N, upper 250m) - psi_{min} (10°S-30°S, upper 250m).

2.4 Statistical method: Singular-Spectrum Analysis (SSA)

Singular-Spectrum Analysis (SSA) is designed to extract information from short and noisy time series and thus provide insight into the unknown or partially known dynamics of the underlying system that generated the series (Ghil et al., 2000).

Colebrook (1978) applied a form of SSA to biological oceanography and noted the duality between the principal component analysis (PCA) in the space and time domain. Broomhead and King (1986) applied the "method of delays" of dynamical system theory to estimate the dimension of and reconstruct the Lorenz attractor using singular-value decomposition on the trajectory method formed by lagged copies of a single time series obtained from the system. Vautard and Ghil (1989) realized the formal similarity between classical lagged-covariance analysis and the method of delays. They exploited the similarity further by pointing out that pairs of SSA eigenmodes corresponding to nearly equal eigenvalues and associated temporal principal components that are nearly in phase quadrature can represent efficiently a nonlinear, anharmonic oscillation.

The SSA expansion is an EOF expansion in which the field contains values at the same location but at different time lags. The leading eigenvectors (known as Time-EOFs or T-EOFs) of the corresponding covariance matrix represent thus the leading time patterns of field. The principal components associated with these T-EOFs are called Time-PCs or T-PCs and can be interpreted as moving averages of the original time series, the averages being weighted by the coordinates of the T-EOFs.

In SSA analysis, any oscillatory behavior present in the original time series stands out as a pair of nearly equal eigenvalues. Their associated T-EOFs and T-PCs have a similar time scale of oscillation, but are out of phase by approximately $\pi/2$. Several objective criteria have been developed by Vautard et al. (1992) to extract these oscillatory pairs. The portion of variability in the original time series that is associated to a given oscillation captured by a pair of modes can thus be isolated by restricting the SSA expansion to the T-EOFs and T-PCs

corresponding to that pair of modes. In this way we can reconstruct the original time series using only the two SSA components of interest.

SSA has been applied extensively to the study of climate variability and to other areas in the physical and life sciences. For example, the climate applications include the analysis of paleoclimatic time series (Vautard and Ghil, 1989), decadal-interdecadal climate variability (Ghil and Vautard, 1991; Lohmann and Latif, 2005) as well as interannual oscillations (Rasmusson et al., 1990; Ghil et al., 2000). A more detailed description of the statistical method is given by Ghil et al. (2000).

3. Unforced tropical Pacific decadal climate variability

3.1 Introduction

Decadal climate variability can be caused by external and internal forcing mechanisms. Among the natural external forcing mechanisms, variations in the incoming solar radiaton and the volcanic activity have been proposed as major sources of decadal-interdecadal varibility (Labitzke, 1987; Lean et al. 1995; Cubash et al., 1997; Robock and Mao, 1995). Decadal-interdecadal variability can also arise from the interactions between and within different sub-components of the climate system, the most important being the atmosphere and ocean.

In this chapter we will investigate the mechanism driving internally generated tropical Pacific decadal climate variability in the ECHAM5/MPI-OM model. The proposed mechanisms for explaining tropical Pacific decadal variability fall into three main categories: (1) tropical-extratropical interactions (Gu and Philander, 1997; Kleeman et al., 1999), (2) purely tropical processes (Knutson and Manabe, 1998; Jin, 2001) and (3) purely extratropical processes teleconnected to the tropical Pacific (Barnet et al., 1999; Pierce et al., 2000). Despite this wealth of suggested mechanisms, there is no consensus on the causes and origins of tropical Pacific decadal variability. In this chapter, we will first briefly describe the observed Pacific decadal variability. We then go on to analyze the mechanisms of decadal variability in the coupled model. Due to insufficient observational data for these timescales coupled models are essential tools.

3.2 Pacific decadal variability in observations

The first EOF of low-pass-filtered SSTAs (Figure 3.1a) shows the pattern of observed decadal climate variability in the Pacific region (25°S-60°N, 120°E-80°W). The observed sea surface temperatures are from Kaplan et al. 1998 dataset that is described in chapter 2.2. Prior
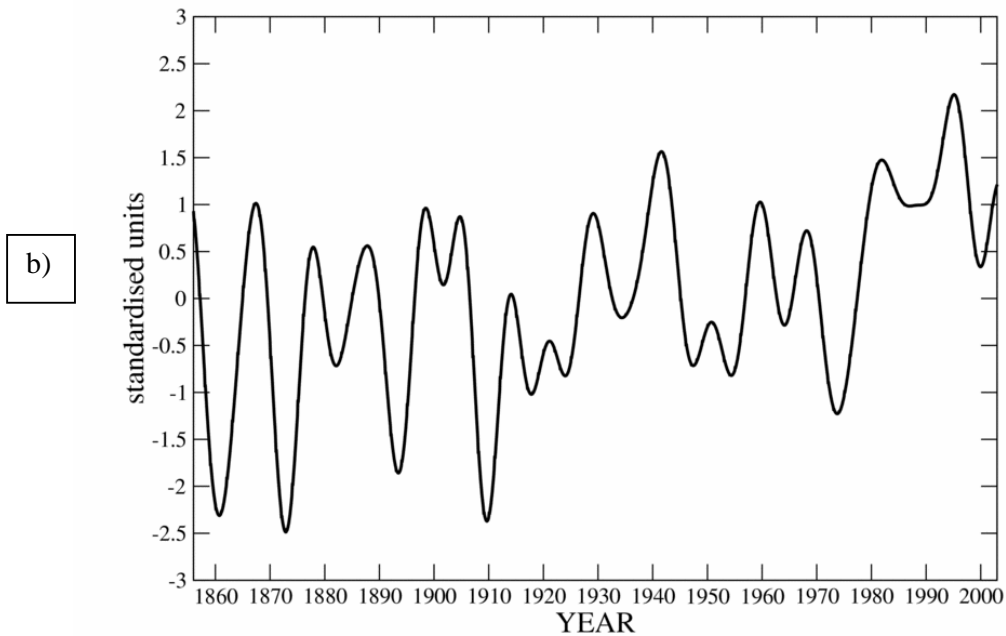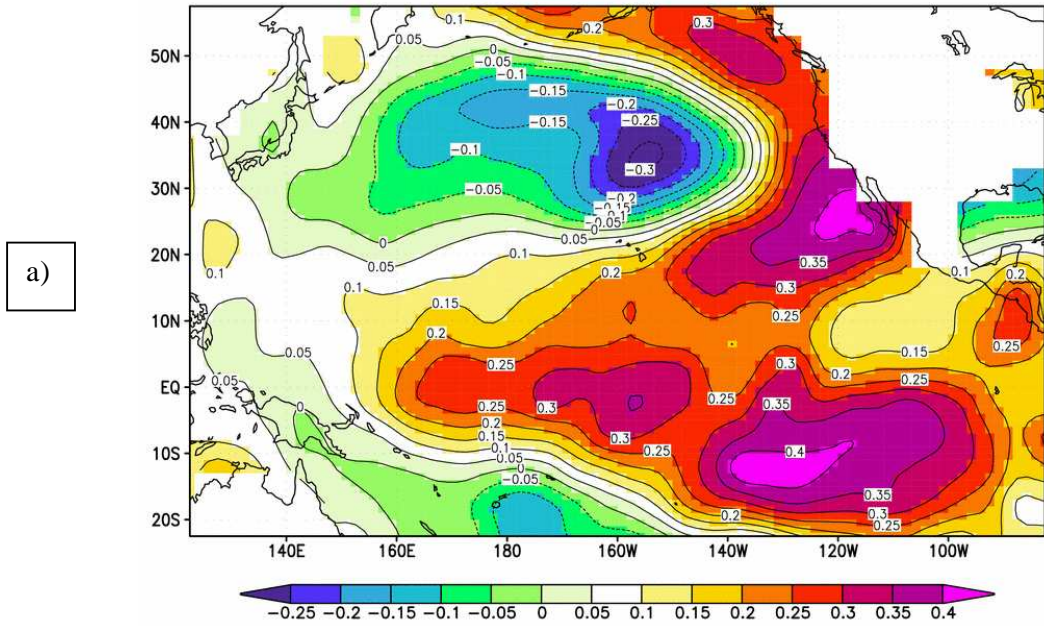
PC1 of the low-pass filtered Pacific SSTA for the observations

Figure 3.1 (a) Spatial pattern, and **(b)** the normalized time coefficient of the dominant EOF mode of observed sea surface temperature anomalies in the Pacific basin. The SSTAs are low-pass filtered to retain the variability longer than 7 years. Contour interval is 0.05 °C/ 1σ of the principal component.

to EOF analysis, the monthly SSTAs were low-pass-filtered using a Fast Fourier Transform (FFT) to retain the variability longer than 7 yr. The first EOF explains about 41% of the total decadal variance. The spatial pattern has a broad triangular shape in the tropical Pacific basin (Figure 3.1a), which is similar to the "ENSO-like decadal" mode of Zhang et al. (1997). It resembles the interannual ENSO pattern, but has a broader meridional extension and with the maximum loading (0.4 °C per standard deviation of the principal component) off the equator in the tropical eastern Pacific, instead of equatorial Pacific. The temporal evolution of this mode is characterized by decadal-bidecadal fluctuations and a clear warming SST trend starting in mid 1970s (Figure 3.1b).

3.3 Tropical decadal variability in ECHAM5-MPIOM model

The decadal scale climate variability in the tropical Pacific has been analyzed using a 1000yr long control integration of the coupled ocean-atmosphere-sea ice general circulation model ECHAM5-MPIOM forced with constant greenhouse gas concentration at pre-industrial levels. In the following, we limit our analysis to the last 500yr of the coupled experiment to avoid the influence of any possible model drift. In order to focus our analysis on decadal variability, a 5-yr running mean is applied to the monthly model data.

As discussed in the previous section, one mechanism for tropical Pacific decadal variability is tropical-extratropical interactions. Several recent observational (McPhaden and Zhang, 2002) and modeling studies using ocean models (Klinger et al., 2002; Nonaka et al., 2002; Solomon et al., 2003) or coupled general circulation models (Kleeman et al., 1999; Merryfield and Boer, 2005; Lohmann and Latif, 2005) suggest the influence of STCs/TCs (subtropical/tropical cells) on decadal climate variability in the tropical Pacific. Figure 3.2 shows the time evolution and the power spectrum of the anomalous 5-yr running mean TC (tropical cell) index for our model simulation. As shown in Figure 3.2a and b, the decadal activity of the TC index varies from decade to decade with a typical period of about 17yr. The 17yr spectral peak is statistically significant at 95% confidence level and suggests the existence of a coupled ocean-atmosphere mechanism that acts at decadal timescales.

Next, the relationships between variations in tropical cell strength and the sea surface temperature over the tropical Pacific Ocean is investigated by means of linear regression. Figure 3.3 displays the simultaneous linear regression coefficient between TC index and
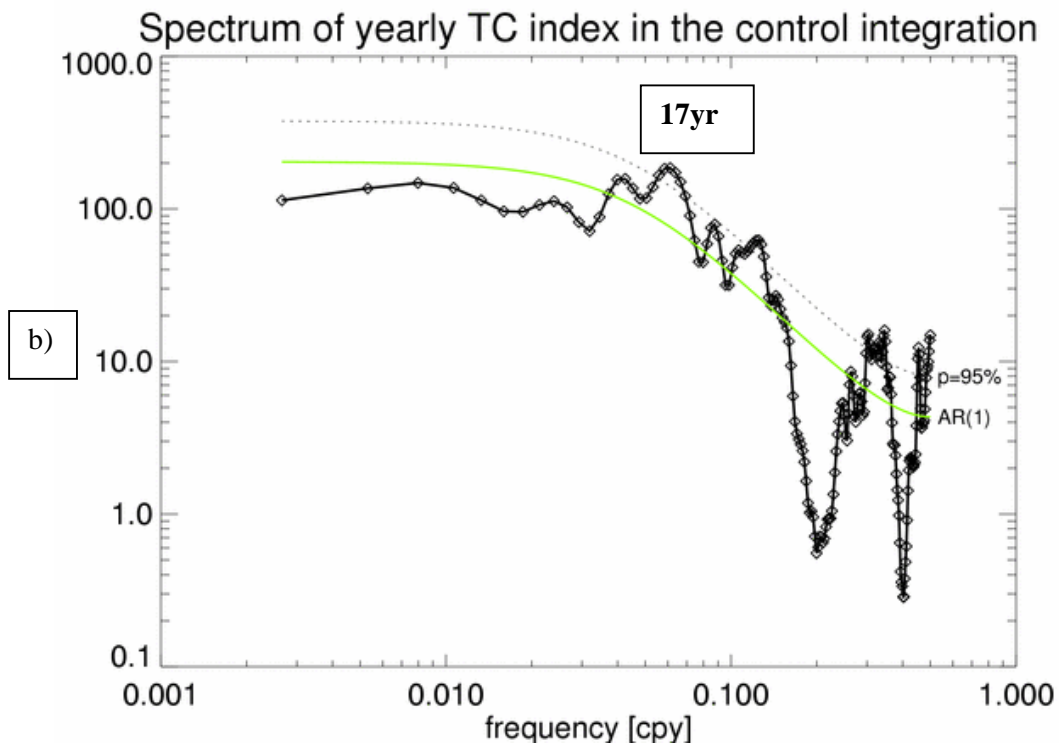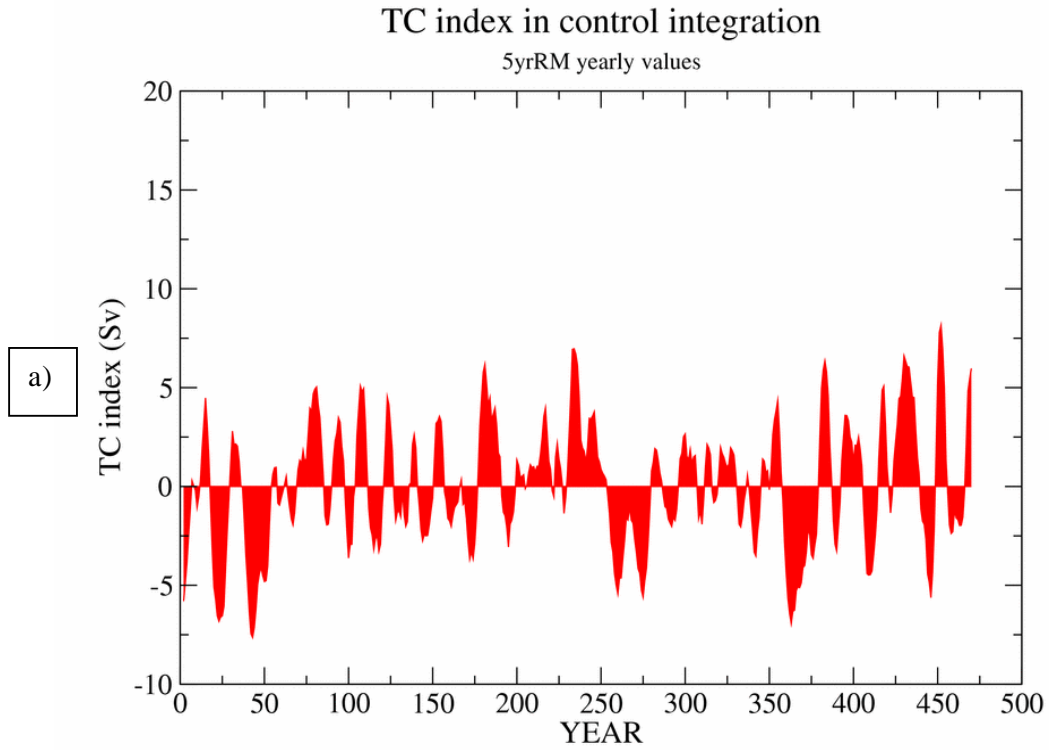
Figure 3.2 (a) Time evolution, and **(b)** the power spectrum (thick solid line) of the anomalous strength of the Tropical Cells (TC) from the control integration. For the definition of the cell strength please see the text. The plotted values in **(a)** have a 5-year running mean applied. The 95% confidence level is plotted as the dotted black line, and the AR1 process fitted to the data as solid green line.
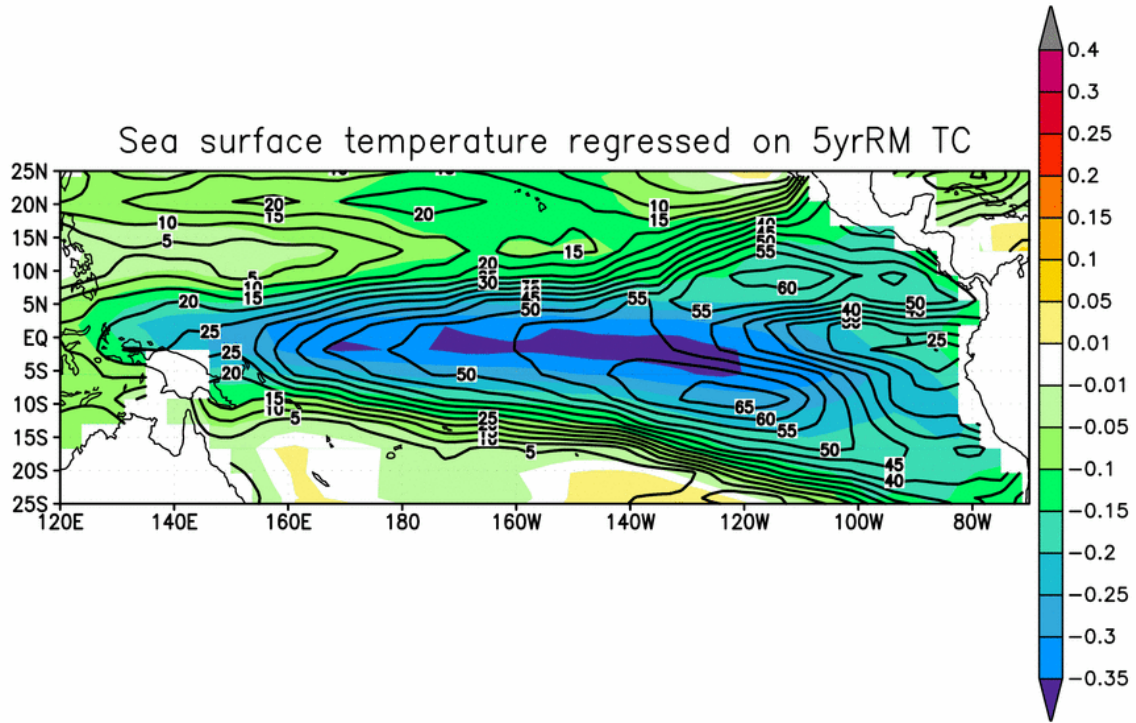
Figure 3.3 Linear regression of the sea surface temperature anomalies (shaded, in °C) over the tropical Pacific regressed on the anomalous strength of the TCs from the control integration. A 5-year running mean low-pass filter was applied to the monthly anomalies before the regression analysis. The explained variance of the regression is plotted with contour lines. The contour interval is 5 %.
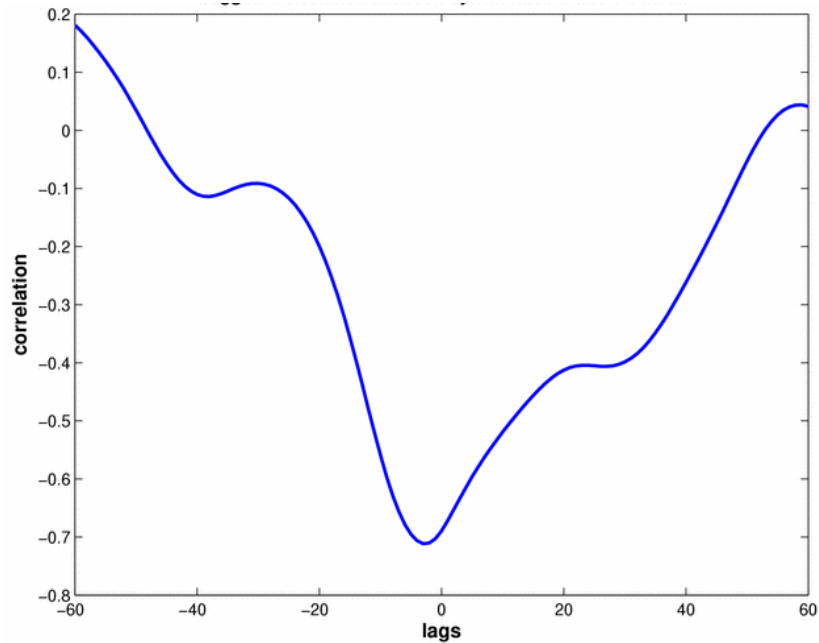
Figure 3.4 The lead-lag correlation function between the Niño-4 SSTA and the anomalous strength of the TCs from the control integration. The 95% significance level according to a t-test is –0.195. A positive (negative) lag indicates that Niño-4 SSTA is leading (lagging).

23

tropical Pacific SST and the associated explained variance. The regression coefficient reaches a maximum of -0.35 °C per standard deviation of TC index in the central-western equatorial Pacific. The associated explained variance is characterized by a horseshoe-like pattern, with maximum values in the central-western equatorial Pacific, extending to the northeast and southeast into the subtropics. This horseshoe-like structure resembles the signature of the observed decadal climate variability in the tropical Pacific (Latif et al.,1997; Lohmann and Latif, 2005; see also Figure 3.1a). The cross-correlation between the TC index and Niño-4 SSTA (sea surface temperature anomalies) amounts to –0.7, with the meridional overturning leading by 3-4 months (Figure 3.4). The correlation coefficient is statistically significant at the 95% level according to a t-test (the threshold value is –0.195). Therefore, an anomalous warm Niño-4 SST goes along with an anomalous weakening of the tropical cells, while the time lag suggests that the variability of the tropical cells is driving the low-pass-filtered SST fluctuations in the Niño-4 region.

We decomposed the monthly TC index time series by means of singular spectrum analysis (SSA). The reconstructed TC index time series using the first two SSA modes is plotted as a red line in Figure 3.5a, while with black color is represented the original TCA time series. The leading temporal modes that accounts for 22% of the TC index variance, has a quasi-decadal timescale. The first two T-EOFs exhibit a pronounced decadal variability with a period of about 17yr (Figure 3.5b). It is worth mentioning that this pair of SSA modes represents the only oscillatory pair isolated in the data by means of SSA. In the following, we will use the reconstructed TC index (hereafter TCdec) to investigate by means of linear regression the spatial structures of decadal climate variability in tropical Pacific. Please note that all the regression coefficients hereafter will describe changes in the atmospheric and oceanic variables per one standard deviation of the TCdec index (1.44 Sv). Furthermore, only the strengthening TC case will be described.

Figure 3.6 shows the pattern for the regression of TCdec index onto the tropical Pacific SST. An increase by one standard deviation in TCdec index is accompanied by a 0.2-0.25°C decrease in tropical Pacific SST, with maximum values in central-western equatorial Pacific and off-equatorial South Pacific. The pattern of associated explained variance is similar to the horseshoe-like structure seen in Figure 3.3, but with smaller values in both equatorial and off-equatorial Pacific. The anticorrelation between the TC strength and Niño-4 SSTA is also maintained at the decadal timescale (not shown). The largest correlation coefficient amounts to –0.4, which is weaker than in Figure 3.4, but still statistically significant at the 95% level.
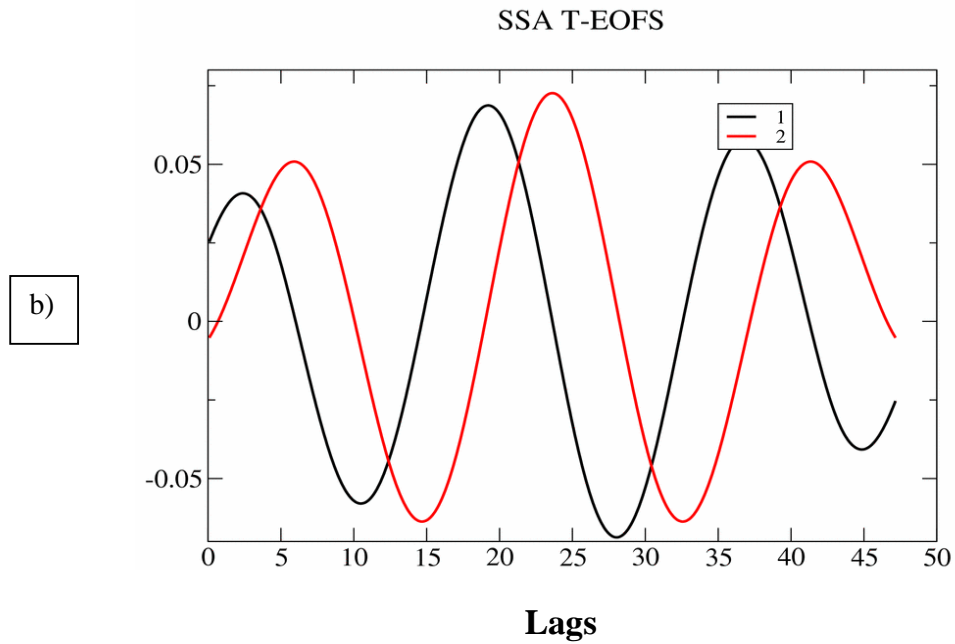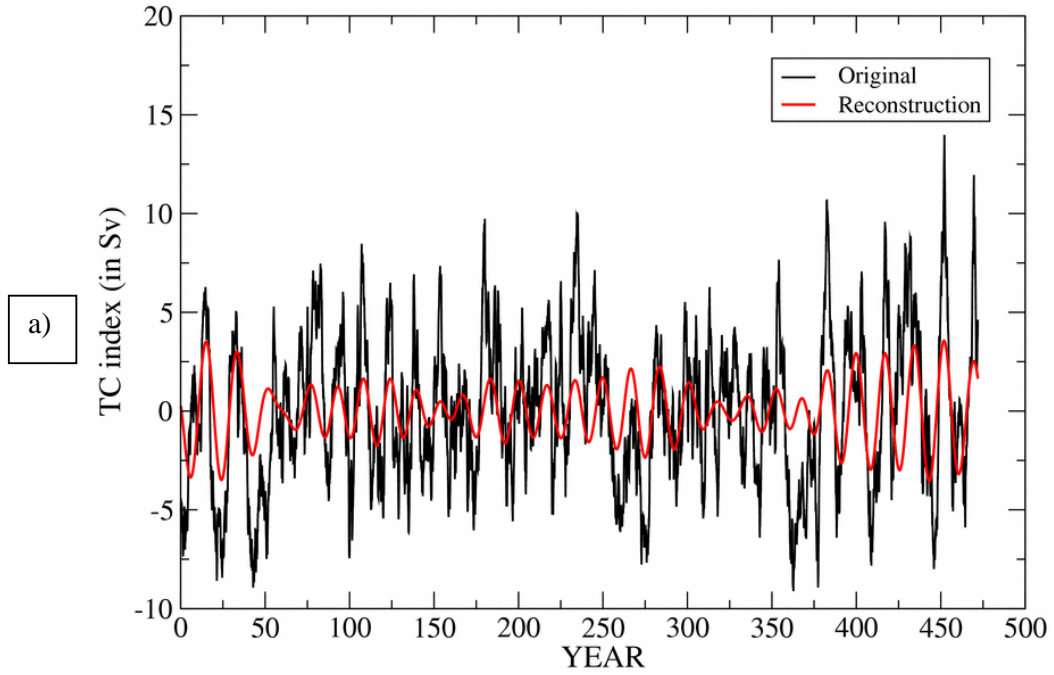
Figure 3.5 (a) Reconstruction (red solid line) of the anomalous strength of the TCs (in Sv) from the Singular Spectrum Analysis using mode 1 and 2. The original anomalous strength of the TCs is represented by the black solid line. **(b)** T-EOFs of the SSA mode 1 (black) and 2 (red).
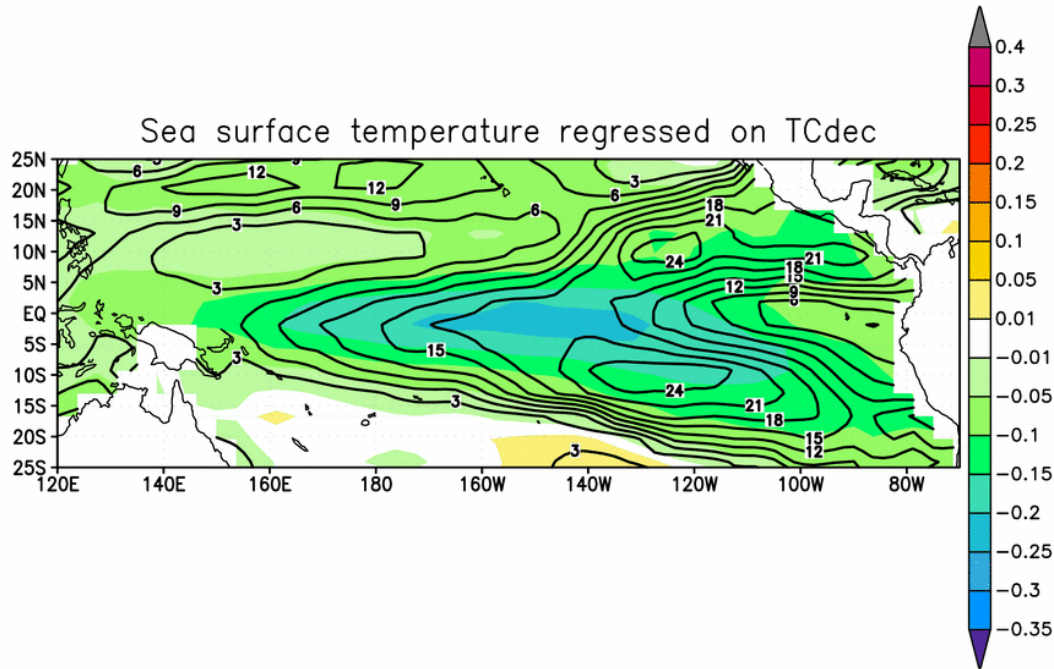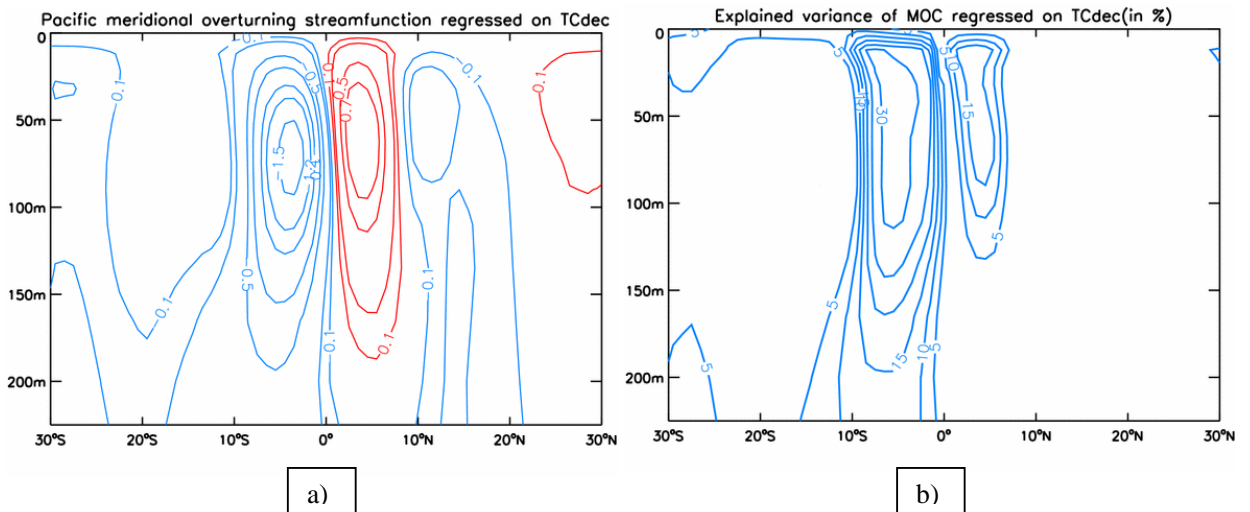
Figure 3.6 Linear regression of the sea surface temperature anomalies (shaded, in °C) over the tropical Pacific on the anomalous strength of the TCdec. A 5-year running mean low-pass filter was applied to the monthly anomalies before the regression analysis. The explained variance of the regression is plotted with contour lines. The contour interval is 5 %.

Figure 3.7 (a) Linear regression of the anomalous upper Pacific meridional overturning streamfunction (in Sv) on the anomalous strength of the TCdec. **(b)** The explained variance of the regression pattern. Contour levels in **(a)** are ±0.1, ±0.3, ±0.5, ±0.7, ±1, ±1.2, and ±1.5 Sv. Contour interval in **(b)** is 5 %.

The regression pattern of the Pacific meridional overturning streamfunction upon the TCdec index suggests a stronger influence of the southern tropical cell on the decadal mode and a very weak contribution of the off-equatorial regions (Figure 3.7). The maximum regression coefficient amounts to 1.5Sv for the southern tropical cell and explains 30% of its variance, compared to 0.7Sv and 15% explained variance for the northern tropical cell.
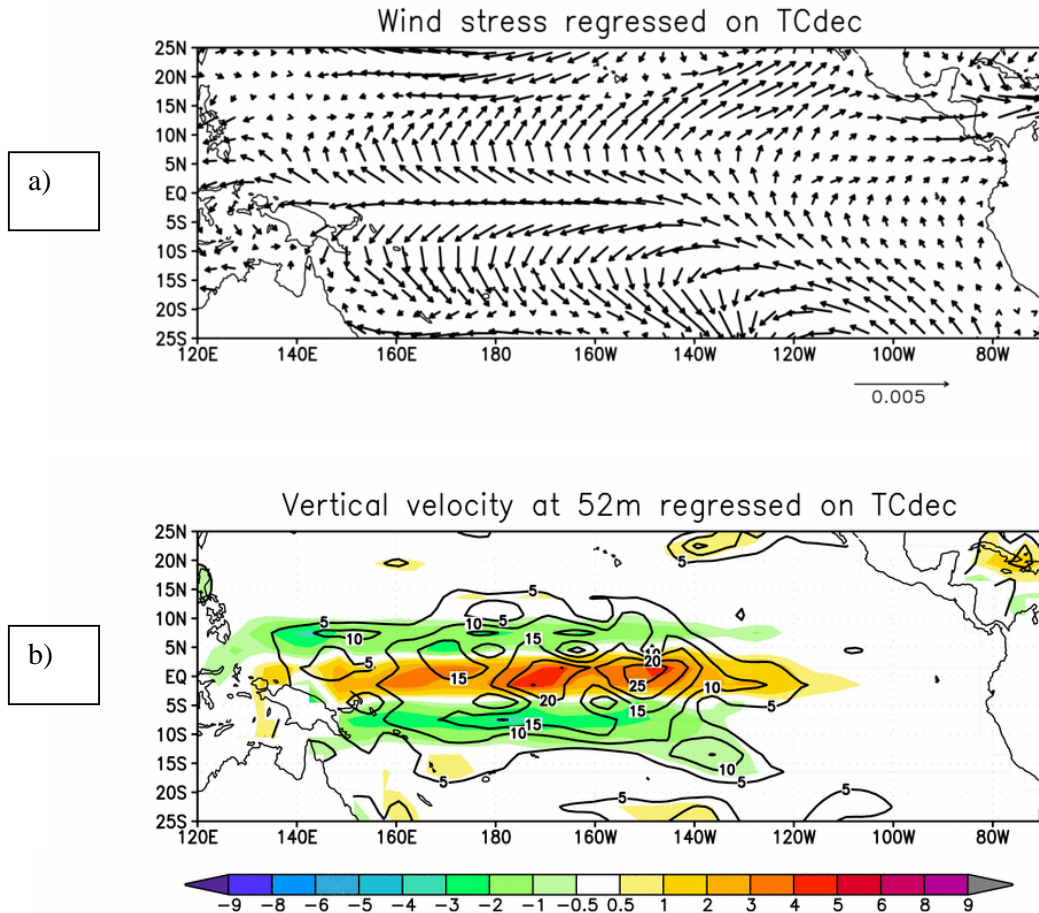
Figure 3.8 (a) Linear regression of the anomalous wind stress (vectors, in N/m^2) on the anomalous strength of the TCdec. The reference vector is 0.005 N/m^2. **(b)** Linear regression of the anomalous ocean vertical velocity (shaded, in cm/day) on the anomalous strength of the TCdec. The explained variance of the regression pattern is plotted with black contour lines. Contour interval is 5 %.

In our model, a spinning up of the tropical cell is accompanied by a strengthening of the trade winds over the central-western equatorial Pacific and tropical South Pacific, with maximum changes of about 0.005 N/m^2 that accounts for 22% of the low-pass-filtered wind stress variability (Figure 3.8a). In response to stronger trade winds, the Ekman transport divergence in the ocean is intensified and this will lead to an increase in the equatorial

upwelling. In this study, we are using the vertical ocean velocity at 52m depth as a measure of the equatorial upwelling. Figure 3.8b shows that the biggest vertical velocity changes (5cm/day) occur in the central-western Pacific, overlapping the area where the wind stress changes are the largest. Consistent with the spinning up of the tropical cells, the vertical velocity regression pattern displays an intensified downwelling between 5° and 10° latitude in both hemispheres. As it can be seen in Figure 3.9a, the regression pattern for the total precipitation amount exhibits a North-South dipole-like structure over South Pacific, indicating a southward shift in the South Pacific Convergence Zone (SPCZ). This displacement of the SPCZ appears to be the cause of a wind stress curl anomaly which drives the Ekman downwelling, that is simulated between 5°S-10°S in western tropical Pacific (Figure 3.9b). A similar, although weaker, precipitation pattern is found over tropical North Pacific, and it resembles a northward shift in the ITCZ. The effect of off-equatorial anomalous wind stress curl favoring Ekman downwelling can be easily identified in Figure 3.10, which displays the regression pattern for the thermocline depth (represented here by the depth of the 20°C isotherm-Z20). A deepening of the thermocline is found between 5°-10° latitude in both hemispheres of the western tropical Pacific west of 150°W during phases of anomalous strong TCdec. There is also a thermocline depth change in the subtropical North Pacific, but we found it not related to the tropical Pacific and therefore, it will not be discussed.

The above-mentioned changes in trade winds will also have an effect on the wind-driven horizontal circulation. A strengthening of the South Equatorial Current (SEC) of the order of 2 cm/s is simulated in the western equatorial Pacific and tropical South Pacific, accompanied by a weaker reduction of the North Equatorial Current (NEC) (Figure 3.11). Due to a strengthened SEC, the horizontal temperature advection will bring cold water from the cold tongue region into the warm pool area and southern tropical Pacific, contributing to the decrease in SST of the decadal mode. A similar circulation pattern is evident from the regression of subsurface currents (horizontal velocity at 100m depth), but with only half the amplitude (not shown).

The net surface heat flux changes associated with strong TC are in opposite sign to SST anomalies over the western equatorial Pacific and tropical South Pacific, and hence damp them in these regions. However, the surface heat flux contributes to cool SST in the eastern equatorial Pacific. The cold SSTA in the tropics associated with the decadal mode induce an anomalous anticyclonic circulation in the South Pacific tilted in the southeast-northwest direction (Figure 3.12b). A weaker Aleutian low is simulated in the North Pacific due to the
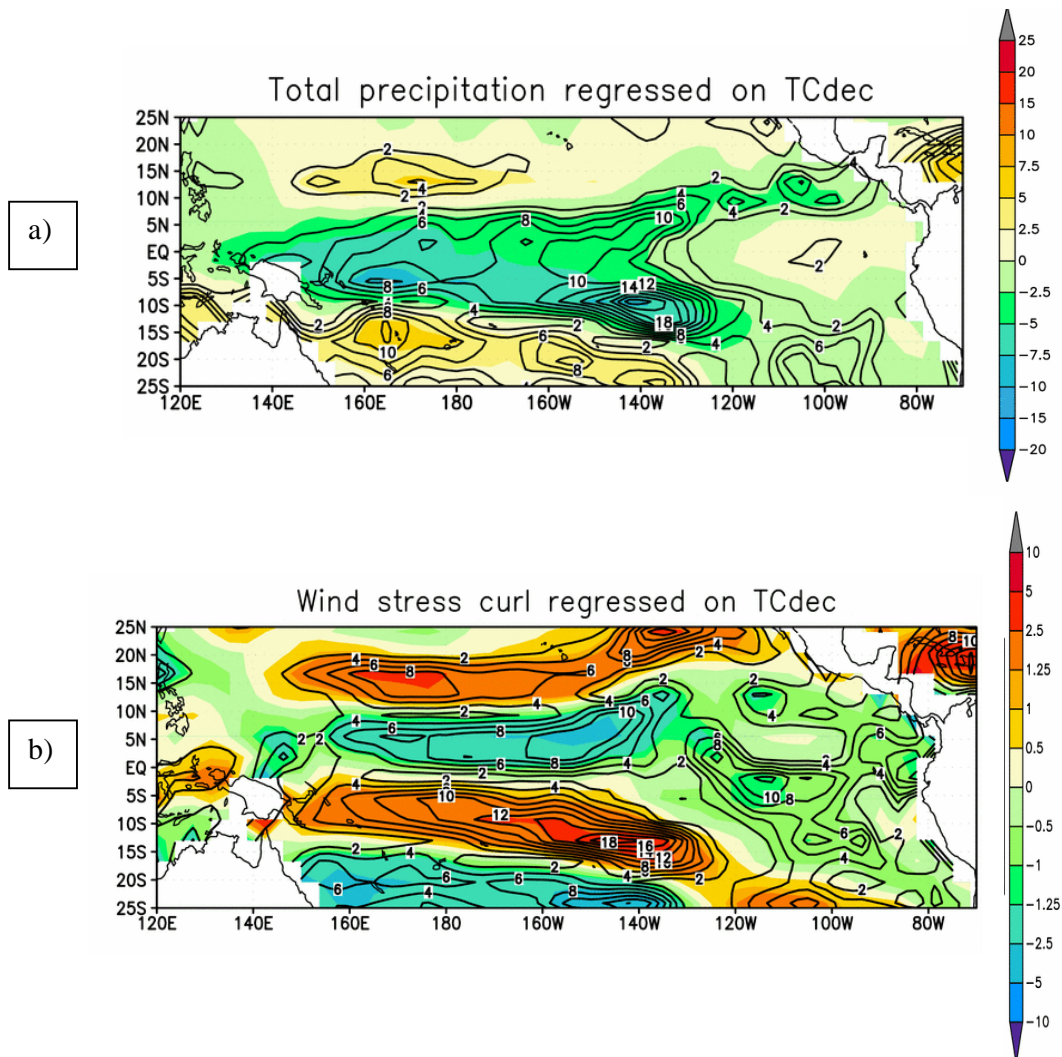
Figure 3.9 (a) Linear regression of the anomalous total precipitation amount (shaded, in mm/month) on the anomalous strength of the TCdec. The explained variance of the regression pattern is plotted with black contour lines. **(b)** Linear regression of the anomalous wind stress curl (shaded, in N/m^3) on the anomalous strength of the TCdec. The explained variance of the regression pattern is plotted with black contour lines. The contour interval of the explained variance is 2 % in both figures.
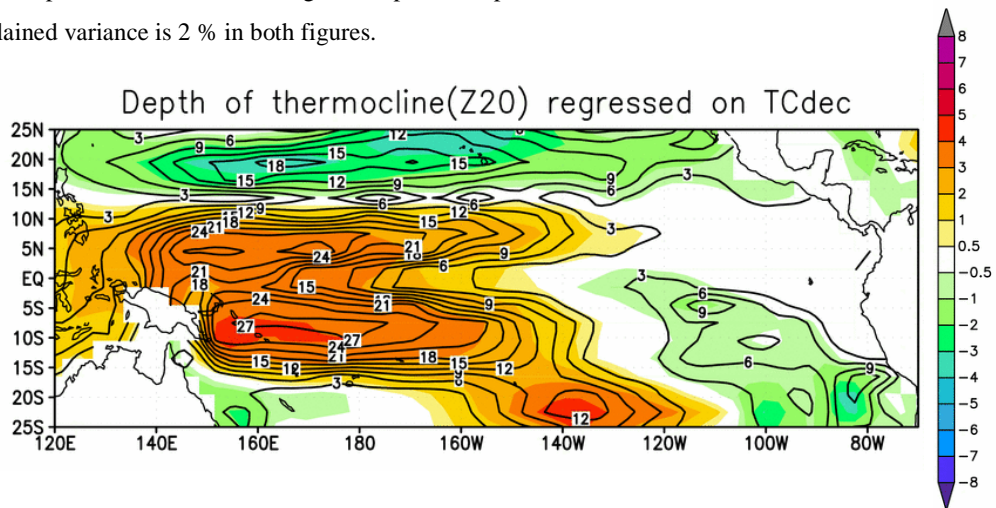

Figure 3.10 Linear regression of the anomalous thermocline depth (shaded, in m) on the anomalous strength of the TCdec. The explained variance of the regression pattern is plotted with black contour lines. The contour interval of the explained variance is 3 %.

29

Ocean surface velocity regressed on TCdec
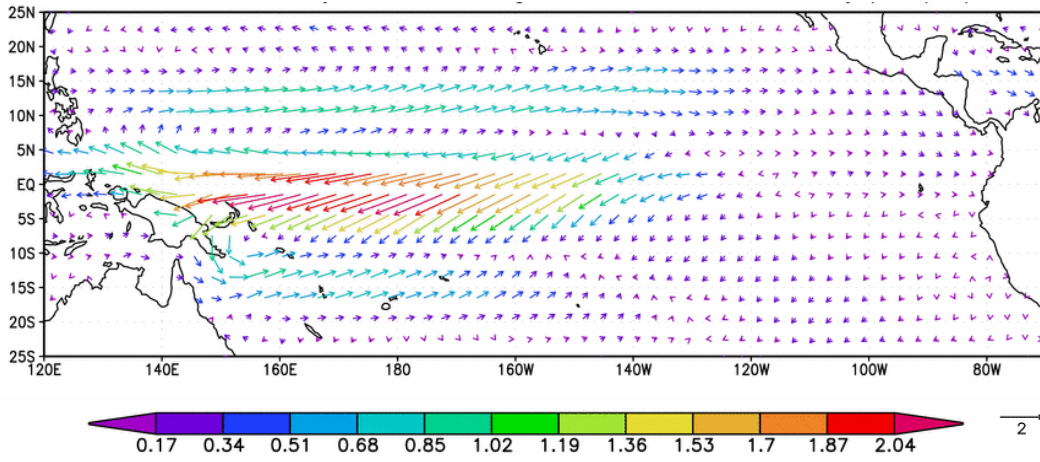
Figure 3.11 Linear regression of the anomalous ocean surface velocity (vectors, in cm/s) on the anomalous strength of the TCdec. The reference vector is 2 cm/s.

a)

b)
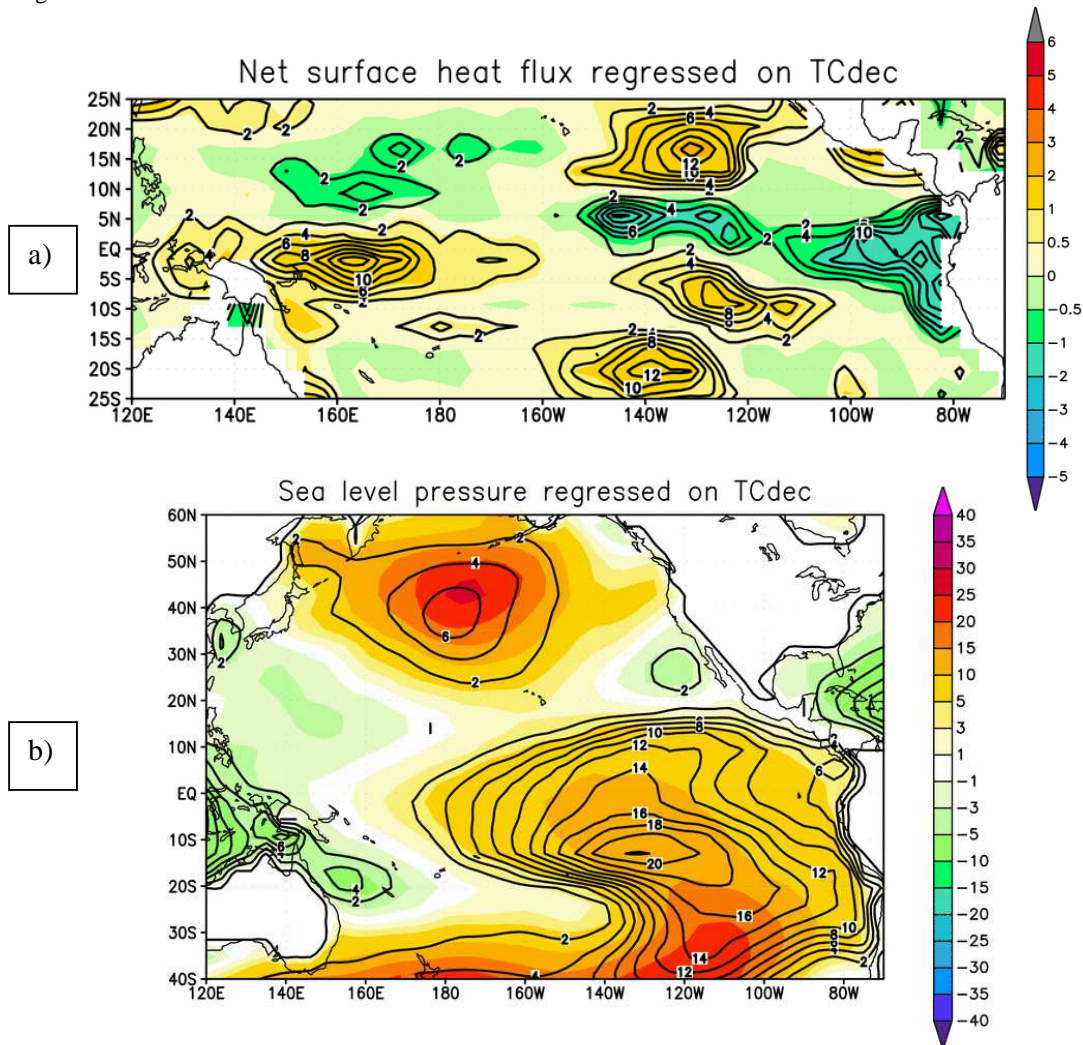
Figure 3.12 (a) Linear regression of the anomalous net surface heat flux (shaded, in N/m^2) on the anomalous strength of the TCdec. The explained variance of the regression pattern is plotted with black contour lines. **(b)** Linear regression of the anomalous sea level pressure (shaded, in Pa) on the anomalous strength of the TCdec. The explained variance of the regression pattern is plotted with black contour lines. The contour interval of the explained variance is 2 % in both figures.

30

teleconnection from the cold tropical Pacific SSTA, also with much less explained variance compared with observations (Alexander et al., 2002).

Since the thermocline processes are likely to play an important role in the tropical variability at decadal timescales, we further examined the behavior of the tropical thermocline depth associated with the decadal mode. The lead-lag regression maps between the depth of the thermocline and the TCdec index are plotted in Figure 3.13 at various time lags, representing one life cycle of the decadal mode. Please note that a positive (negative) lag indicates that the thermocline depth is lagging (leading). At zero-lag (Figure 3.13e), besides the deepening of the thermocline over the western tropical Pacific, a deeper thermocline is simulated in the central South Pacific between 15°S-30°S, accompanied by an elevated thermocline at the same latitudes in the eastern South Pacific. As the time progresses (Figure 3.13 f-i), a clockwise propagation pattern of the thermocline depth anomalies in the tropical South Pacific is emerging. The eastward movement of the Z20 anomalies along the equator is followed by the development of thermocline depth anomalies of the same sign in the eastern tropical Pacific near the South American coast, which will propagate westward along the 20°S-30°S till about 160°W and then farther, northwestward, towards the warm pool area. From the lead-lag regression pattern we can also infer a 16-17yr period of the decadal thermocline variability that is consistent with the period of our decadal mode.

This mode's evolution is such that when the tropical cells are spinning up and lead to a negative sea surface temperature anomaly in the central equatorial Pacific, a positive sea level pressure anomaly is developed over the southern tropical Pacific via the atmospheric teleconnection. Associated with the anomalous anticyclonic circulation, a positive wind stress curl anomaly is induced with a SE-NW orientation from about 20°S-120°W to 5°S-150°E. The corresponding downward Ekman pumping anomaly will cause the local oceanic thermocline to deepen and thus generate warm subsurface temperature anomalies. The anomalous warm subsurface signal will further extend westward and northward towards the equatorial western Pacific. After reaching the western equatorial Pacific, the positive temperature signal will move eastward along the equator, where it will replace the original negative temperature anomaly and weaken the tropical cells owing to a reduced equatorial upwelling. A similar evolution, but with an opposite sign, will subsequently follow for the second half of the decadal mode's cycle.

Now we will try to find out the cause for the propagation of the subsurface temperature signal in tropical South Pacific and along equatorial Pacific. In an observational study, Luo and Yamagata (2001) speculated that in the western Pacific, the northwestward
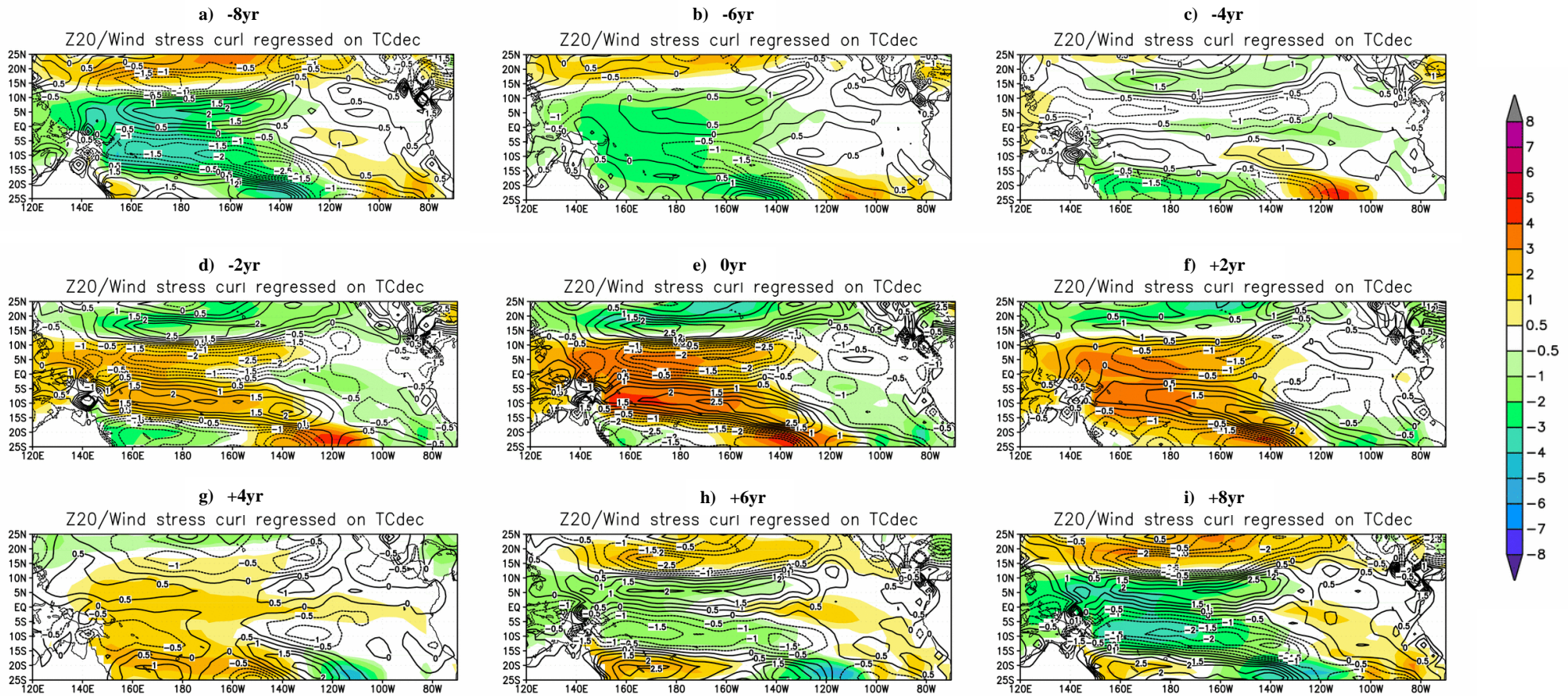
Figure 3.13 Lead-lag regression of the anomalous thermocline depth (shaded, in m) and wind stress curl (black contours, in N/m^3) on the anomalous strength of the TCdec. Lags are –8yr **(a)**, -6yr **(b)**, -4yr **(c)**, -2yr **(d)**, 0yr **(e)**, +2yr **(f)**, +4yr **(g)**, +6yr **(h)**, and +8yr **(i)**. A positive (negative) lag indicates that TCdec is leading (lagging). The contour interval is 0.5 N/m^3.

and northward propagation of subsurface temperature anomalies could be a result of Rossby wave propagation and/or of the mean flow advection (Gu and Philander, 1997). Based on the analysis of OGCM data, Capotondi and Alexander (2001, 2003) have shown that the tropical centers of thermocline variability at 10°S and 13°N are associated with first-mode baroclinic Rossby waves forced by anomalous Ekman pumping, with the most important forcing factor - the zonal coherence of the Ekman pumping - becoming more pronounced at decadal timescales. A recent study by White et al. (2003) proposes a tropical decadal mode involving a westward propagation of Rossby waves along 15°S from Tahiti to western boundary near Australia in about 5 years. To test whether the coupled Rossby wave propagation is active in our model at decadal timescales, we plotted in Figure 3.14 the low-pass filtered anomalies (5yr running mean applied) of the thermocline depth along the 20°S for 50 years of our simulation. The propagation is quite fast; taking about 2-3 years for the thermocline depth anomalies to propagate from 120°W to 150°E. Therefore, the propagation of subsurface signal is not due to the propagation of coupled Rossby waves generated in the eastern subtropical South Pacific.
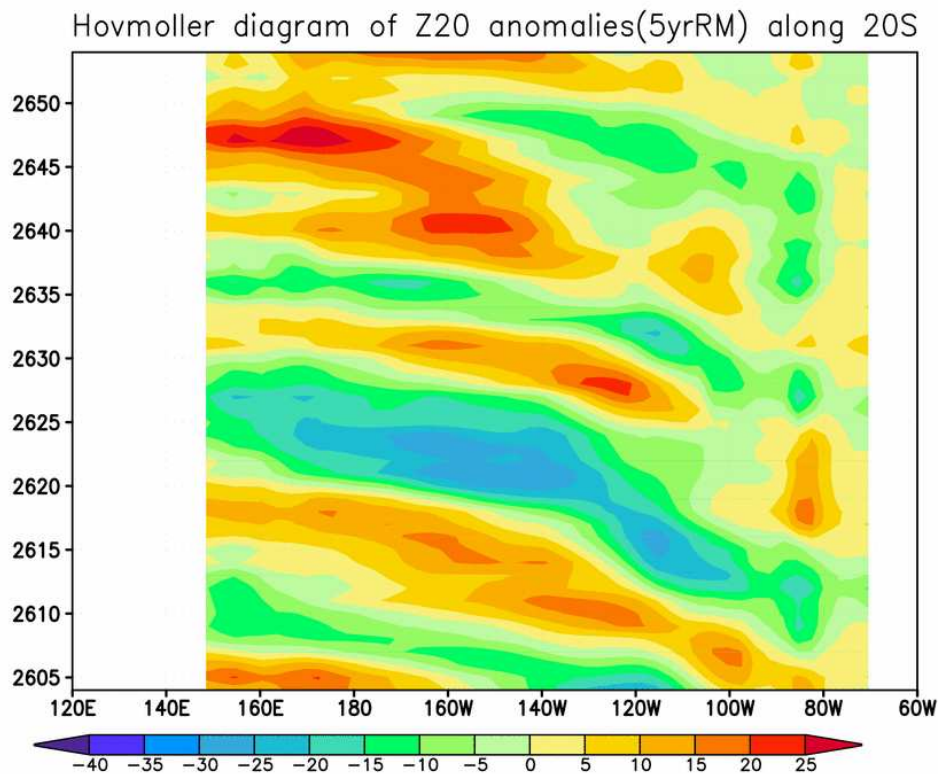
Figure 3.14 Hovmoller diagram of the anomalous thermocline depth (in m) in the Pacific Ocean along 20°S for a period of 50 years of the simulation.

Next, we investigate the behavior of the equatorial ocean heat content (OHC) associated with this decadal mode by means of lead-lag linear regressions. The ocean heat content used in our study is defined as the vertically averaged temperature over the upper 500m of the water column. Figure 3.15a shows the lead-lag regression between the low-pass filtered OHC averaged between 1.5°S-1.5°N along the equatorial Pacific and the TCdec index, while Figure 3.15b displays the lead-lag regression of 150°E-140°W zonally averaged OHC and the TCdec index. Please note that a positive lag indicates that the OHC is lagging.

The regression pattern in Figure 3.15a indicates that the decadal mode is associated with an east-west seesaw and a slow eastward propagation of the equatorial heat content anomalies. At lag zero, a positive OHC anomaly pattern develops in the central-western Pacific, while east of 150°W, a weaker negative OHC anomaly leads the positive western anomalies by 1 year. After about 5 years, the positive western anomalies are connected with eastern OHC anomalies of the same sign, suggesting an eastward propagation that leads to the opposite phase. The pattern and the time evolution of the oceanic heat content associated with the decadal mode suggest that the ENSO recharge/discharge mechanism proposed by Jin (1997) for the tropical Pacific interannual variability might operate at the decadal timescales in the model.

The propagation of the subsurface signal in the South Pacific is too fast to be explained solely by the mean advection or the Rossby wave propagation. Instead, the local ocean-atmosphere interactions in the western Tropical Pacific seem to play an important role in the fast westward and equatorward movement of the subsurface temperature anomalies. The maximum variability of the OHC at the decadal timescales is located around 10°S and 7°N in western-central tropical Pacific (Figure 3.15b). The local OHC fluctuations center in the tropical South Pacific is stronger than the one in the tropical North Pacific, and both lead the equatorial OHC by 1-2 years. The OHC fluctuations in the tropical western Pacific require a local atmospheric forcing: the variations in Ekman pumping velocity generated by the atmospheric teleconnections from the central equatorial Pacific lead the heat content variations by about 1-2 years (not shown).

Our results are in accordance with recent observational and modeling studies. Analyzing the mechanisms responsible for ENSO-like decadal (7-35 years) variability in observations, Luo and Yamagata (2001) argued that the South Pacific acts as an external thermal source to discharge/recharge the tropical ocean and therefore, inducing the decadal fluctuations of the ENSO-like phenomenon. They propose a 14 years period for the decadal phenomenon and underline the role of western tropical South Pacific, where the SPCZ is

located, as a key region for ENSO-like decadal variability. Investigating a coupled ocean-atmosphere model, Luo et al. (2003) found that a similar mechanism can explain ENSO-like decadal variations in their model.
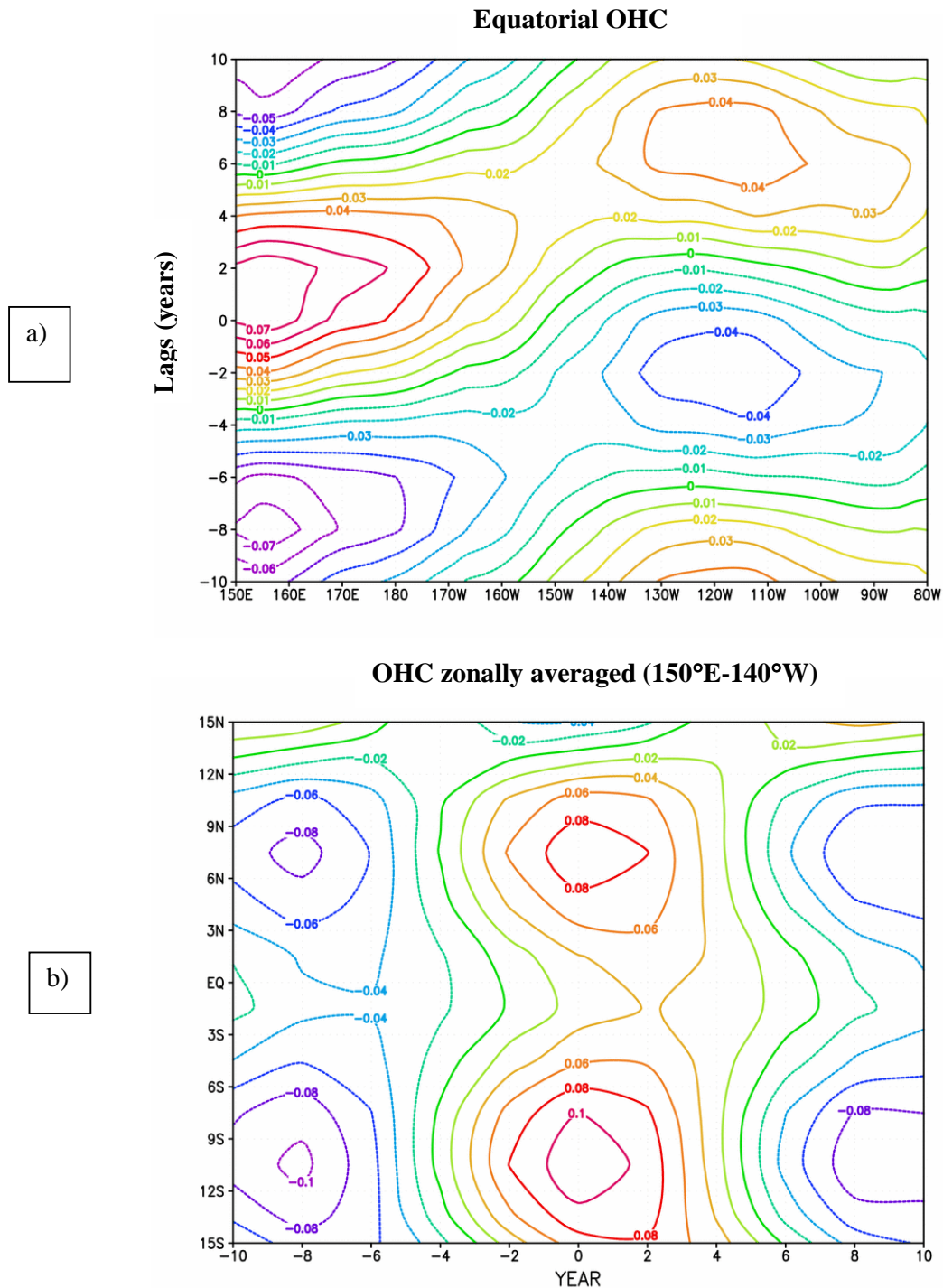
Equatorial OHC

OHC zonally averaged (150°E-140°W)

Figure 3.15 Lag-regression of anomalous Pacific Ocean heat content (OHC, in °C) on the anomalous strength of the TCdec from –10yr to 10yr. A positive (negative) lag indicates that TCdec is leading (lagging). In **(a)** the OHC is averaged between 1.5°S-1.5°N. In **(b)** the OHC is zonally averaged between 150°E-140°W. Contour interval is 0.01 °C in **(a)** and 0.02 °C in **(b)**.

35

3.4 ENSO decadal modulation

We will now investigate whether the decadal mode of the model is associated with changes in ENSO characteristics. To test this hypothesis, we computed composite maps of SST standard deviation for periods of strong positive (TCdec > 1 std) and strong negative (TCdec < -1std) values of the decadal mode index. The composites for strong positive events and the composites for strong negative events are computed separately, and then subtracted. Figure 3.16 shows that periods of strong positive TCdec are associated with periods of increased ENSO variability and vice versa, and therefore contribute to the decadal modulation of ENSO activity. A positive TCdec period is associated with an intensified zonal SST contrast and a deepening of the thermocline in the western tropical Pacific. According to Zebiak and Cane (1987) and Meehl et al. (2001), these changes in the mean background state are expected to accompany an enhanced ENSO activity. A more detailed discussion about the affect of decadal changes in the mean background state of the equatorial Pacific Ocean on ENSO variability will be given in the Chapter 4 of the thesis.

SST composites for TCdec (°C/ 1 stddev TCdec)
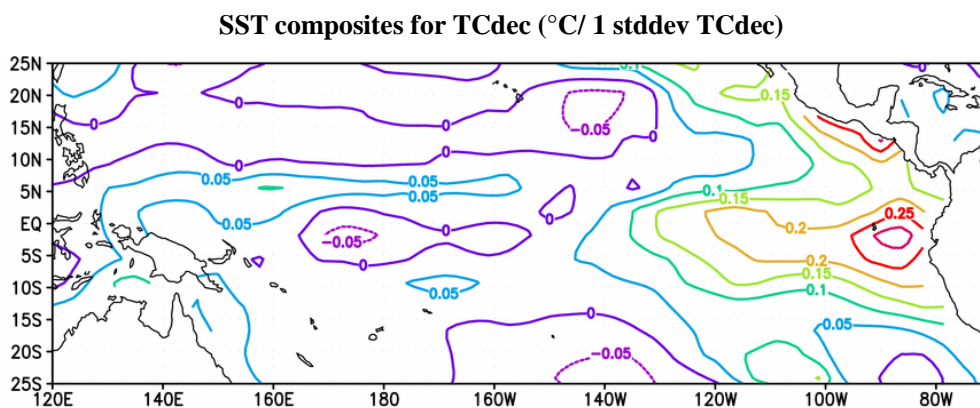
Figure 3.16 Composite difference map for strong positive minus strong negative TCdec of the SST standard deviation (in °C). The threshold value for the composite is one standard deviation of the TCdec index. Contour interval is 0.05 °C.

4. Sensitivity to density perturbations in the subtropics – impact on the mean state

4.1 Introduction

In this chapter we use ECHAM5-MPIOM coupled ocean-atmosphere-sea ice model to study the mechanisms responsible for subtropical-tropical interactions in the Pacific region at decadal timescale. To investigate the climate response of the equatorial Pacific system to density variations in the subtropical surface climate, and to estimate the relative contributions of North and South Pacific to the subtropical-tropical connections, we carried out a number of sensitivity experiments. In these experiments idealized sea surface temperature anomalies and sea surface salinity anomalies were added over certain domains in the North and South Pacific. Additionally, similar uncoupled integrations with the AGCM ECHAM5 model were performed.

In the following we will mainly focus on the impact of the Pacific subtropical sea surface temperature anomalies on the mean state of the ocean and atmosphere. The mean climate adjustment to the sea surface salinity will be only briefly discussed. The impact of subtropical Pacific on tropical climate variability, with an emphasis on ENSO modulation, will be analyzed in the next chapter of the thesis.

4.2 Experimental setup of the coupled experiments

The Pacific equatorial climate response to sea surface temperature and sea surface salinity variability in the subtropical Pacific is examined by prescribing idealized SST/SSS anomalies over North Pacific, respectively South Pacific subtropics. Two domains were selected, one in the subtropical North Pacific (hereinafter NPac) between 170°W-125°W, 23°N-31°N and the second one in the subtropical South Pacific (hereinafter SPac) between 135°W-75°W, 23°S-31°S. The two selected domains (Figure 4.1) correspond to the subduction areas proposed by Gu and Philander (1997). In selecting the size of the forcing

domains, the relative coarse horizontal resolution of the coupled model was also taken into consideration.

SST= sea surface temperature

SSS= sea surface salinity

a)

b)
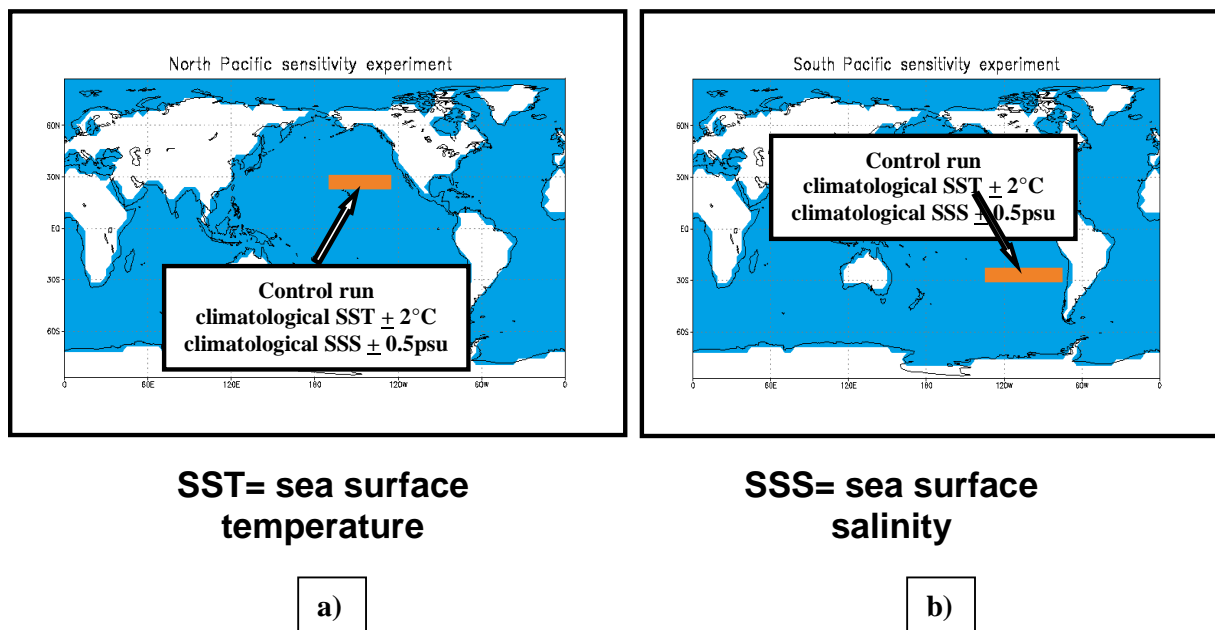
Figure 4.1 Selected domains of the individual sensitivity experiments: (a) North Pacific experiment (NPac), **(b)** South Pacific experiment (SPac).

We have imposed a homogenous two degree warming/cooling on the top of the mean seasonal cycle of the control run over the NPac and SPac domains. The SST anomalies were kept constant for 200 years. Figure 4.2a shows the SST response in both NPac and SPac domains, for a global warming experiment performed with the same coupled climate model. This integration represents a CO_2 sensitivity experiment in which a "1% CO_2 concentration increase per year to quadrupling" is imposed for the first 140 years, and then, the CO_2 forcing is kept constant at 4xCO_2 level for about 750 years. Therefore, the prescribed 2°C anomaly is beyond the range of intrinsic coupled variability, but is within the range of the expected global warming change in the subtropical Pacific in the model (Figure 4.2a) and in literature (Kerr, 2004; Lea, 2004). The negative (-2°C) SST sensitivity experiments were performed in order to study the equatorial response to an idealized cooling in the subtropical Pacific. To assess the linearity of the equatorial response to the anomaly strength, we have also conducted experiments with half of the forcing: +1°C /-1°C.

Similar sensitivity simulations were performed imposing a ±0.5 psu and ±0.25 psu sea surface salinity anomaly forcing. The imposed salinity forcing is also within the range of sea surface salinity change in the above-mentioned global warming experiment for both NPac and

The SST response for a global warming experiment (1% CO2 increase until 4xCO2)
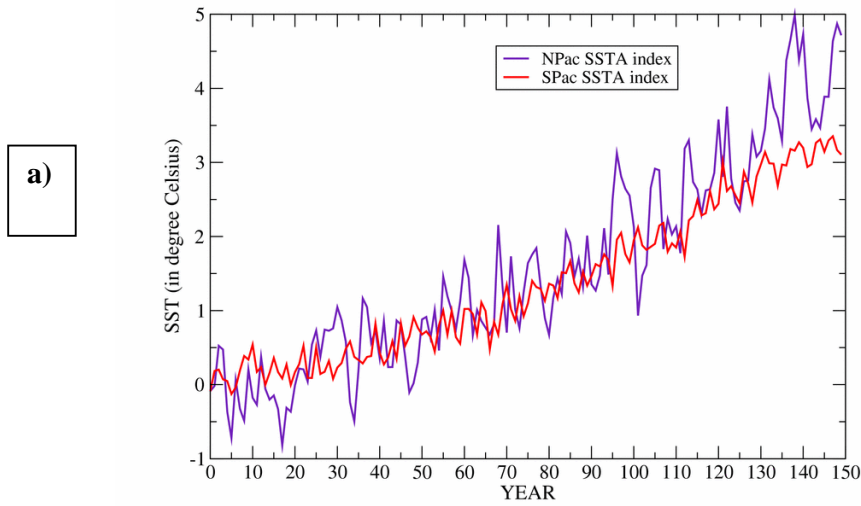
The sea surface salinity response in a global warming experiment (1% CO2 increase until 4xCO2)
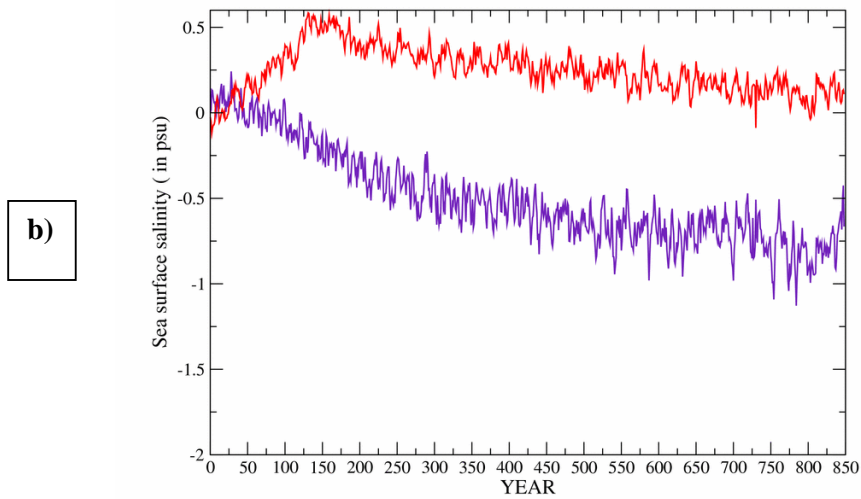
Figure 4.2 Evolution of the anomalous annual **(a)** SST and **(b)** SSS response averaged over the NPac (blue line) and SPac (red line) domains during a global warming experiment. The anomalies are computed relative to the mean of the control integration.

SPac domains (Figure 4.2b). The full forcing (0.5psu) sea surface salinity experiments were conducted for 70 years and the half-forcing experiments for only 30 years. A longer integration for the sea surface temperature experiments compared to sea surface salinity experiments was required in order to assess the statistically significant changes in tropical Pacific interannual variability. Such changes in tropical Pacific interannual variability were not simulated in the sea surface salinity experiments.

39

4.3 South Pacific sensitivity experiment (SPac+2°C)

In the following part we will discuss the +2°C experiment in the South Pacific (SPac+2°C). The response of the coupled experiment is computed as a difference between the mean of a variable over the whole 200 years of the experiment and the mean of the control run for the same period. Only the response that exceeds the 95% significance level according to a two-sided Student's t-test is plotted.

Figure 4.3 displays the simulated response of sea surface temperature in the SPac+2°C experiment. The mean SST response exhibits an equatorial warming, which reaches a maximum of 0.9°C in the central-eastern equatorial Pacific. The warming represents 45% of the SST forcing. This SST pattern will lead to a reduced zonal SST gradient between West and Central-East Pacific, which in turn will influence ENSO variability. This aspect will be discussed in the next chapter.

Tropical Indian and Atlantic oceans also experience an SST warming of about 0.2°C - 0.3°C (not shown). A dipole-like pattern can be noticed south of Australian continent with a 0.8°C SST cooling in the southwest and a 1°C SST warming in the southeast. In the North Pacific, a warming of 0.7°C along the western coast of Canada and Gulf of Alaska and an even higher 0.9°C warming near Kamchatka are simulated (Figure 4.3).
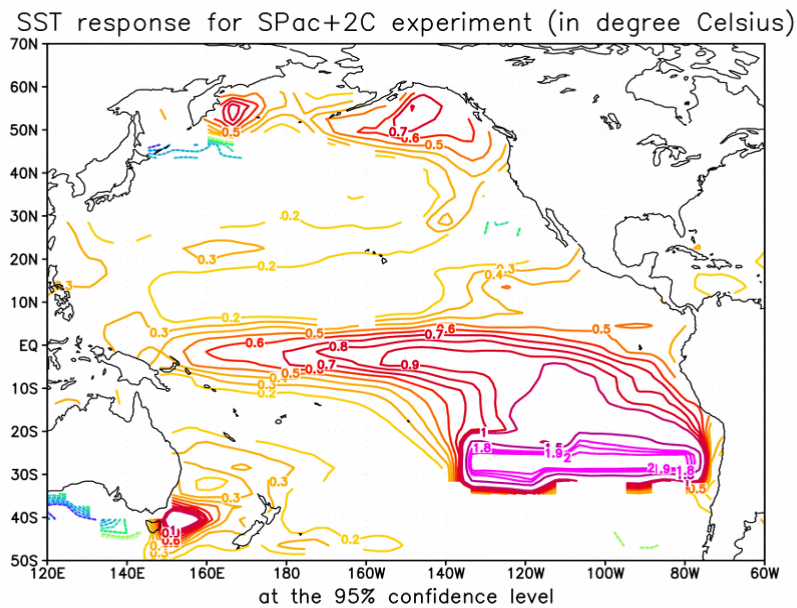
Figure 4.3 Anomalous Pacific Ocean SST (in °C) response in the SPac+2°C experiment. Contour interval is 0.1°C. Please note that values in the range (-0.2°C, +0.2°C) are not plotted.

a) Equatorial SST response for SPac+2C(in degree Celsius)

b) Equatorial thermocline response for SPac+2C

at the 95% confidence level
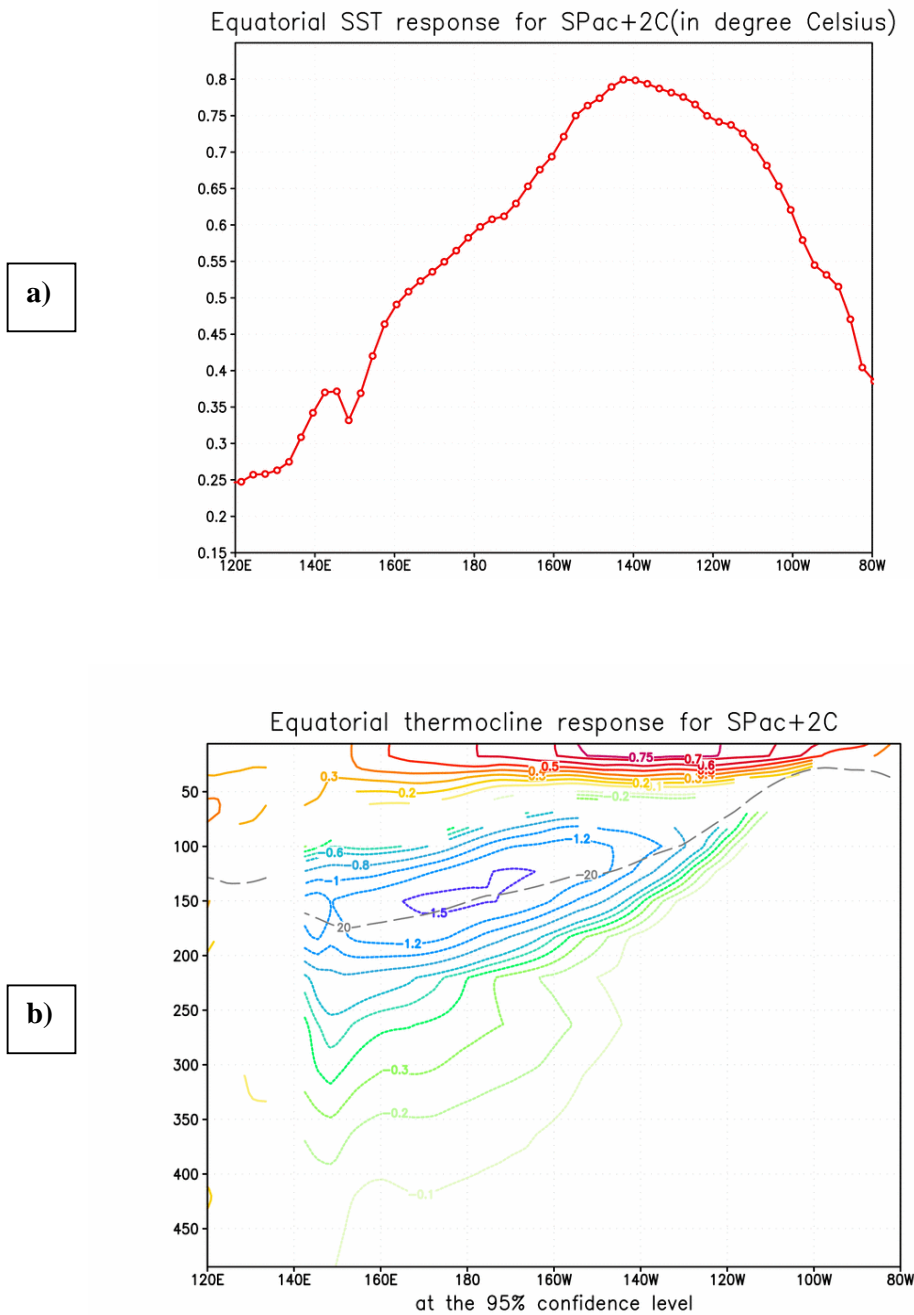
Figure 4.4 Mean climate changes in **(a)** SST (in °C) and **(b)** the thermocline temperature in SPac+2°C experiment, averaged in a 5°N - 5°S equatorial strip of Pacific Ocean. In **(b),** the dashed gray line represents the mean depth of the 20°C isotherm in the control integration. The contour levels in **(b)** are –1.5°C, -1.2°C, -1.0°C, -0.8°C, and -0.6°C, followed by a 0.1°C contour interval.

41
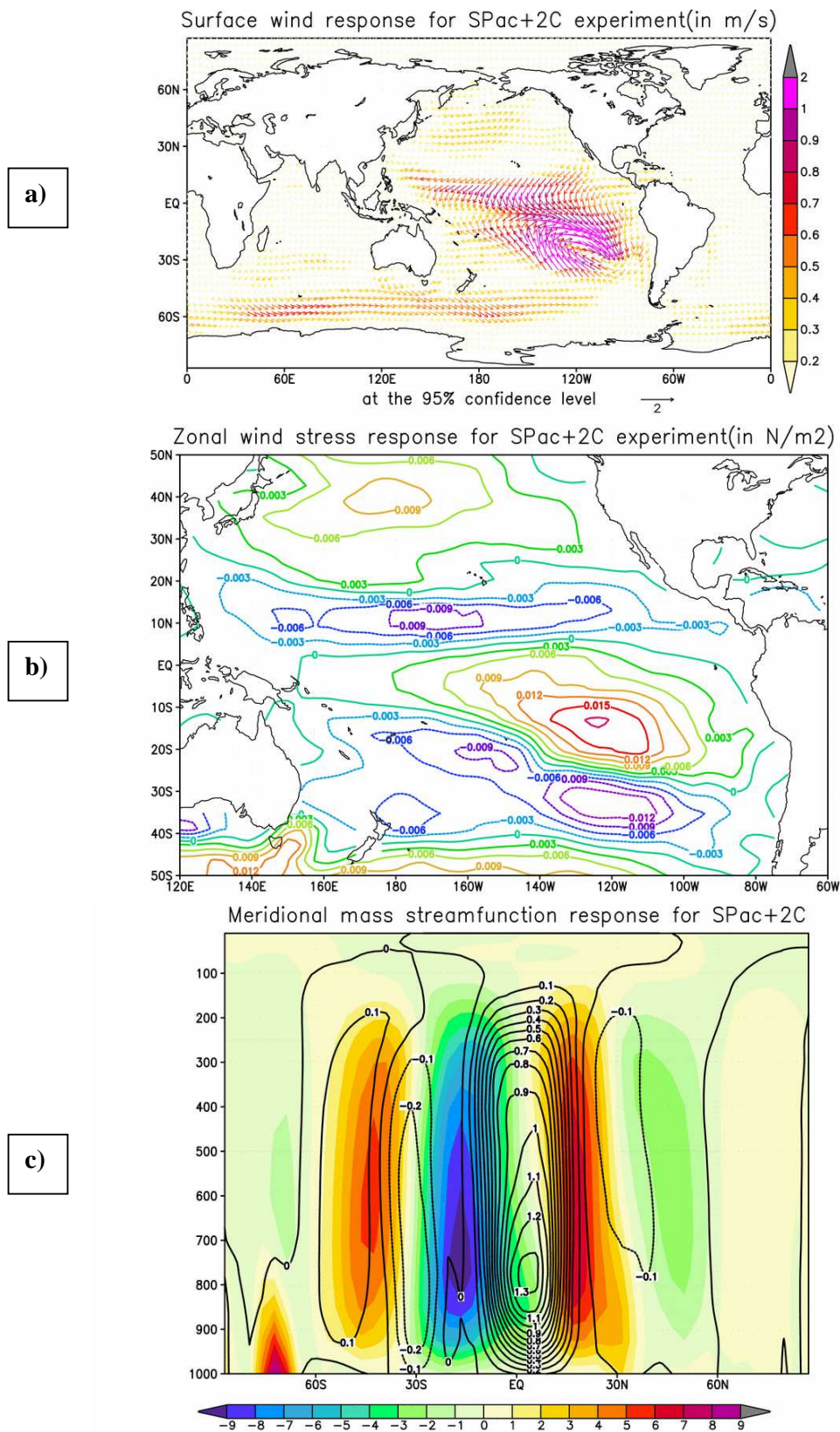
Figure 4.5 Anomalous Pacific Ocean **(a)** surface winds (in m/s) and **(b)** zonal wind stress (in N/m^2) in the SPac+2°C experiment. The reference vector of surface wind is 2 m/s. The contour interval in **(b)** is 0.003 N/m^2. Anomalous atmospheric meridional mass streamfunction in the SPac+2°C experiment (black contours) and the mean atmospheric meridional mass streamfunction of the control integration (shaded, in 10^{10}Kg/s) are plotted in **(c)**. Contour interval in **(c)** is 0.1x 10^{10}Kg/s.

These changes in the surface climate can be obtained through both the "atmospheric bridge" (AB) and "oceanic tunnel" (OT). As it can be seen from Figure 4.4a, the mean SST change averaged in a 5°N-5°S equatorial strip of Pacific reaches a maximum between 150°W and 130°W, where it exceeds 0.9°C. In figure 4.4b, the mean change of the Pacific 5°N-5°S averaged equatorial thermocline temperature is plotted. The thick black dashed line represents the position of the depth of the 20°C isotherm in the control integration. The fast "atmospheric bridge" is not very effective in changing the equatorial subsurface temperature, due to the strong equatorial upwelling that inhibits the downward penetration of the surface atmospheric heat flux forcing. In the equatorial ocean, the temperature anomaly decreases downward towards the subsurface till about 75m in western Pacific and till about 50m in central and eastern Pacific. A negative subsurface temperature anomaly that reaches –1.5°C at 180°E and 150 m depth is simulated along the mean upper thermocline (Figure 4.4b), leading to an enhanced overall vertical temperature gradient. This dynamic response of the ocean will be discussed latter in the chapter. The negative subsurface temperature anomaly weakens slightly over the period of the simulation. This maybe the result of the equatorward oceanic subduction process in OT.

The mean state changes in the tropics resulting from the subtropical warming are consistent with the changes in the atmospheric Hadley cells and oceanic meridional overturning circulation. We have plotted the anomalous Pacific Ocean surface winds and zonal wind stress in Figure 4.5a and b. The southeasterly trades over the South Pacific Ocean are significantly weakened and the northeasterly trades strengthened. This is due to a decreased South Pacific and an increased North Pacific meridional sea surface temperature contrast. As a result of above-mentioned changes in trade winds, the atmospheric Hadley circulation is southward displaced (Figure 4.5c).

The local atmospheric response (Figure 4.6a) to the SSTA in the subtropical South Pacific displays a linear baroclinic response with a surface low (2hPa at the sea level) and an upper level high (40m in the geopotential height response at 250hPa). In addition to the local changes, the sea level pressure response exhibits an anomalous high associated with anticyclonic circulation over the western North and South tropical Pacific. It reaches 1.6 hPa near the southeastern coast of Australia. A remarkable remote feature is the deepening of the Aleutian Low in the North Pacific. This appears to be a result of the atmospheric teleconnection from the tropics (Figure 4.6b). The local vertical air temperature response

43

shows a strong warming of up to 1.5°C at 250hPa (Figure 4.6a). All three tropical oceans present an anomalous increase in the vertical air temperature that extends southward up to 60S° (not shown). This vertical warming response over the tropical oceans is intensified with the altitude and reaches 0.8°C at 250 hPa.
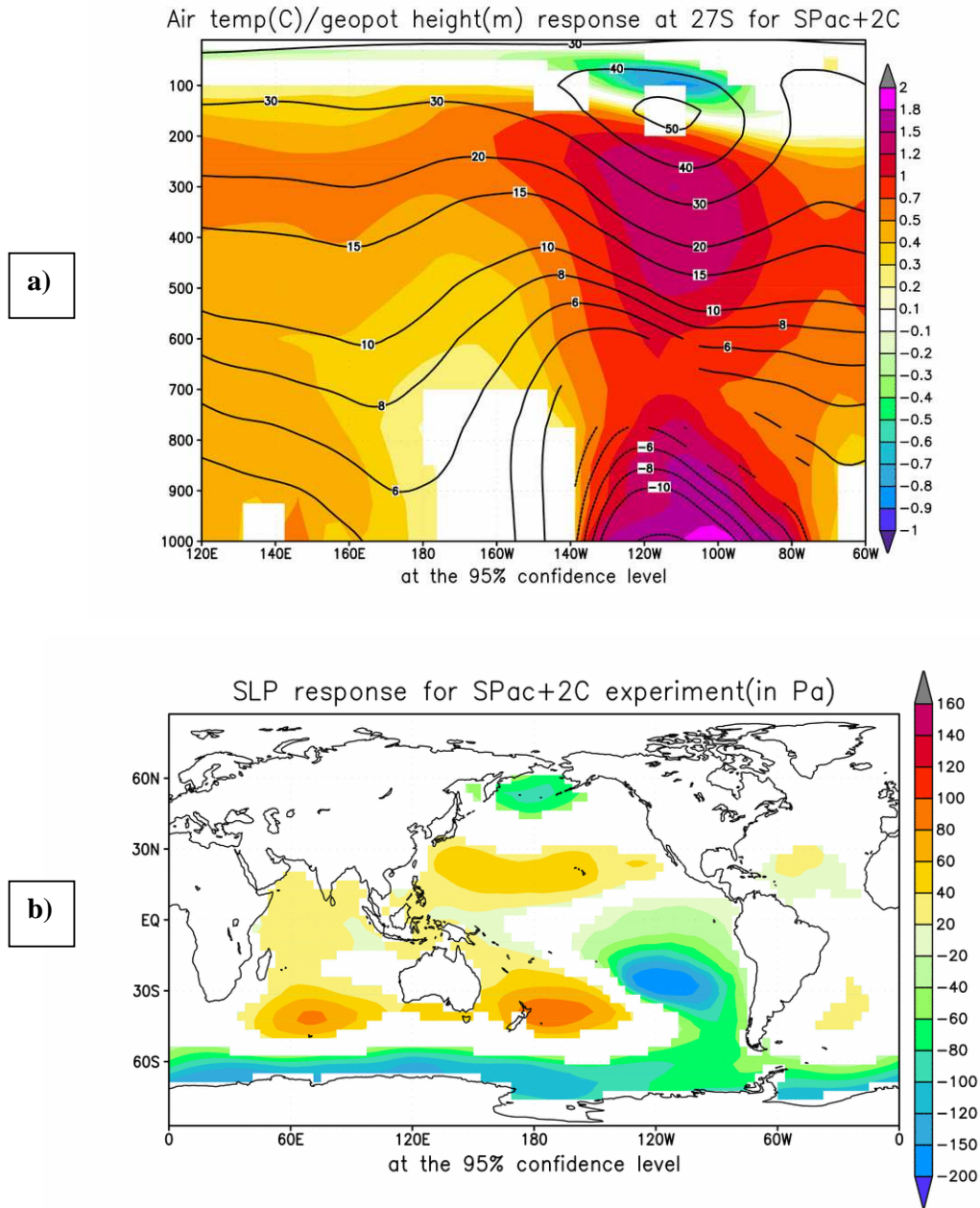

Figure 4.6 (a) Anomalous Pacific Ocean vertical air temperature (shaded, in °C) and geopotential height (black contours, in m) at 27°S latitude in the SPac+2°C experiment. The contour interval is 2m for values less than 10m, and then, the contour levels are 15m, 20m, 30m, 40m and 50m. **(b)** Anomalous sea level pressure (in Pa) response in the SPac+2°C experiment.
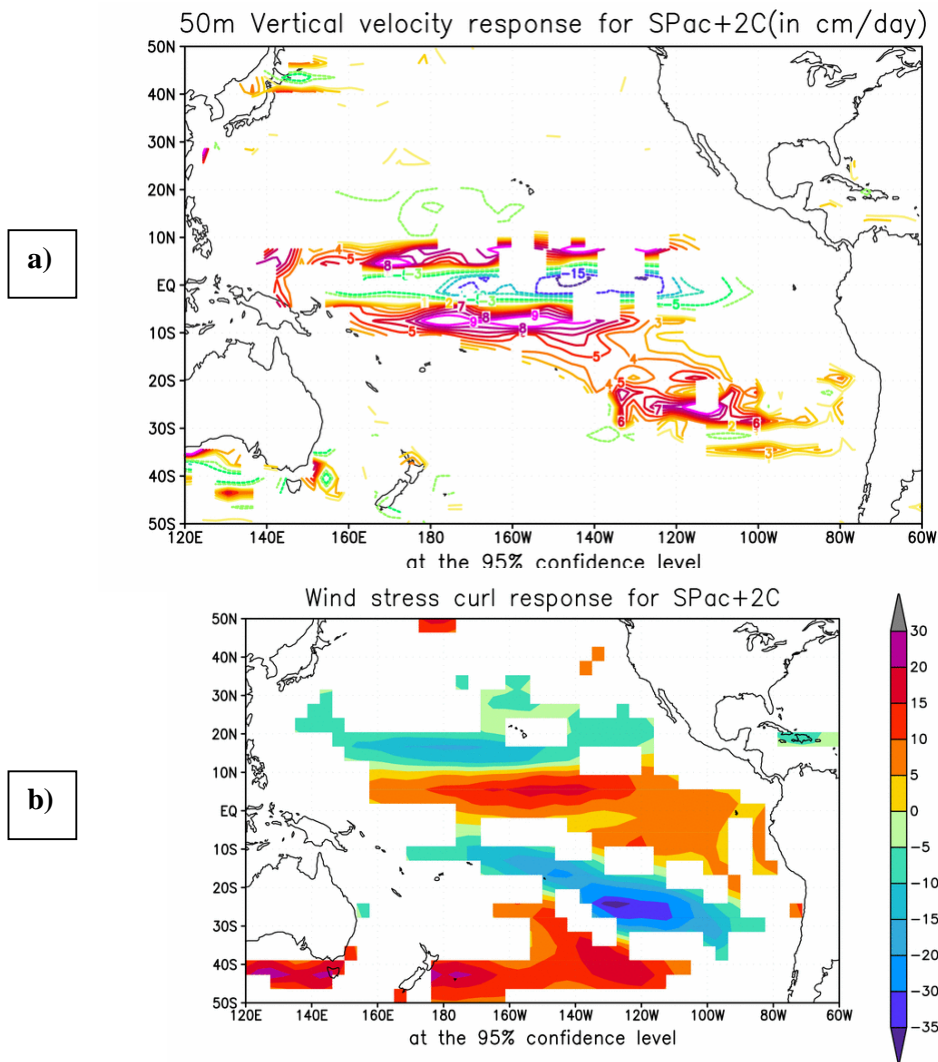
Figure 4.7 Anomalous Pacific Ocean (**a**) vertical velocity at model level 50m (contours, in cm/day) and (**b**) wind stress curl (in 10^{-9} N/m^3) in the SPac+2°C experiment. The contour interval for positive values is 1 cm/day, while the contour levels for negative values are –3, -5, -7, -10, -15, -20 cm/day.
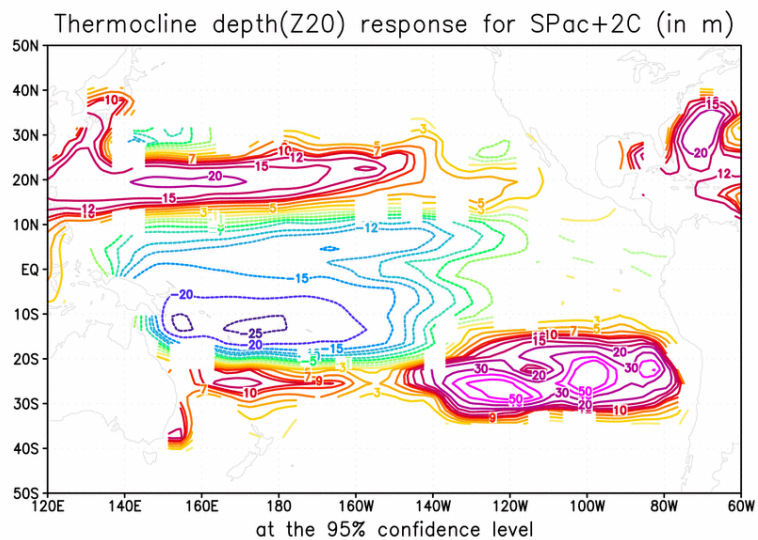
Figure 4.8 Anomalous Pacific Ocean depth of thermocline (in m) in the SPac+2°C experiment. The contour levels are –25, -20, -15, -12, -10, -7, -5, -3, -1, 1, 3, 5, 7, 9, 10, 12, 15, 20, 30, 40 and 50 m.

Weaker equatorial trade winds will lead to a reduced equatorial Ekman divergence in the ocean, which in turn will decrease the equatorial upwelling of the colder subsurface waters. This is clearly seen in the anomalous vertical velocity at 52 m depth (Figure 4.7a). The strongest vertical velocity changes appear in the central equatorial Pacific, between 160° W and 120° W, where the wind stress changes are the largest (Figure 4.5b). In this area of the equatorial Pacific, a reduction of 20 cm/day or about 25% of the mean upwelling is obtained. An upwelling favorable wind stress curl is simulated between 5° and 10° latitude in the central-western tropical Pacific of the both hemispheres (Figure 4.7b). In the south this shifted eastward and southward (10°S-30°S) towards the forcing area. The off equatorial changes in the wind stress curl are visible not only in the vertical velocity response, but also in the depth of the thermocline changes. A shoaling of the thermocline can be found between 10°N and 20°S in the western tropical Pacific with a maximum anomaly of 25m between 5°S-15°S (Figure 4.8). Furthermore, a deepening of the thermocline appears between about 10°N to 25°N in the tropical North Pacific (Figure 4.8).
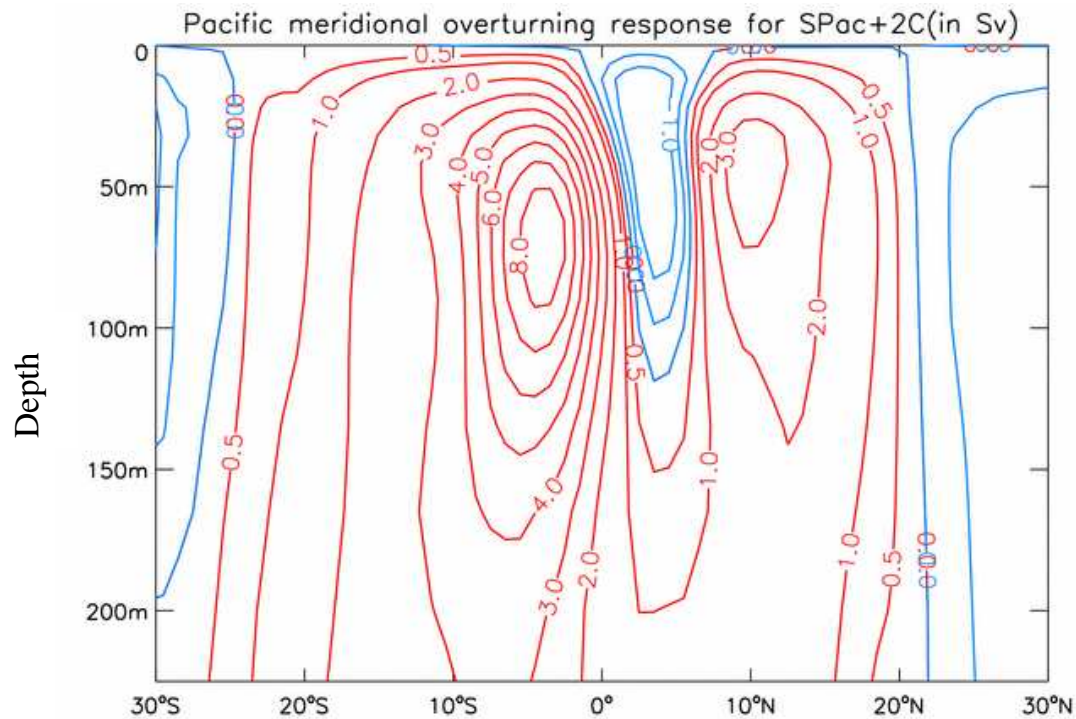
Figure 4.9 Anomalous Pacific Ocean meridional overturning streamfunction (in Sv) in the SPac+2°C experiment. Contour levels are -1, -0.5, -0.3, 0.5, 1, 2, 3, 4, 5, 6, 7 and 8 Sv.

The above-mentioned changes in equatorial upwelling and tropical downwelling are associated with a weakening of the Pacific tropical cells (Figure 4.9). The tropical cell index (see Chapter 2.3 for a definition of TC and STC indices) shows a decrease of about 8 Sv (1Sv = 10^6 m^3/s), which is equivalent to a 10% reduction in TC strength relative to the control integration (the red curve in Figure 4.27a). The weakening of the TC comes primarily from a slowing of the southern cell (Figure 4.9), which exhibits a 17% reduction in strength compared to only 2% for the northern cell. The strength of southern Pacific subtropical cell is decreasing, while the strength of the northern Pacific subtropical cell is increasing. The simulated changes in the depth of the thermocline might also lead to changes in the slope of the thermocline, and thus contribute to the changes in the strength of tropical/subtropical cells. The shoaling of the thermocline in the west will decrease the zonal slope of the thermocline that itself will reduce the equatorward flow within the thermocline and slow down the tropical cells and the southern subtropical cell. On the contrary, the deepening of the thermocline between 10°N-25°N will increase the zonal slope, leading to an increased equatorward flow within the thermocline and to a speed up of the northern subtropical cell.

The changes of equatorial trade winds will also influence the wind-driven horizontal circulation. Figure 4.10a shows a weakening of the South Equatorial Current of the order of 8 cm/s as a result of weakened southeasterly trade winds. On contrary, the North Equatorial Current has strengthened by up to 6 cm/s due to the intensification of the northeasterly trades. Relative strong meridional velocity anomalies are simulated close to the equator and in western tropical South Pacific, which reflect the weaker Ekman divergence. Considering the mean zonal temperature gradient in the tropical Pacific, the horizontal current anomalies will advect warmer water from the warm pool area zonally toward the east and also meridionally into the cold tongue area. In the tropical North Pacific, the westward horizontal currents anomalies will bring colder water from the eastern tropics into the warm pool. This will lead to a much reduced warming between 5°N-20°N. The anomalous mean barotropic streamfunction suggests a strengthening and southward displacement of the subtropical gyre in the North Pacific (Figure 4.10b).

In addition to ocean dynamics, changes in net surface heat flux will also affect sea surface temperature. The response in the net surface heat flux displays a local damping effect on the sea surface temperature of up to 60 W/m^2 (Figure 4.11a). This anomalous surface heat flux is mainly due to an intensified evaporation over the forcing area (not shown). This is not surprisingly, since the latent heat flux is the dominant term in the air-sea heat exchange. The fresh water flux (P-E) changes (Figure 4.11b) reflect mostly the changes in precipitation. An
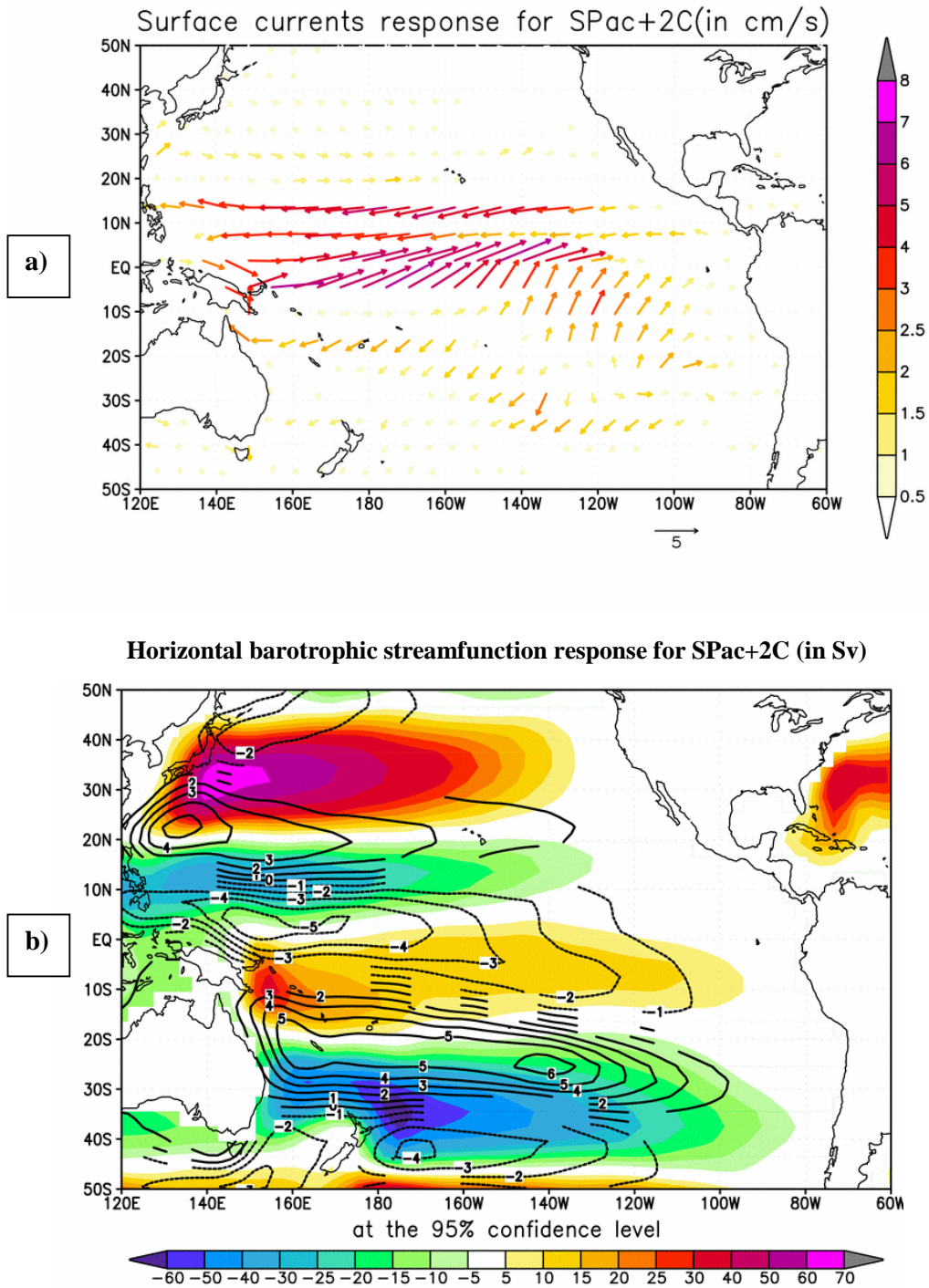
Figure 4.10 (a) Anomalous Pacific Ocean surface current velocity (in cm/s) in the SPac+2°C experiment. The reference vector of surface velocity is 5 cm/s. **(b)** Anomalous horizontal barotrophic streamfunction (black contours, in Sv) in the SPac+2°C experiment and the mean horizontal barotrophic streamfunction in the control integration (shaded, in Sv). The contour interval is 1 Sv.
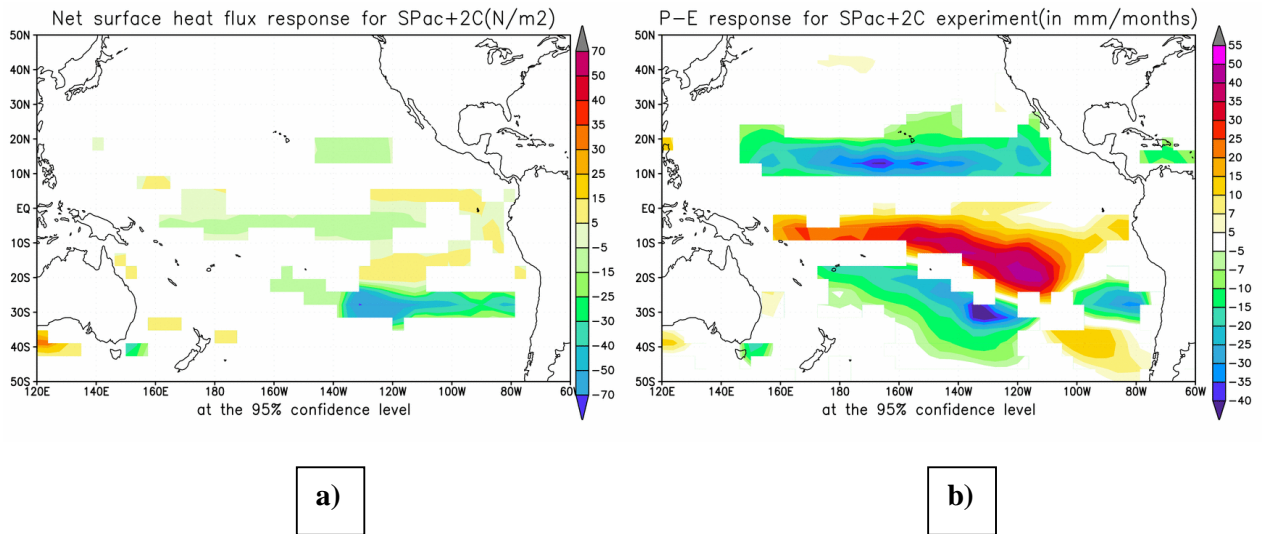
Figure 4.11 Anomalous Pacific **(a)** net surface heat flux (in N/m^2) and **(b)** fresh water flux (precipitation-evaporation, in mm/month) in the SPac+2°C experiment.
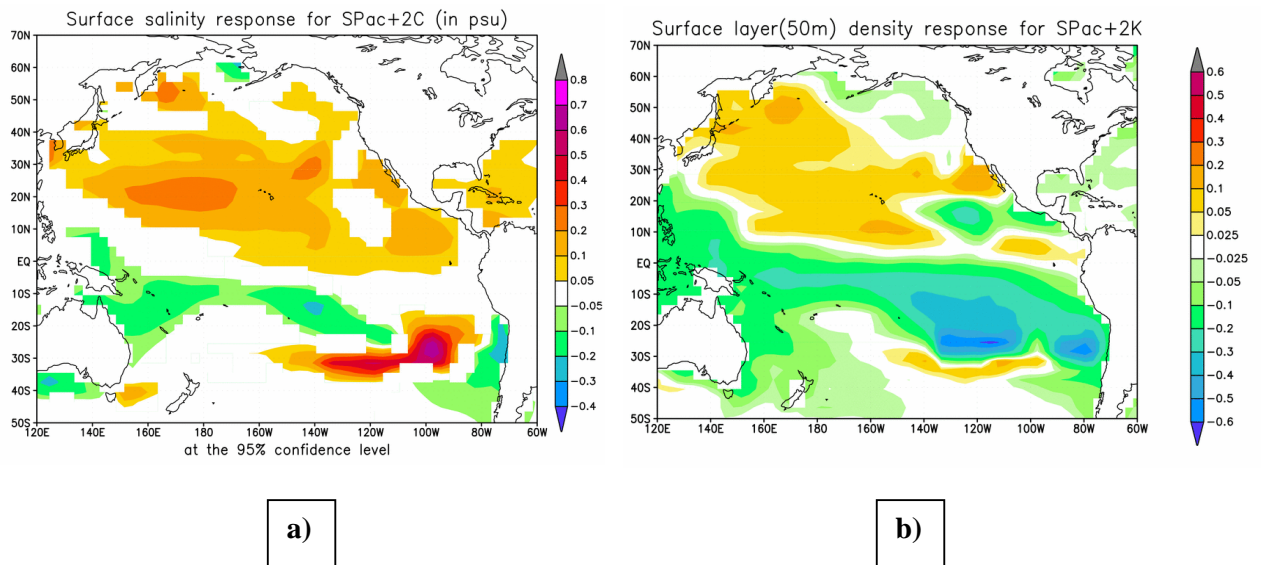
Figure 4.12 Anomalous Pacific **(a)** surface salinity (in psu) and **(b)** upper level density (in Kg/m^3) in the SPac+2°C experiment. The anomalous upper level density was computed as the anomalous ocean density averaged over the upper 50 m.

increase in the total precipitation of about 50 mm/month has been simulated over the area with a positive sea surface temperature anomaly in the equatorial Pacific and tropical eastern South Pacific. In the tropical North Pacific, between 10°N and 20°N, a reduction in the total precipitation of about 35 mm/month is simulated. A decrease in precipitation, but of a smaller scale, appears in the western subtropical South Pacific. In the tropics increases in latent heating are typically associated with local decreases in sea level pressure. This is consistent with the sea level pressure changes in our experiment. The area of increased precipitation exhibits a reduction in the sea level pressure, while the decreased precipitation areas overlap regions with anticyclonic circulation (i.e. high sea level pressure).

In Figure 4.12a we plotted the surface salinity response. An increase of 0.2 psu in the surface salinity is simulated between 10°N-30°N over the North tropical Pacific, as a result of reduced precipitation and horizontal advection of more saline water from the eastern subtropical North Pacific. The South Pacific salinity response shows a 0.6 psu increase in salinity over the forcing domain, and a 0.2 psu freshening of the surface waters in the warm pool area. As a result of the described changes in sea surface salinity and temperature, we found a significant response in the density of upper North and South Pacific Ocean. Figure 4.12b shows a change in the ocean density averaged over the upper 50m: a decrease in density in the tropical South Pacific due to a combined effect of warmer temperatures and lower salinity; this is accompanied by a reduction in the North Pacific ocean mainly due to changes in salinity.

4.4 North Pacific sensitivity experiment (NPac+2°C)

We turn now to the description of the sensitivity experiment in which a two degree sea surface temperature anomaly was imposed over the domain in subtropical North Pacific (NPac+2°C). Figure 4.13 shows the mean response in sea surface temperature over the whole length of the simulation relative to the control integration. The spatial structure of the sea surface temperatures response displays a warming in the tropical Pacific between 10°S-30°N. Relative to the forcing domain, the SST warming decreases westward and southwestward toward the warm pool region. The equatorial SST warming reaches 0.5°C in the western Pacific and 0.3°C in the cold tongue area leading to a slightly increase in the zonal temperature contrast (Figure 4.14a). As a consequence of the warming in the tropical Pacific, a 0.2°C-0.3°C SST warming is simulated in the tropics of Indian and North Atlantic Ocean.
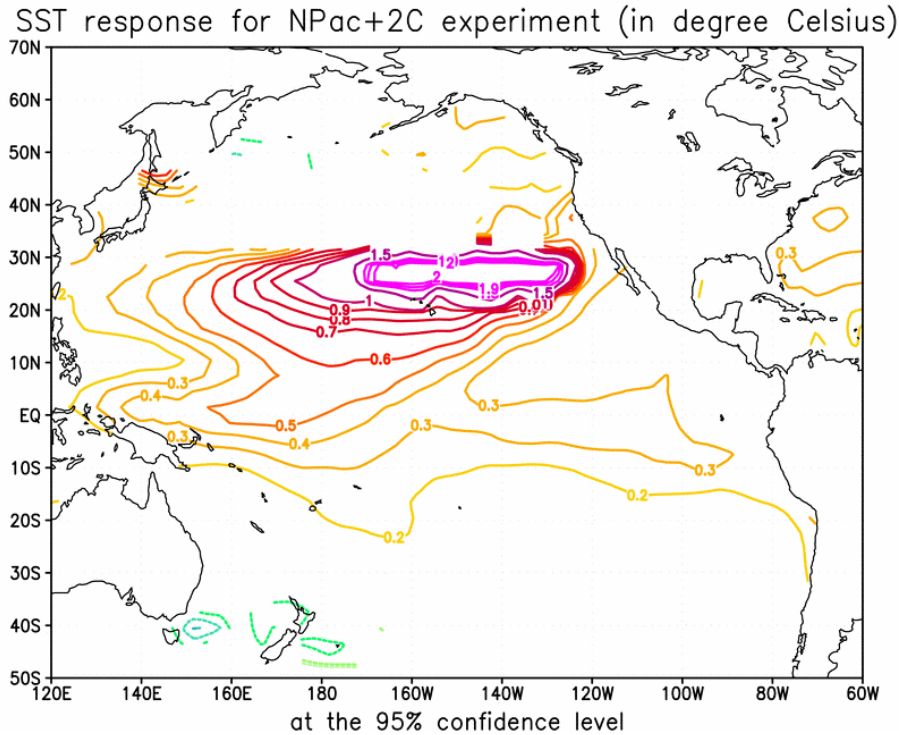
Figure 4.13 Anomalous Pacific Ocean SST (in °C) response in the NPac+2°C experiment. Contour interval is -0.1°C. Please note that values in the range (-0.2°C, +0.2°C) are not plotted.

The North Pacific subtropical warming has also affected the equatorial Pacific thermocline temperature (Figure 4.14b). In the equatorial upper ocean, a positive subsurface temperature anomaly is found till about 200m depth where it reaches 0.3°C. In the far western equatorial Pacific, a negative temperature anomaly up to –0.4°C is simulated between 50m and 450m depth.

As shown in Figure 4.15a, the local response to the subtropical North Pacific warming exhibits a linear baroclinic pattern: an anomalous warm-low response downstream of the forcing area at the surface (1.2 hPa in the sea level pressure) and a warm-ridge response in the upper levels (a 30m geopotential height change at 250 hPa). An anomalous anticyclonic circulation of about 1.2 hPa in sea level pressure is simulated in the South Pacific, close to the Antarctic continent (Figure 4.15b). This anomalous anticyclonic circulation overlaps an area with increased sea ice cover. A negative surface air temperature anomaly of about –0.6°C accompanies the change in sea ice, suggesting that the anticyclonic response is a result of the positive sea ice-albedo feedback.

The above-mentioned changes in the sea level pressure can also be seen in the surface wind and zonal wind stress changes, and are a result of modified meridional temperature
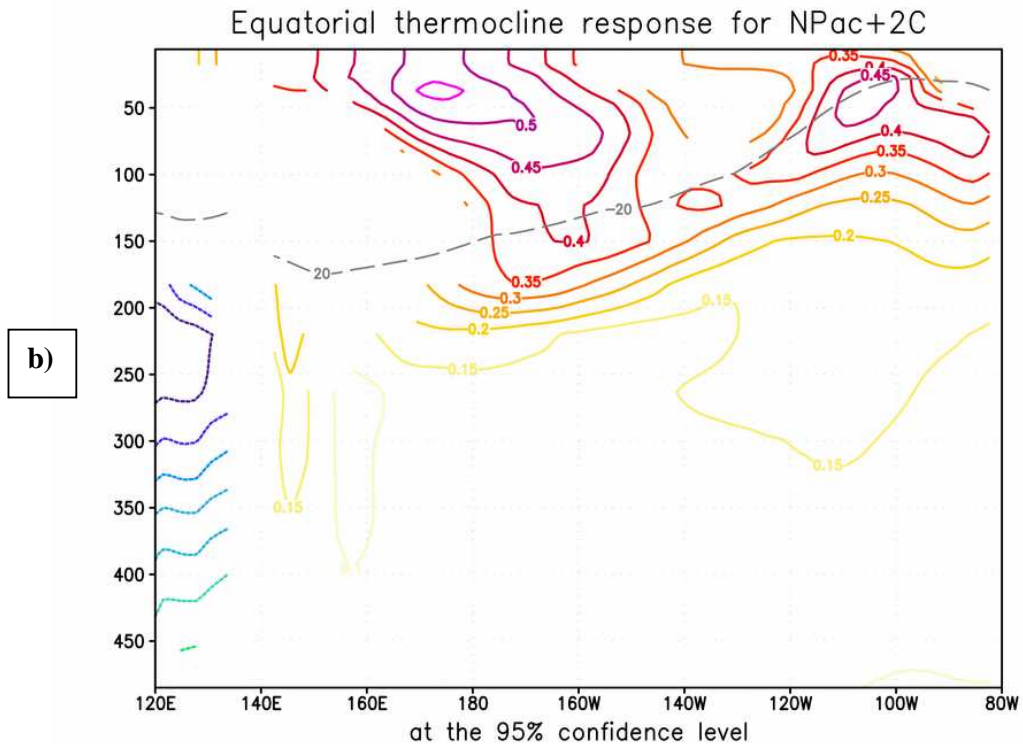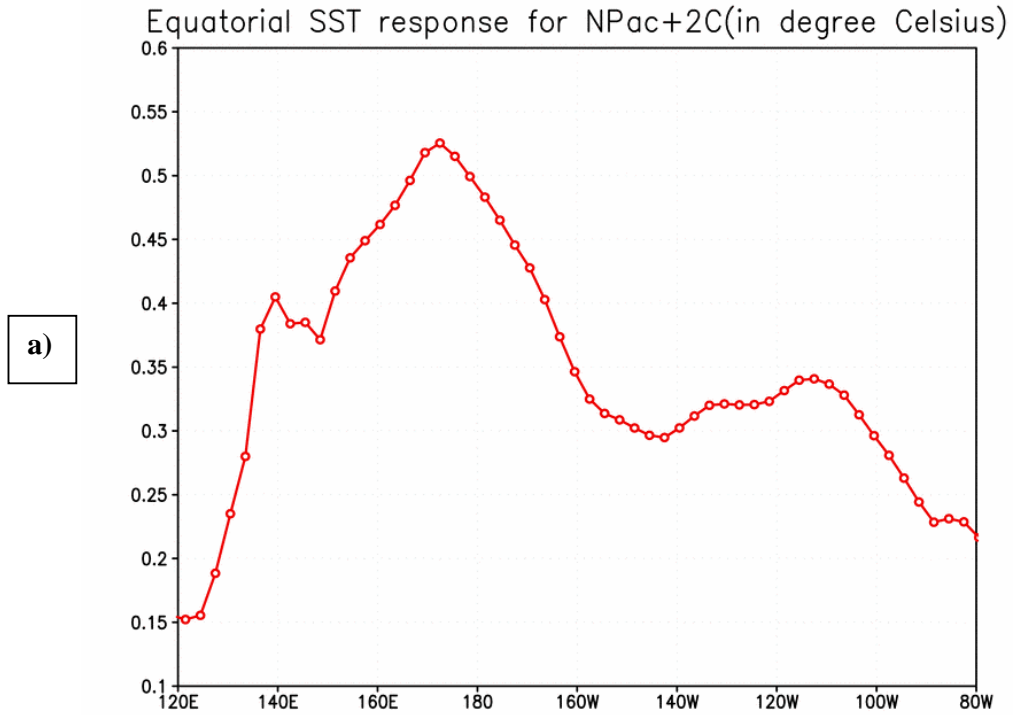
Figure 4.14 Mean climate changes in **(a)** SST (in °C) and **(b)** the thermocline temperature in NPac+2°C experiment, averaged in a 5°N - 5°S equatorial strip of Pacific Ocean. In **(b)**, the dashed gray line represents the mean depth of the 20°C isotherm in the control integration. The contour interval is 0.05 °C.
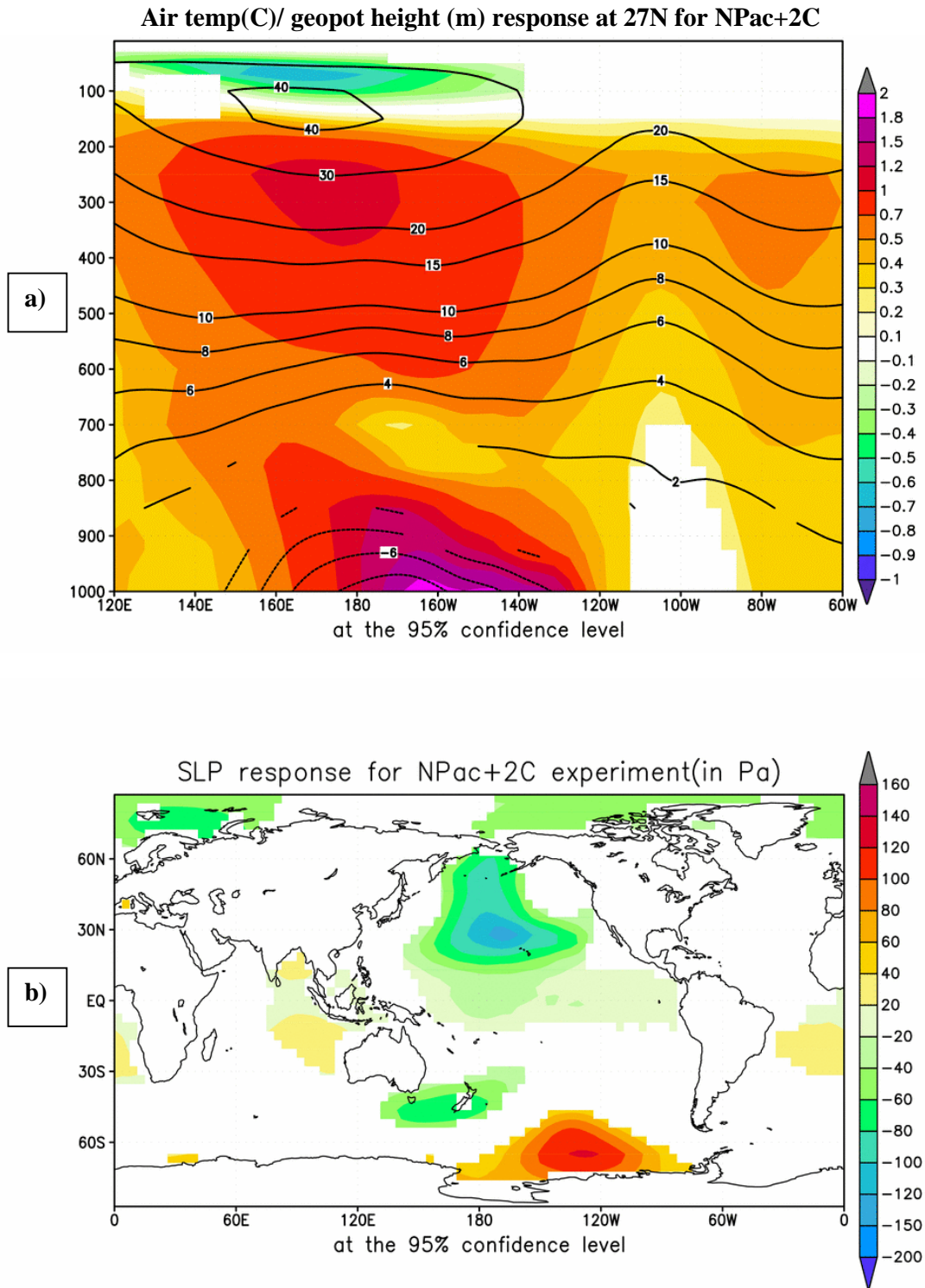
Figure 4.15 (a) Anomalous Pacific Ocean vertical air temperature (shaded, in °C) and geopotential height (black contours, in m) at 27°N latitude in the NPac+2°C experiment. The contour interval is 2m for values less than 10m, and then, the contour levels are 15m, 20m, 30m and 40m. **(b)** Anomalous sea level pressure (in Pa) response in the SPac+2°C experiment.
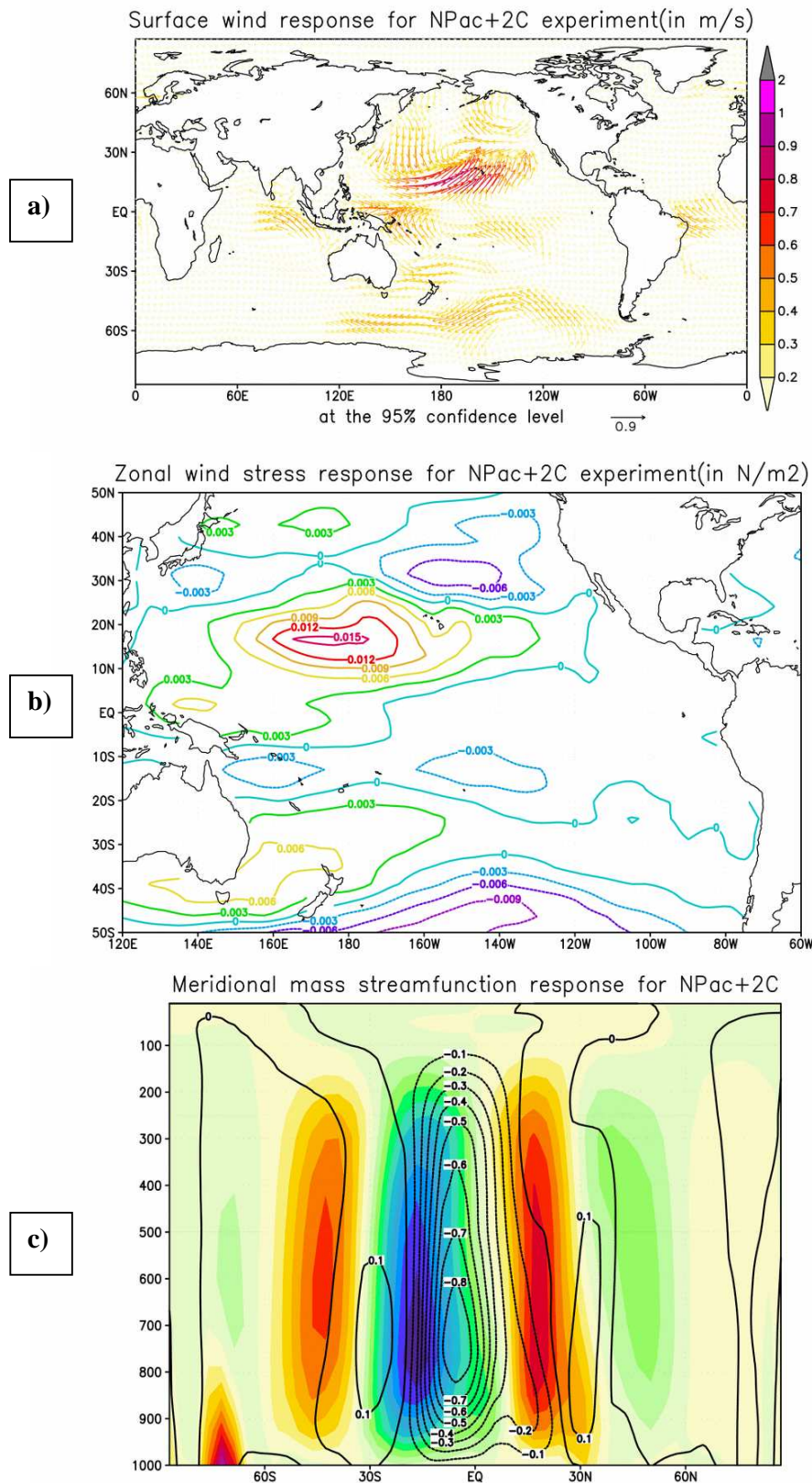
Figure 4.16 Anomalous Pacific Ocean **(a)** surface winds (in m/s) and **(b)** zonal wind stress (in N/m^2) in the NPac+2°C experiment. The reference vector of surface wind is 0.9 m/s. The contour interval in **(b)** is 0.003 N/m^2. Anomalous atmospheric meridional mass streamfunction in the NPac+2°C experiment (black contours) and the mean atmospheric meridional mass streamfunction of the control integration (shaded, in 10^{10}Kg/s) are plotted in **(c)**. Contour interval in **(c)** is 0.1x 10^{10}Kg/s.

gradient (Figure 4.16a and b). The southeasterly trades strengthen in the tropical South Pacific oceans due to an intensified meridional thermal contrast, while the northeasterly trades weaken as a consequence of a decreased meridional thermal contrast in the tropical North Pacific.   The anomalous low, which spans almost the whole North Pacific Ocean, is responsible for the warming found along the west coast of North America. The anomalous southerly warm air advection has raised the air surface temperature in the northeastern North Pacific by about 0.4°C -0.6°C. On the contrary, the anomalous northerly cold air advection prevents the surface warming in the northwestern North Pacific and leads to a slight cooling near Kamtchatka (Figure 4.13).

As a consequence of the changes in trade winds, the Hadley circulation is shifted northward (Figure 4.16c). The resulting anomalous descending motion between 10°S-20°S leads to a decrease in precipitation of about 15-20 mm/month in all three tropical oceans. The anomalous ascending motion, which enhances the convective activity, leads to an increase in precipitation between 5°N-5°S. The biggest precipitation changes are simulated in the South Pacific Convergence Zone (SPCZ) and the warm pool region of West Pacific (Figure 4.17b). Another area that exhibits an increase in the precipitation amount up to 25 mm/month is located in the central tropical North Pacific between 10°N-30°N. Changes in the net surface heat flux can also influence sea surface temperature. The net surface heat flux response exhibits a damping effect onto the sea surface temperature over the forcing area. In the central tropical Pacific between 10°N-20°N, however, the net surface heat flux contributes to the SST warming (Figure 4.17a).
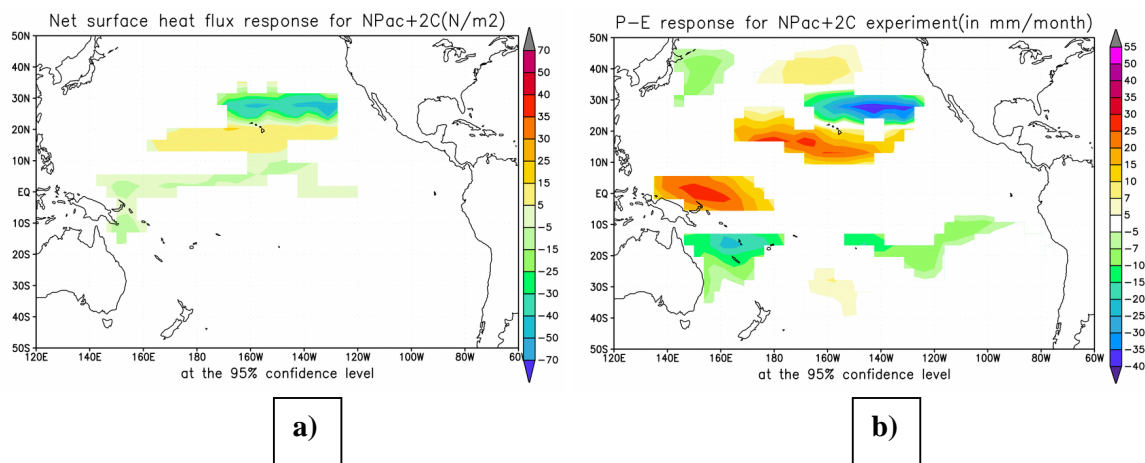
Figure 4.17 Anomalous Pacific **(a)** net surface heat flux (in N/m^2) and **(b)** fresh water flux (precipitation-evaporation, in mm/month) in the NPac+2°C experiment.
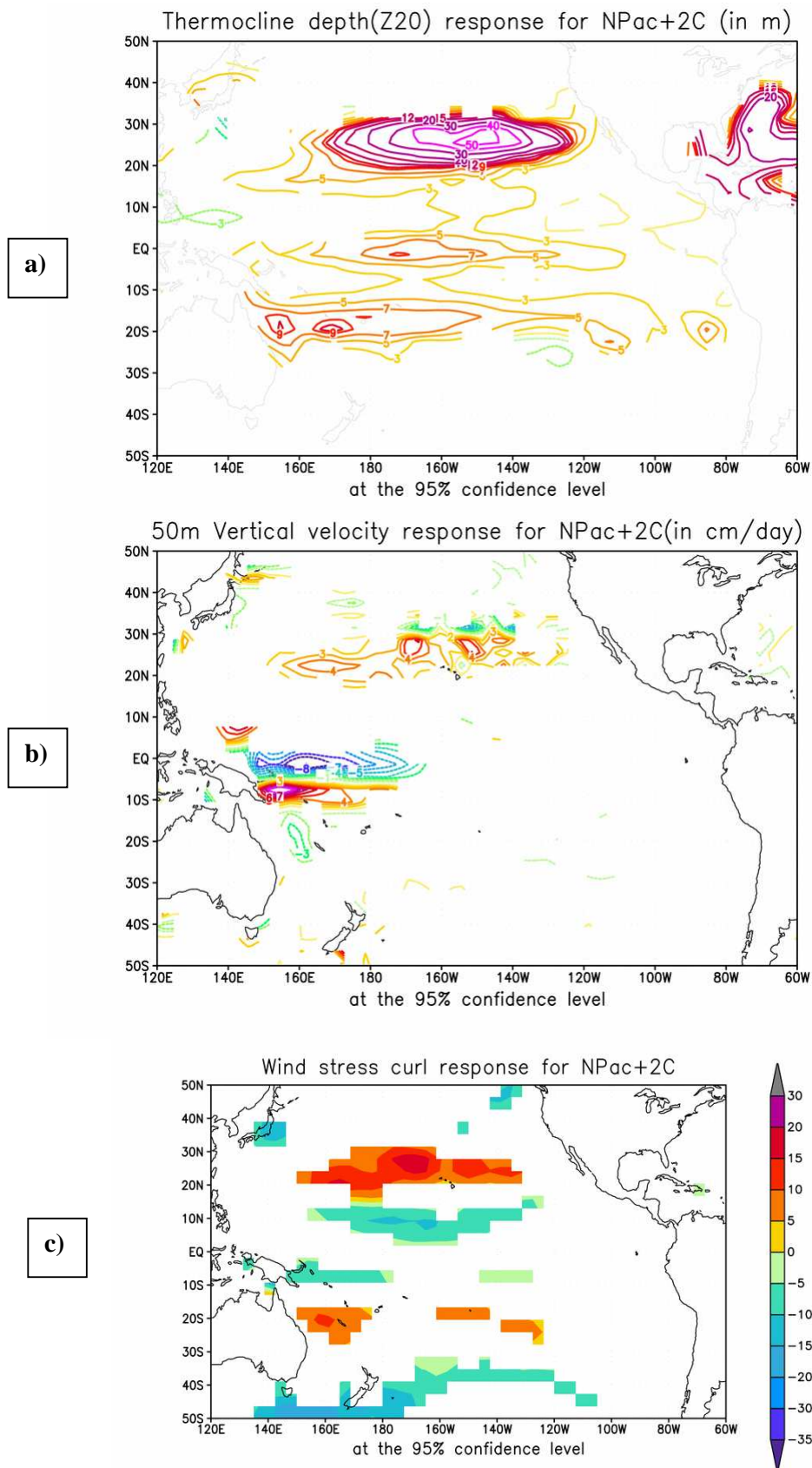
Figure 4.18 Anomalous Pacific Ocean **(a)** depth of thermocline (in m), **(b)** vertical velocity at model level 50m (contours, in cm/day) and **(c)** wind stress curl (in 10^{-9} N/m^3) in the NPac+2°C experiment. In **(a)** the contour levels are -3, -1, 1, 3, 5, 7, 9, 10, 12, 15, 20, 30, 40 and 50 m. The contour interval in **(b)** is 1 cm/day.

56

The simulated weakening of the trade winds affects the equatorial upwelling and the thermocline depth in both the North and South tropical Pacific (Figure 4.18a,b). Relative to the control run, the upwelling in NPac+2°C experiment exhibits a reduction of 9 cm/day in the western equatorial Pacific accompanied by an anomalous upwelling between 5°S-10°S in the western South Pacific (Figure 4.18b). In the central tropical North Pacific, an anomalous upwelling is simulated between 20°N-30°N. The warming in the subtropical North Pacific induces a deepening of the thermocline of up to 50 m over the central-eastern tropical North Pacific, accompanied by a 8m deepening of the thermocline in the central equatorial Pacific and around 20°S in the western tropical South Pacific (Figure 4.18a). The simulated changes in the depth of the thermocline and in the upwelling are accompanying changes in the strength of subtropical/tropical cells in both North and South Pacific (Figure 4.19). Apart from the weakening of the off-equatorial downwelling, the deepening of the thermocline in the central-eastern tropical North Pacific will decrease the zonal slope of the thermocline, reducing the equatorward flow within thermocline and therefore, spinning-down the northern branch of the subtropical and tropical cell in the Pacific Ocean by about 3 Sv. On the contrary, the deepening of the thermocline in the western tropical South Pacific increases the zonal slope of the thermocline, which itself might increase the equatorward flow within the thermocline and spin-up the southern STC.
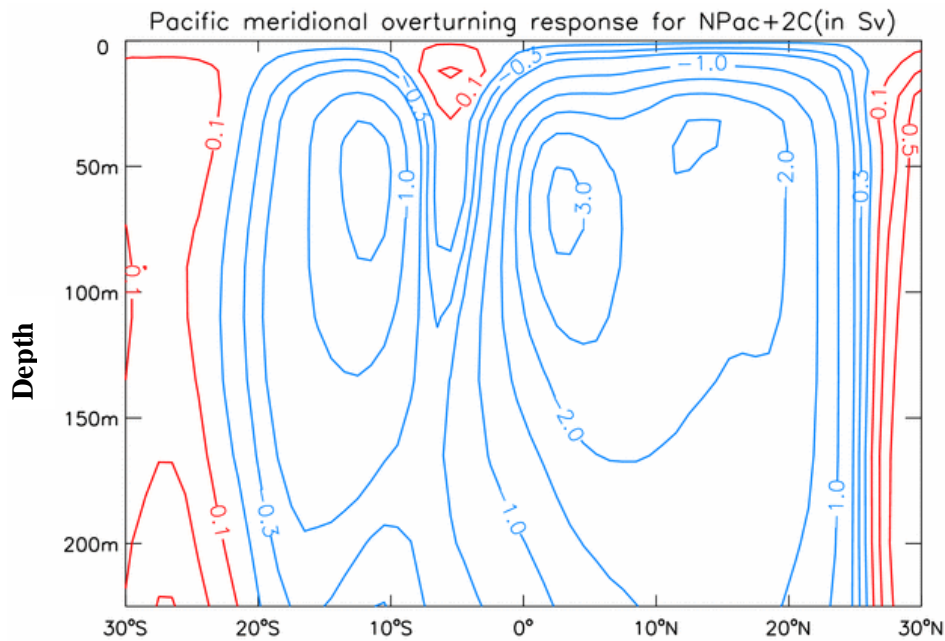
Figure 4.19 Anomalous Pacific Ocean meridional overturning streamfunction (in Sv) in the NPac+2°C experiment. Contour levels are –3.5, -3, -2.5, -2, -1.5, -1, -0.5, -0.3, -0.1, 0.1, 0.3 and 0.5 Sv.
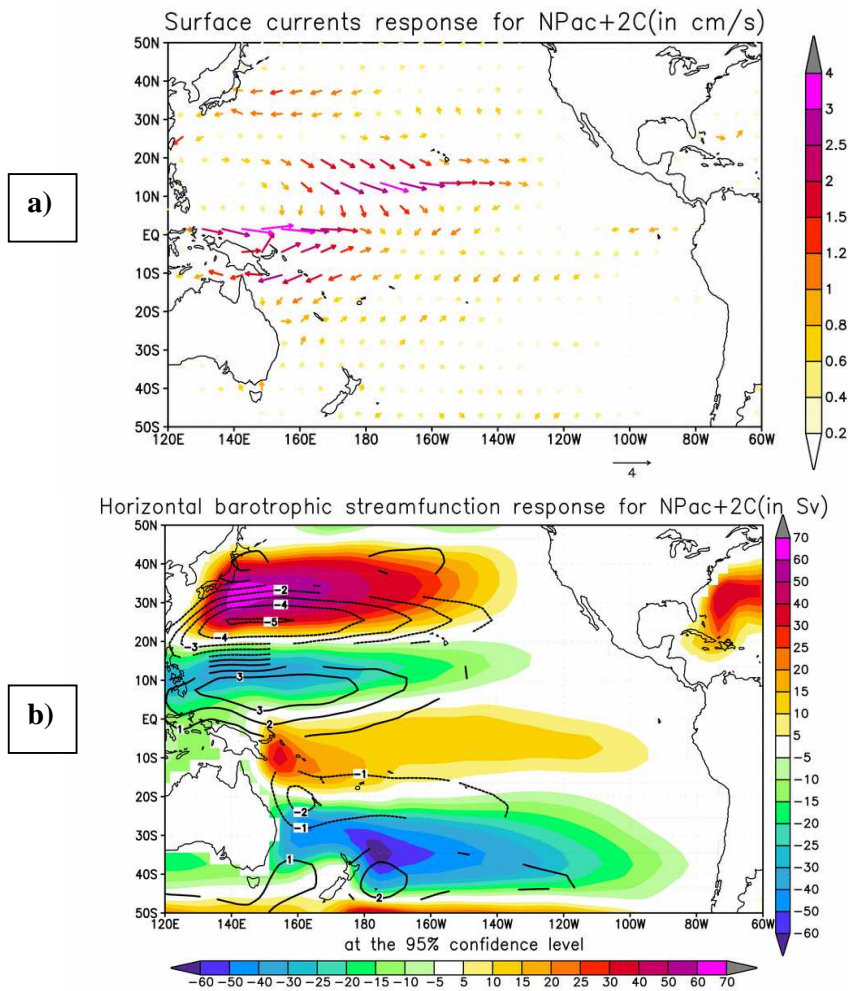
Figure 4.20 (a) Anomalous Pacific Ocean surface current velocity (in cm/s) in the NPac+2°C experiment. The reference vector of surface velocity is 4 cm/s. **(b)** Anomalous horizontal barotrophic streamfunction (black contours, in Sv) in the NPac+2°C experiment and the mean horizontal barotrophic streamfunction in the control integration (shaded, in Sv). The contour interval is 1 Sv.
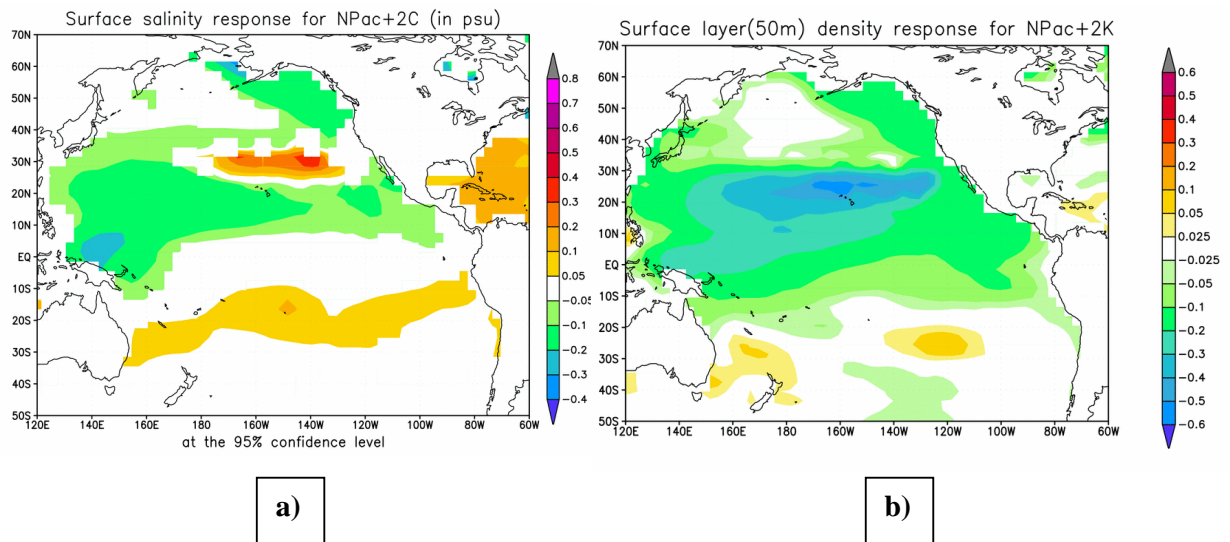
Figure 4.21 Anomalous Pacific **(a)** surface salinity (in psu) and **(b)** upper level density (in Kg/m^3) in the NPac+2°C experiment. The anomalous upper level density was computed as the anomalous ocean density averaged over the upper 50 m.

58

The horizontal oceanic circulation is also affected by the change in the trade winds (Figure 4.20a). The biggest changes in horizontal currents are found in the tropical Pacific Ocean, where the South and North Equatorial Currents weaken by about 4 cm/s. The meridional velocity anomalies simulated close to the equator, especially in the North Pacific, reflect a weaker Ekman divergence. The anomalous mean barotropic streamfunction changes (Figure 4.20b) show a weakening of about 5 Sv and a slightly southward shift of the North Pacific subtropical gyre circulation.

There is a sea surface salinity response to the simulated changes in freshwater flux (Figure 4.21a). The intensified precipitation over most of the tropical and western North Pacific causes a reduction in sea surface salinity of about 0.1-0.2 psu, with the maximum SSS reduction in the warm pool area of western Pacific. In contrast, over the forcing area, the surface salinity is increased by 0.2 psu due to intensified evaporation. The increase in precipitation over central-western tropical North Pacific, combined with a warming of the upper ocean leads to a decrease in the upper layer density over the whole tropical North Pacific (Figure 4.21b).

4.5 Comparison of the impact of South and North subtropical warming/cooling on the tropics

After describing the affect of subtropical positive SST perturbation on the mean climate state, we will now try to quantify the relative contribution of North and South subtropical Pacific to the tropical climate. We will also discuss the impact of subtropical warming versus subtropical cooling. Figure 4.22 displays the tropical Pacific response in sea surface temperature in the following experiments: NPac+2°C, NPac-2°C, SPac+2°C and SPac-2°C. The simulated changes in the Pacific equatorial thermocline for the same experiments are shown in Figure 4.23. The equatorial Pacific SST change, computed as the sea surface temperature response averaged between 5°S-5°N and 120°E-80°W, is +0.58°C in the SPac+2°C experiment comparing to +0.35°C in the NPac+2°C or about 65% larger for the South Pacific experiment. A similar difference is simulated for the cooling experiments: a 2°C cooling in the subtropical South Pacific causes a 0.62°C cooling of the equatorial Pacific SST compared to only 0.35°C in the subtropical North Pacific experiment. Furthermore, the thermal forcing of subtropical South Pacific has a maximum impact on eastern tropical Pacific climate, while the impact of subtropical North Pacific is mostly confined to the western

tropical Pacific (Figure 4.23a compared to Figure 4.23c). The subtropical North and South Pacific oceans also have a different impact on the equatorial thermocline structure (Figure 4.23).
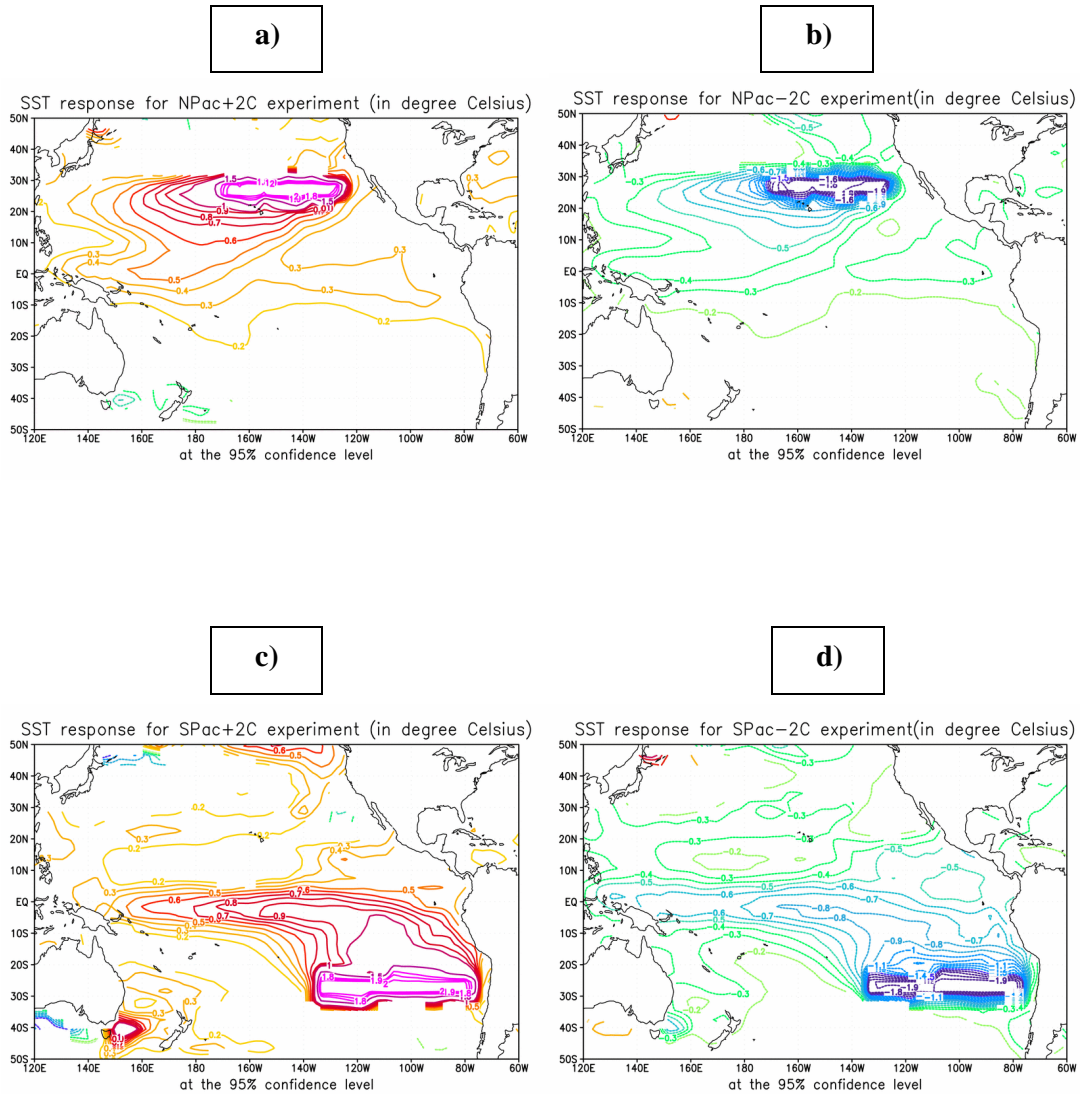
Figure 4.22 Anomalous Pacific Ocean SST (in °C) response in the **(a)** NPac+2°C, **(b)** NPac-2°C, **(c)** SPac+2°C and **(d)** SPac-2°C experiments. In **(a)** and **(c)**, the contour interval is 0.1°C. In **(b)** and **(d)**, the contour interval is -0.1°C. Please note that values in the range (-0.2°C, +0.2°C) are not plotted.
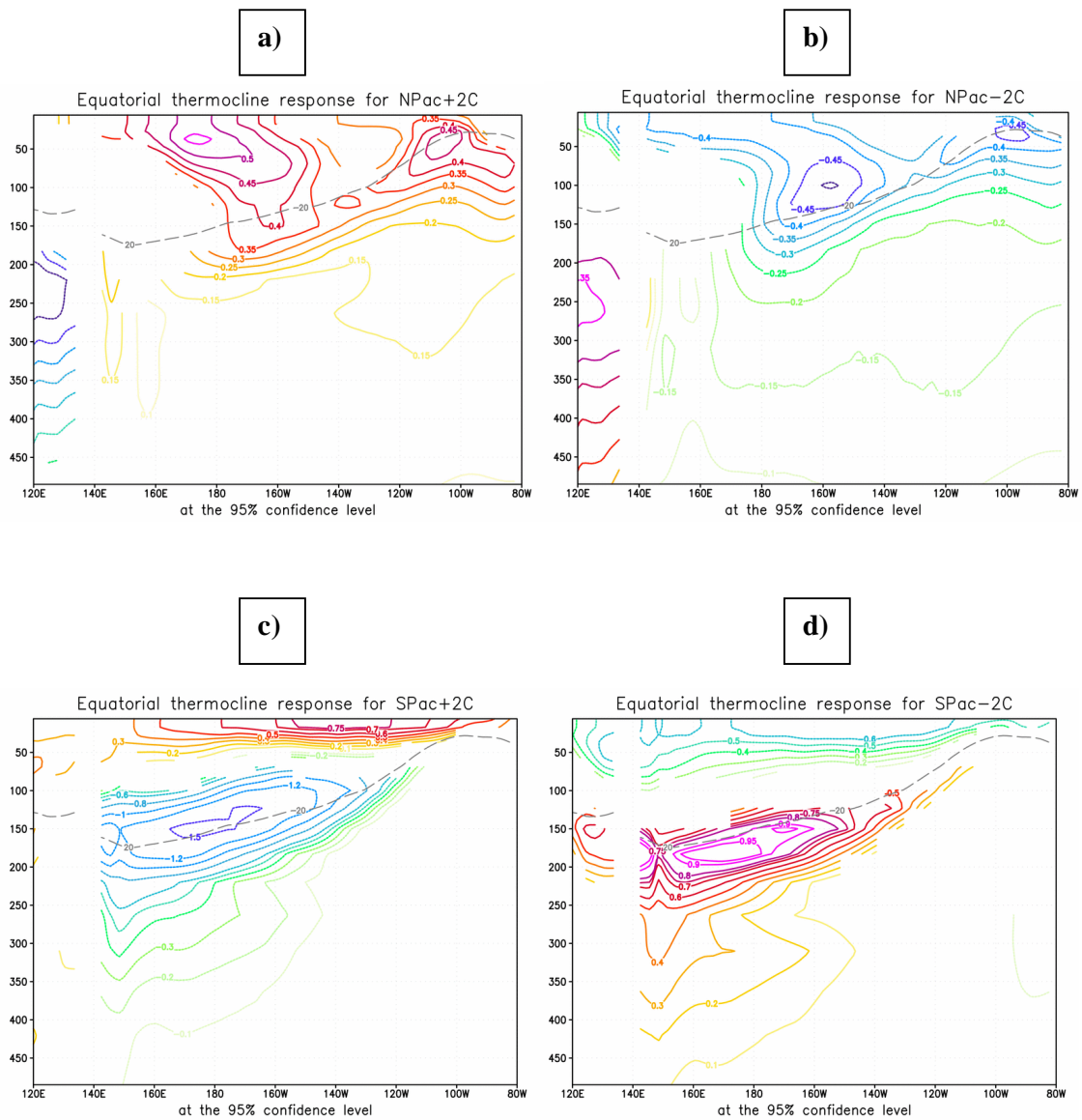
Figure 4.23 Mean climate changes in the thermocline temperature in **(a)** NPac+2°C, **(b)** NPac-2°C, **(c)** SPac+2°C and **(d)** SPac-2°C experiments, averaged in a 5°N - 5°S equatorial strip of Pacific Ocean. The contour interval in **(a)** and **(b)** is 0.05°C, while the contour interval in **(d)** is 0.1°C. The contour levels in **(c)** are –1.5°C, -1.2°C, -1.0°C, -0.8°C, and -0.6°C, followed by a 0.1°C contour interval. The dashed gray line represents the mean depth of the 20°C isotherm in the control integration.

We will now focus on explaining the different impact of North and South Pacific, limiting the discussion to the warming experiments (NPac+2°C and SPac+2°C). Figure 4.24 displays the mean sea surface temperature response computed for the first 10yr, 30yr and for the whole 200yr of the experiment, while Figure 4.25 shows the simulated mean response in equatorial subsurface temperature.
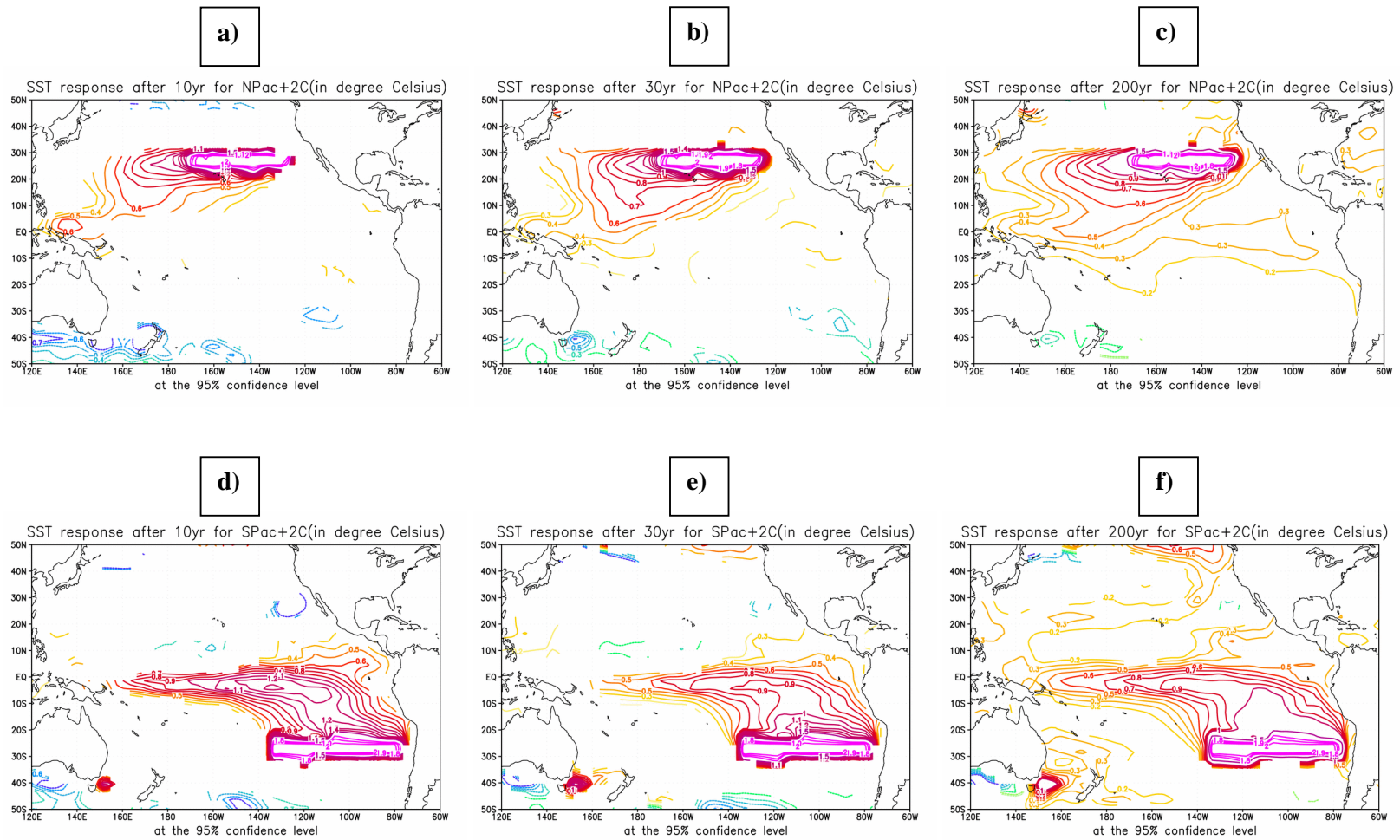
Figure 4.24 Anomalous Pacific Ocean SST (in °C) after the first 10 years **(a)**, 30 years **(b)** and after 200 years **(c)** in the NPac+2°C experiment. Anomalous Pacific Ocean SST (in °C) after the first 10 years **(d)**, 30 years **(e)** and after 200 years **(f)** in the SPac+2°C experiment. The contour interval is 0.1°C. Please note that values in the range (-0.2°C, +0.2°C) are not plotted.
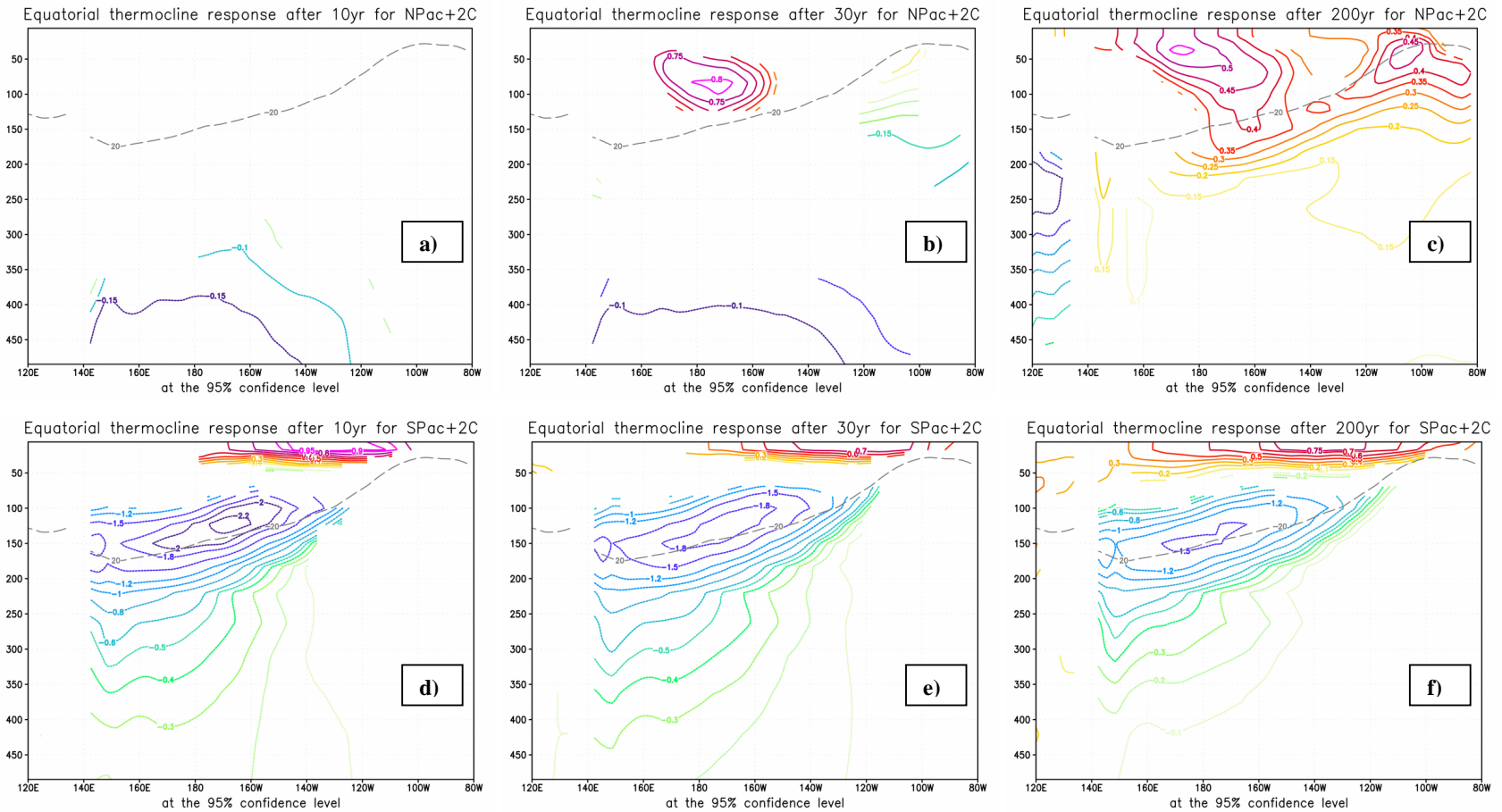
Figure 4.25 Mean climate changes in the thermocline temperature after the first 10 years **(a)**, 30 years **(b)** and after 200 years **(c)** in the NPac+2°C experiment. Mean climate changes in the thermocline temperature after the first 10 years **(d)**, 30 years **(e)** and after 200 years **(f)** in the SPac+2°C experiment. The contour interval in **(a)**, **(b)** and **(c)** is 0.05°C. The contour levels in **(d)**, **(e)**, **(f)** are -2°C, -2.2°C, –1.8°C, –1.5°C, -1.2°C, -1.0°C, -0.8°C, and -0.6°C, followed by a 0.1°C contour interval. The dashed gray line represents the mean depth of the 20°C isotherm in the control integration.

63

After only 10 years of simulation, the equatorial response in the SPac+2°C experiment is almost fully developed (see Figure 4.24d in comparison to Figure 4.24e,f). This rapid increase in the equatorial SST suggests a dominant role of the "atmospheric bridge" in the remote impact of subtropical South Pacific. Anomalous northwesterly trades that reduce the evaporative heat loss in the eastern tropical South Pacific, accompany the enhanced warming in the subtropical South Pacific. In this way the subtropical South Pacific warming extends farther into the eastern tropics. The pattern is indicative of the coupled wind-evaporative-SST (WES) feedback between the atmosphere boundary layer and ocean (Xie and Philander, 1994). After reaching the equator, the SST anomalies are further intensified by the local coupled ocean-atmosphere feedback. The WES feedback not only leads to a very fast change of equatorial SST, but also forces a delayed adjustment of the meridional overturning circulation in the upper Pacific (Figure 4.27a). Therefore, the tropical SST change will be further amplified due to a reduced equatorward cold water transport and equatorial upwelling (Figure 4.7a). The slow ocean connection between subtropical South Pacific and tropics can also be accomplished by the equatorward subduction of anomalous warm water by the mean circulation (Gu and Philander, 1997) through the interior oceanic pathways that are opened due to the absence of a potential vorcity barrier in the South Pacific. In Figure 4.26 we plotted the time evolution of equatorial Pacific heat content anomaly in the SPac+2°C experiment, taken here as an index of the vertically averaged ocean temperature over the upper 450m. The positive trend (0.35°C/200yr) of equatorial Pacific heat content suggests that ocean tunnel plays also a role in the South Pacific subtropical-tropical connections at multi-decadal timescale. In the first years of the simulation, the dynamical adjustment of the equatorial thermocline to the zonal wind stress changes associated with the fast "atmospheric bridge" leads to a warming in the surface accompanied by a cooling at depth (Figure 4.25d), followed by a slow warming from below by the "ocean tunnel" as the experiment continues.

The equatorial climate change in response to a warming in subtropical North Pacific is confined to the westernmost part of the warm pool region during the first 10yr of the experiment (Figure 4.24a), accompanied by no significant mean changes in the subsurface temperature (Figure 4.25a). The very fast increase in SST over the west Tropical Pacific can also be attributed to the WES coupled feedback. The cyclonic response in sea level pressure in the North Tropical Pacific is associated with anomalous southwestern trades that will warm the SST through a reduction in evaporation. The propagation of warmed SST towards the warm pool region is accompanied by westerly wind anomalies that will further reduce the evaporative heat loss and warm the sea surface (Figure 4.16b). Our results are in accordance

with a recent study done by Wu et al. (2006). Using both observations and a coupled ocean-atmosphere model, they have proposed the WES feedback as a possible mechanism for the extratropical-tropical connections in the North Pacific and suggested that the recent tropical Pacific decadal climate variability originates from the extratropical North Pacific.
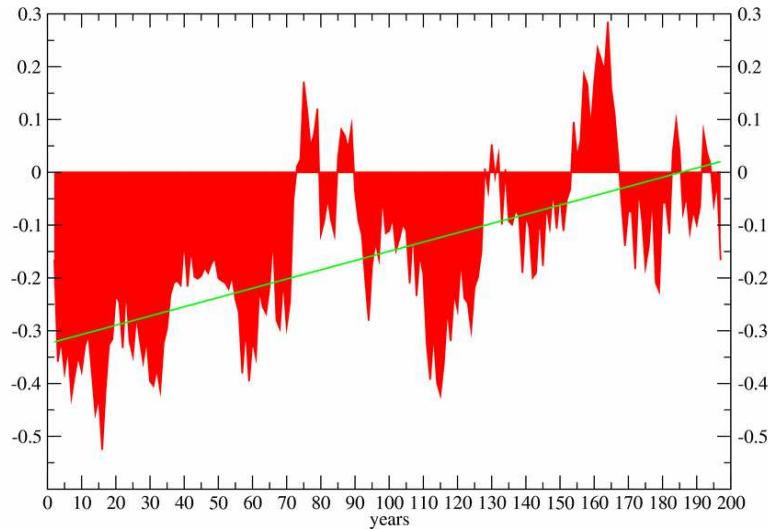

Figure 4.26 Time evolution of the equatorial Pacific annual heat content anomaly (in °C) averaged over 5°N-5°S, 140°E-80°W in the SPac+2°C experiment. The vertically averaged ocean temperature over the upper 450 m is used as a proxy of the ocean heat content. To highlight the low frequency variability, a 5-yr running mean is applied to the index.
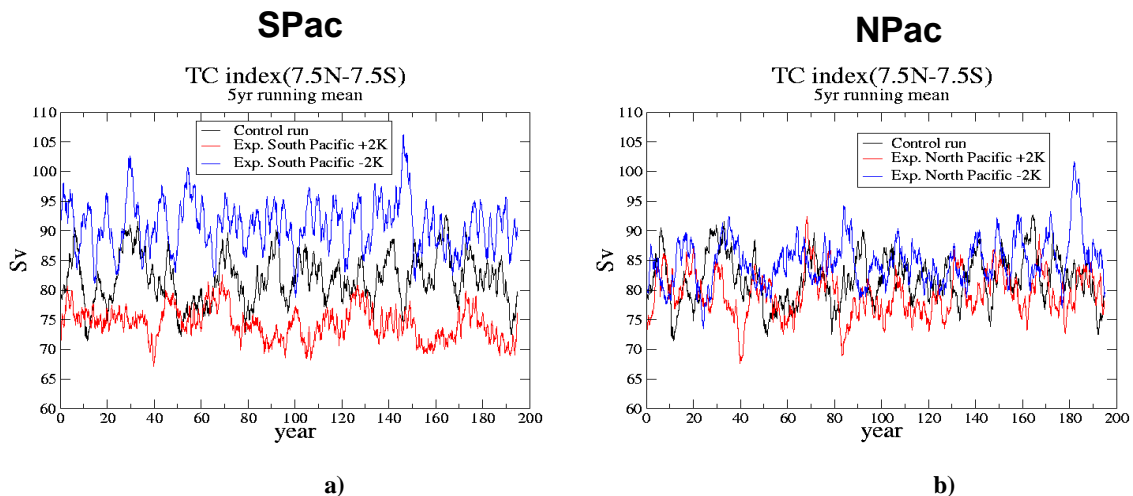
Figure 4.27 Time evolution of the anomalous Tropical Cell (TC) strength (in Sv) in the **(a)** South Pacific and **(b)** North Pacific experiment. For the definition of the cell strength see Chapter 2.3. The TC strength of the control integration is represented by the black curve in both panels. Red color is used for the warming experiments and blue color for the cooling experiments. To highlight the multi-decadal variability, a 5-yr running mean is applied to each index.

While the same fast "atmospheric bridge" seems to act in both North and South Pacific experiments, the amplitude and the spatial extension of the response is very different. Even after 30yr of simulation, the SST warming in the NPac+2°C experiment is limited to the western Tropical Pacific between 120°E-180°E, reaching a maximum of only 0.5°C (Figure 4.24b,c). At the same time, a 0.8°C warming appears in the upper equatorial ocean between 50m-150m and tends to propagate eastward along the thermocline (Figure 4.25b,c). This SST warming from below suggests a more important role for the "ocean tunnel" compared to the "atmospheric bridge" in the NPac+2°C experiment. Since changes in shallow meridional overturning circulation are not large in the NPac+2°C experiment (Figure 4.27b compared to Figure 4.27a), due to the quite small changes in the equatorial zonal wind stress (Figure 4.16b), the dominant mechanism in OT remains the isopycnal transport of anomalous temperature signal from the North Pacific through the western boundary pathway. A possible explanation for the weak impact of the subtropical North Pacific warming is the so-called "thermodynamic thermostat" that might control the warm pool region. Due to this thermodynamical feedback, the SST will warm for as much as necessary for the upward surface heat flux to balance the imposed downward flux (Seager and Murtugudde, 1997).

Since there is no significant atmospheric response (not shown) to the salinity perturbations in the subtropical Pacific Ocean, we can see the SSSA experiments as a study of the "oceanic tunnel". In both North and South Pacific SSSA experiments, the slow oceanic connection between subtropical and tropical Pacific is accomplished only through the equatorward subduction of anomalous saline water by the mean circulation. In the South Pacific experiment, the subducted salinity anomalies can reach equatorial Pacific via the interior pathway, while in the North Pacific experiment; the water carrying the salinity signals has to travel first all the way to the western boundary and then, equatorward.

A first order linear response is simulated for full ($\pm$2K) and half-forcing ($\pm$1K) sea surface temperature sensitivity experiments in both North and South Pacific. Although the Tropical Pacific climate response to an enhanced surface warming/cooling in the subtropics is to first order linear, the negative thermal forcing appears to have a stronger impact on equatorial Pacific thermocline. A 2°C cooling in subtropical South Pacific results in a decrease in equatorial ocean temperature that penetrates till about 100m depth (Figure 4.23d), in comparison with only 50m depth for the warming experiment (Figure 4.23c). Besides the vertical displacement of the thermocline, a bigger change in the vertical mixing (not shown) may explain the larger subsurface temperature anomaly in the SPac-2°C experiment
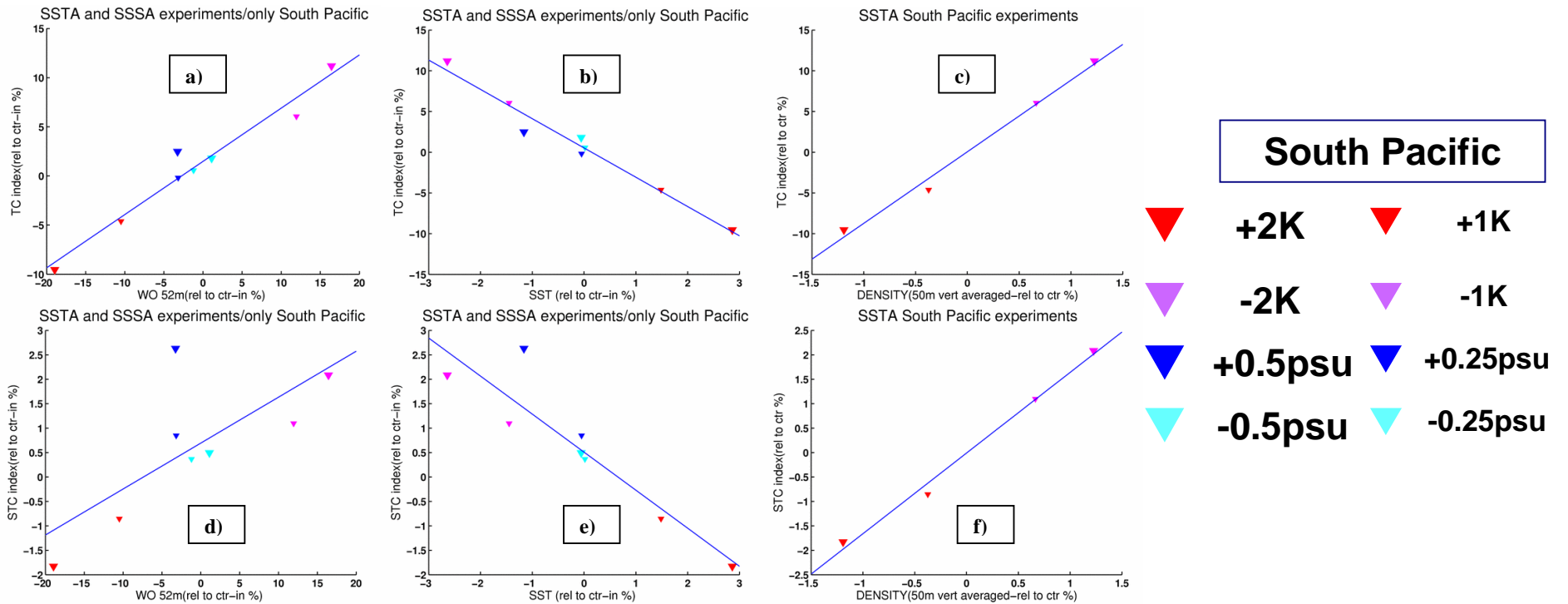
Figure 4.28 Dependence between the anomalous TC strength **(a)** /STC strength **(d)** and the anomalous ocean vertical velocity in the Niño3 region of the eastern equatorial Pacific in the South Pacific SSTA and SSSA experiments. Dependence between the anomalous TC strength **(b)** /STC strength **(e)** and the anomalous sea surface temperature in the Niño3 region of the eastern equatorial Pacific in the South Pacific SSTA and SSSA experiments. Dependence between the anomalous TC strength **(c)** /STC strength **(f)** and the anomalous upper ocean density change over the forcing area in the South Pacific SSTA experiments. All the anomalous changes are expressed in percentage of the mean values in the control integration.

67

compared to the SPac+2°C experiment. Similarly, a greater impact of the subtropical cooling on equatorial thermocline is found in the North Pacific experiments (not shown).

The South Pacific contribution to the modulation of tropical climate is also revealed in Figure 4.28, which presents the relationship between the simulated changes in TC/STC index and changes in sea surface temperature and equatorial upwelling in eastern Pacific for all South Pacific experiments (SSTA and SSSA forcing). For the scatter plots in Figure 4.28, we used the simulated relative changes defined as the variable change divided by the mean of the control run for the respective variable. A strong linear dependence is found between the TC index and the strength of eastern equatorial upwelling (Figure 4.28a), while an inverse linear dependence is obtained between the TC index and eastern equatorial SST (Figure 4.28b) in our South Pacific simulations. A similar dependence, although not as strong as for the tropical cells, is suggested by the Figure 4.28d,e for the subtropical cells. As Figure 4.28c,f shows a linear dependence exists between TC/STC index and upper ocean density change over the forcing area for the South Pacific SST experiments. We could not see a relationship between the strength of TC/STC and eastern equatorial Pacific SST/upwelling in our North Pacific simulation. This behavior might be also due to much smaller changes in the shallow meridional overturning circulation in our North Pacific simulations (Figure 4.27a comparing to Figure 4.27b).

Comparing the warming and the cooling experiments in both North and South Pacific, we can conclude that the subtropical South Pacific appears to "affect" more to the equatorial ocean temperature change than the subtropical North Pacific. The larger contribution of the South Pacific is consistent with observational (Johnson and McPhaden, 1999) and modeling studies using an OGCM (Yang et al, 2004) or fully coupled GCM (Yang et al, 2005; Yang and Liu, 2005). The partial coupling idealized experiments employed by Yang et al. 2005 show that the impact of South Pacific extratropical thermal forcing (poleward of 30°S) on the tropical climate is 30%-50% larger than the impact of North Pacific extratropics. It is worth mentioning that Yang et al. 2005 investigated only the affect of extratropical Northern and Southern Hemisphere warming on tropical Pacific climate. In our sensitivity experiments, we found an asymmetric impact of the North and South Pacific Ocean on the tropical climate not only in the case of enhanced subtropical warming, but also for an enhanced subtropical cooling.

4.6 Relative role of the atmosphere and ocean in tropical-subtropical interactions

To further quantify the role of air-sea interactions and ocean dynamics in the simulated tropical climate response to the subtropical surface warming/cooling, we performed sensitivity experiments, similar to the coupled ones, with the AGCM ECHAM5. The sea surface temperature and sea ice monthly climatology of the coupled control run were used to force the AGCM. The AGCM was run under these conditions for 36 years and the last 30 years of the integration will constitute our AGCM control run (ACTR). After allowing a 6 years spin up period, we have imposed a +2°C degree sea surface temperature anomaly over the North Pacific (refer to as ANPac+2°C), respectively South Pacific domain (refer to as ASPac+2°C), and run the model for 30 years. All the mean climate changes are derived as the difference between the mean of each AGCM experiment and the mean of control run ACTR over the whole period of the sensitivity run. Only the statistically significant changes at 95% level according to a two-sided Student's t-test are discussed here.

Figure 4.29a displays the annual mean geopotential height change at 1000 hPa for the ASPac+2°C experiment. In contrast to the coupled experiment, the atmospheric response of the AGCM experiment to the warming in the subtropical South Pacific is mostly confined to the Southern Hemisphere and has no response in the equatorial Pacific. Correspondingly, the change in the surface wind displays a cyclonic anomalous circulation that is limited to the eastern subtropical South Pacific (Figure 4.30). The local geopotential height response (Figure 4.29b) to the imposed boundary forcing features a surface low (15m at 1000hPa or 2hPa in sea level pressure) beneath the upper level high (a 15m geopotential height change at 250hPa). Although the local geopotential height response is linear baroclinic in both the coupled and uncoupled experiments, the changes are bigger in the former. Besides a large local increase in evaporation rate (30mm/month) over the forcing area, accompanied by a similar magnitude reduction in evaporation to the north of it, the subtropical heating also produces changes in precipitation. An increase in precipitation of up to 70 mm/month is found on the western margins of the heating zone, while a decrease in precipitation of up to 40 mm/month is simulated to the north and west of the forcing area as a result of reduced evaporation rate due to anomalous westerlies winds. The SST anomalies in the subtropical South Pacific produce changes that reach the middle and upper troposphere (not shown).
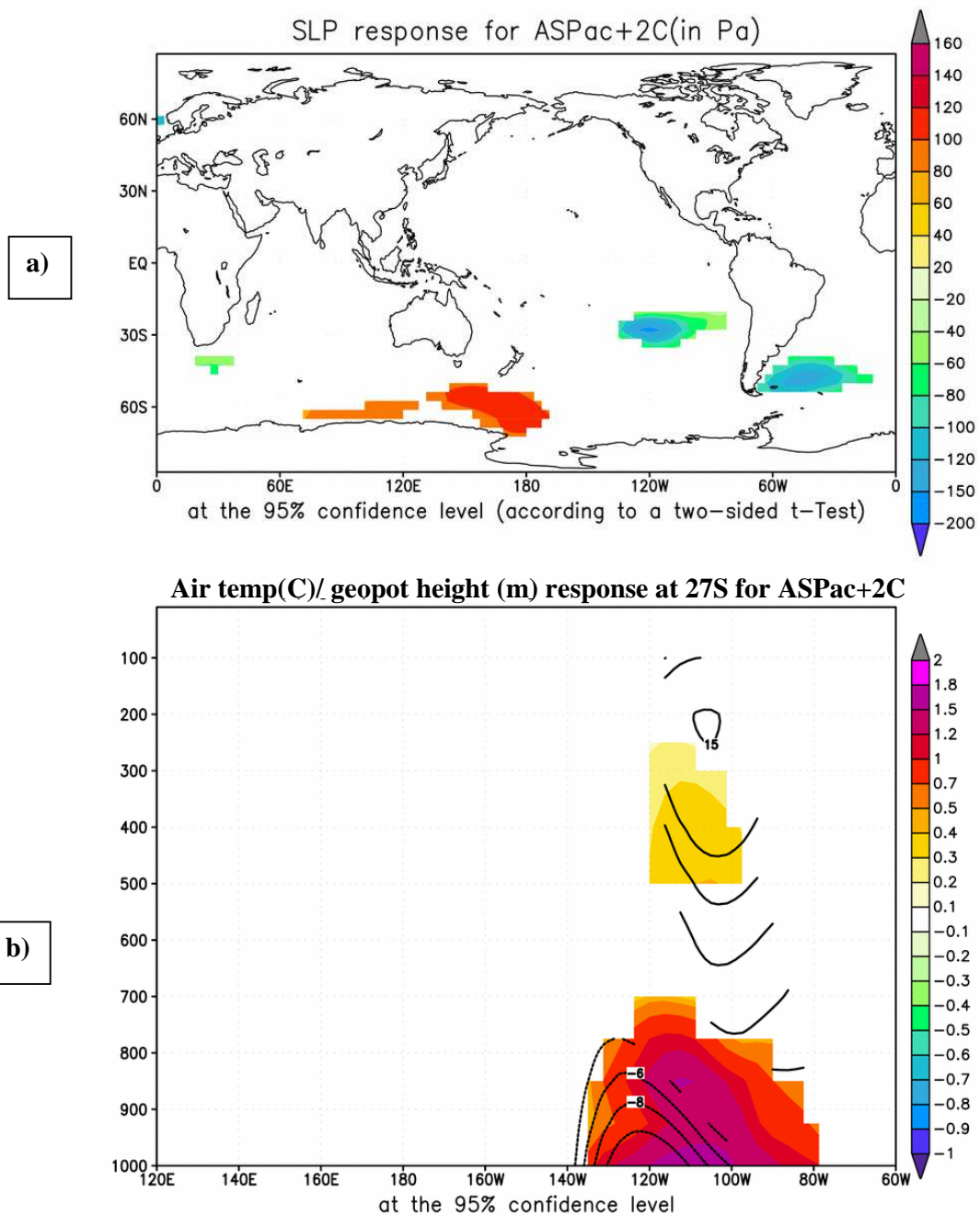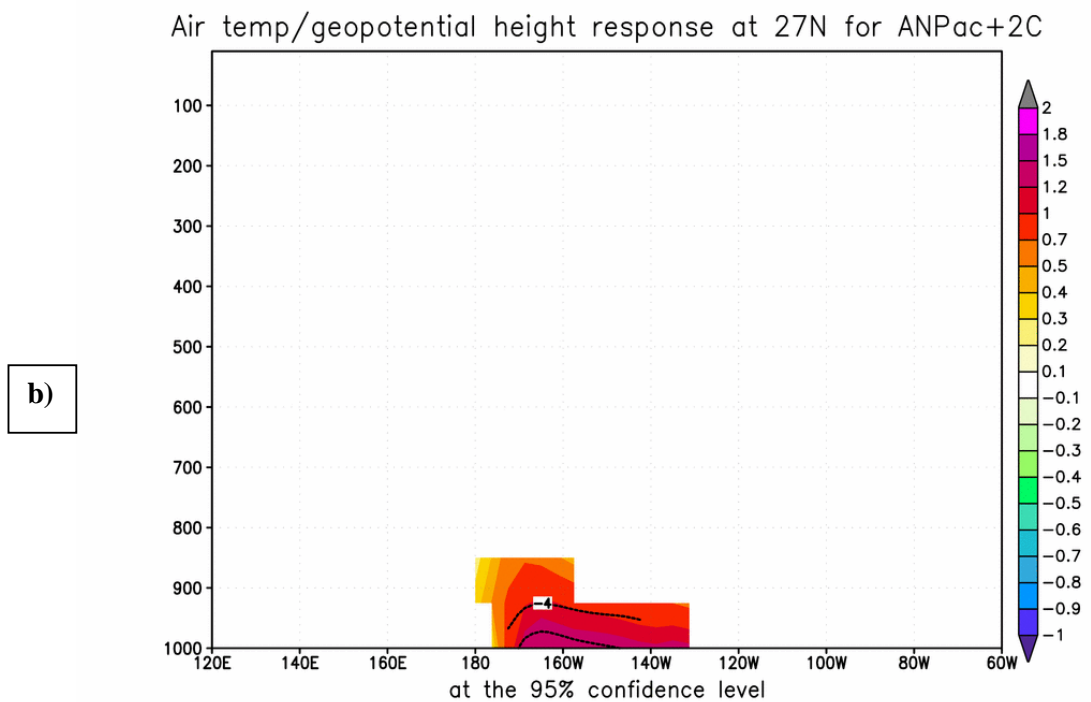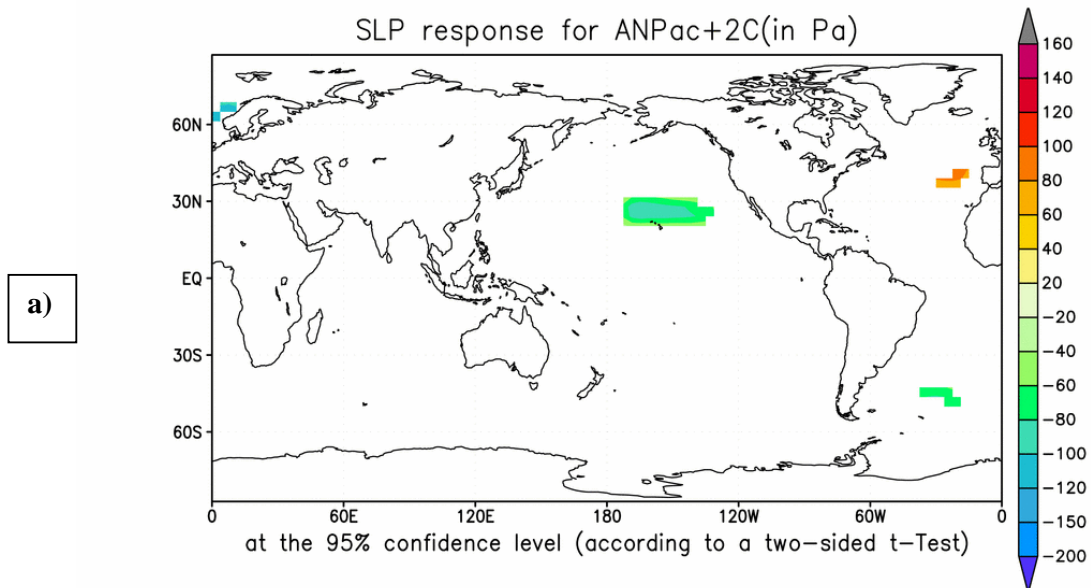
Figure 4.29 (a) Anomalous sea level pressure (in Pa) response in the ASPac+2°C experiment. **(b)** Anomalous Pacific Ocean vertical air temperature (shaded, in °C) and geopotential height (black contours, in m) at 27°S latitude in the ASPac+2°C experiment. The contour interval is 2m.
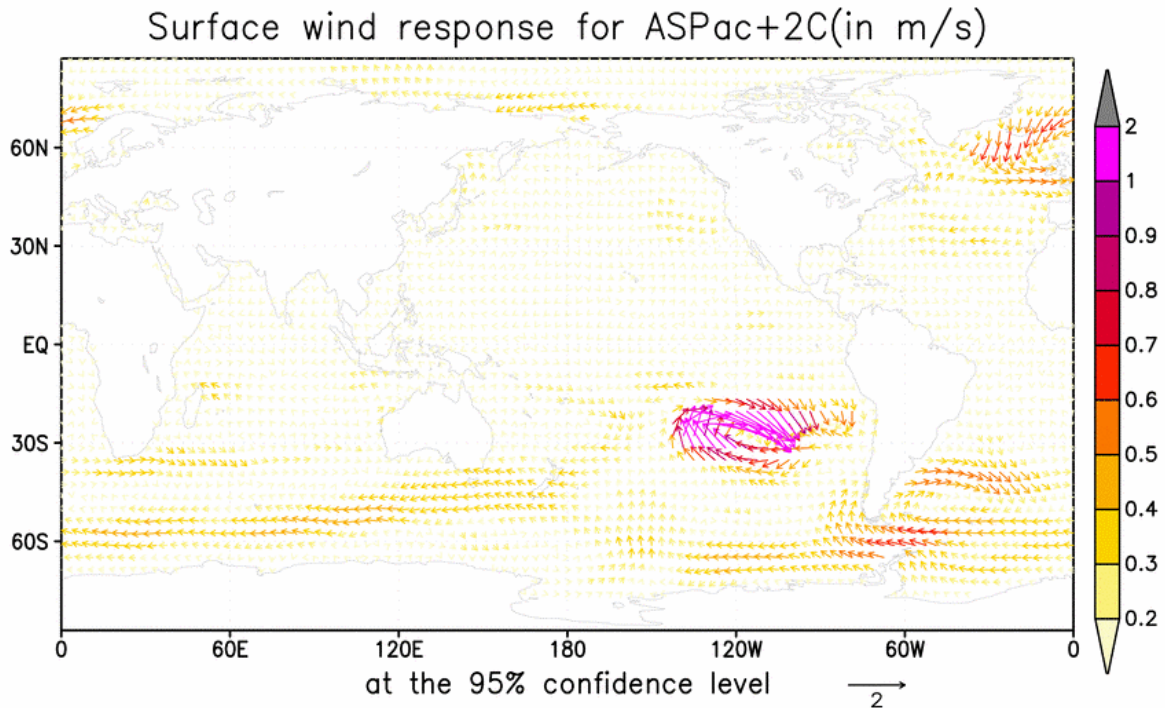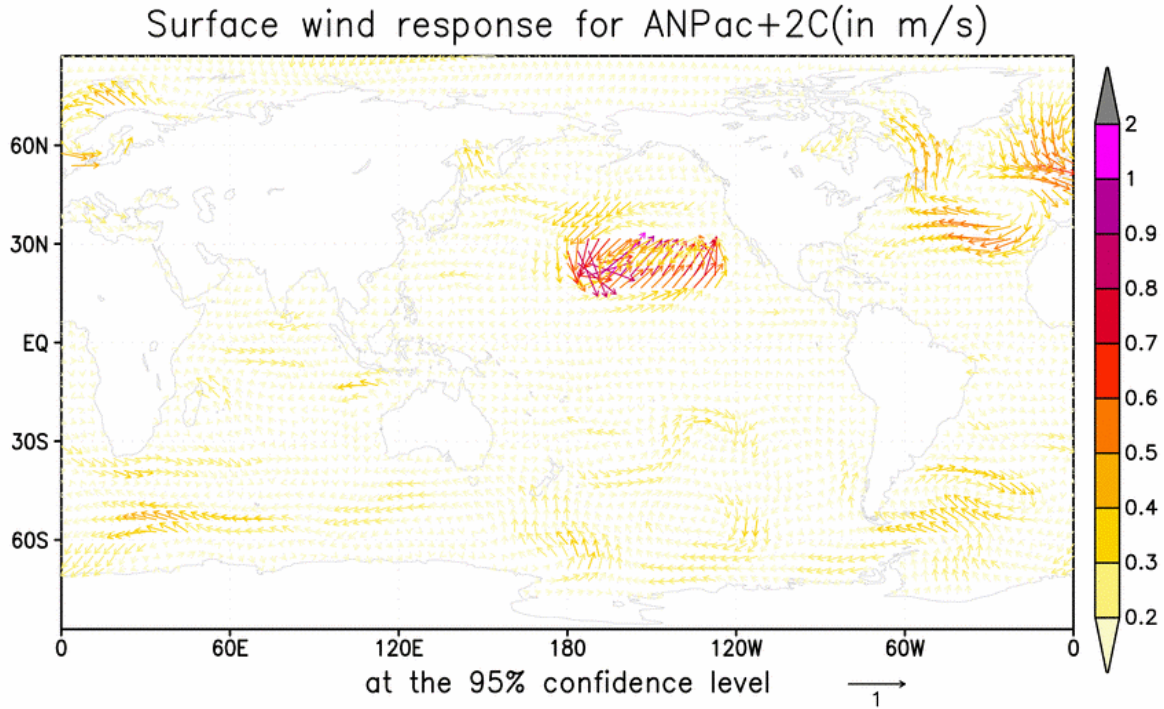
Figure 4.30 Anomalous Pacific Ocean surface winds (in m/s) in the ASPac+2°C experiment. The reference vector of surface wind is 2 m/s.

Comparing with the South Pacific experiment, the atmospheric response to the subtropical warming in the North Pacific is much weaker. The geopotential height changes (Figure 4.31a) are confined to the Northern Hemisphere, where they exhibit a local surface anomalous low (7m at 1000hPa or 1hPa in sea level pressure) without any signal in the upper troposphere (Figure 4.31b). Similar to ASPac+2°C experiment, significant changes in the surface wind are restricted to the forcing region, but are about half magnitude (Figure 4.32). As a result of the SST damping, the evaporation rate has increased over the forcing area by 40 mm/month. Additional features of the local response include a reduction in evaporation of up to 25 mm/month to the south and west of the heating zone and a modest increase in precipitation in the western margins. The difference in the atmospheric response to the North Pacific subtropical warming can be also seen in the vertical response, with air temperature changes limited to the lower troposphere (not shown).

71

Figure 4.31 (a) Anomalous sea level pressure (in Pa) response in the ANPac+2°C experiment. **(b)** Anomalous Pacific Ocean vertical air temperature (shaded, in °C) and geopotential height (black contours, in m) at 27°N latitude in the ANPac+2°C experiment. The contour interval is 2m.

Figure 4.32 Anomalous Pacific Ocean surface winds (in m/s) in the ANPac+2°C experiment. The reference vector of surface wind is 1 m/s.

As it was described in the above paragraphs, the atmospheric response to the warming in the subtropical North and South Pacific for the AGCM experiments is mostly confined to the forcing's hemisphere contrary to the global response of the coupled experiments. The local atmospheric response is similar for the AGCM and the fully coupled experiments, although weaker and with no significant vertical response in the case of North Pacific AGCM run. The weaker atmospheric response to the thermal forcing in subtropical North Pacific might also contribute to the smaller impact of the North Pacific Ocean to the tropical climate. The reason for this weaker atmospheric response to the subtropical North Pacific SST forcing is not yet clear.

We can conclude that air-sea interactions and ocean dynamics are very important for the equatorial Pacific response to the sea surface anomalies in the subtropical Pacific.

73

5. Sensitivity to density perturbations in the subtropics -Impact on the tropical Pacific climate variability

5.1 Introduction

While air-sea interactions responsible for El Niño-Southern Oscillation (ENSO) are centered in the equatorial Pacific Ocean, changes in the tropical convections associated with ENSO influence the global atmospheric circulation. The effect of El Niño-Southern Oscillation (ENSO) on the subtropical/extratropical climate has been extensively studied over the past decades (Trenberth et al., 1998; Alexander et al., 2002), with a focus on the tropical-extratropical connection in the North Pacific (Alexander et al., 2002; Deser et al., 2004). In contrast, our understanding of the influence of subtropical/extratropical climate on ENSO is very limited. In this chapter, we will use the idealized experiments described in Chapter 4 to investigate the impact of subtropical density perturbations on the tropical Pacific climate variability.

5.2 Subtropical density perturbations impact on ENSO

Several paleoclimatic studies show that ENSO has undergone significant climate shifts in the history in response to a background climate change (Liu et al., 2000; Cole, 2001; Tudhope et al., 2001; Rosenthal and Brocolli, 2004). ENSO has also changed during the past decades (Fedorov and Philander, 2000, 2001). How ENSO phenomenon is responding to a background state change is a very actual issue (Van Oldenborgh et al., 2005; Zelle et al., 2005; Merryfield, 2006; Guilyardi, 2006; Meehl et. al, 2006b), with major implications on global warming impact studies. However, the GCMs projections of the ENSO properties in a future, warmer climate, reveal different responses: from increased amplitude due to a stronger thermocline (Timmermann et al., 1999; Collins, 2000) to a decreased amplitude due to a reduced zonal SST gradient (Knutson et al., 1997), or even no change in amplitude (Meehl et
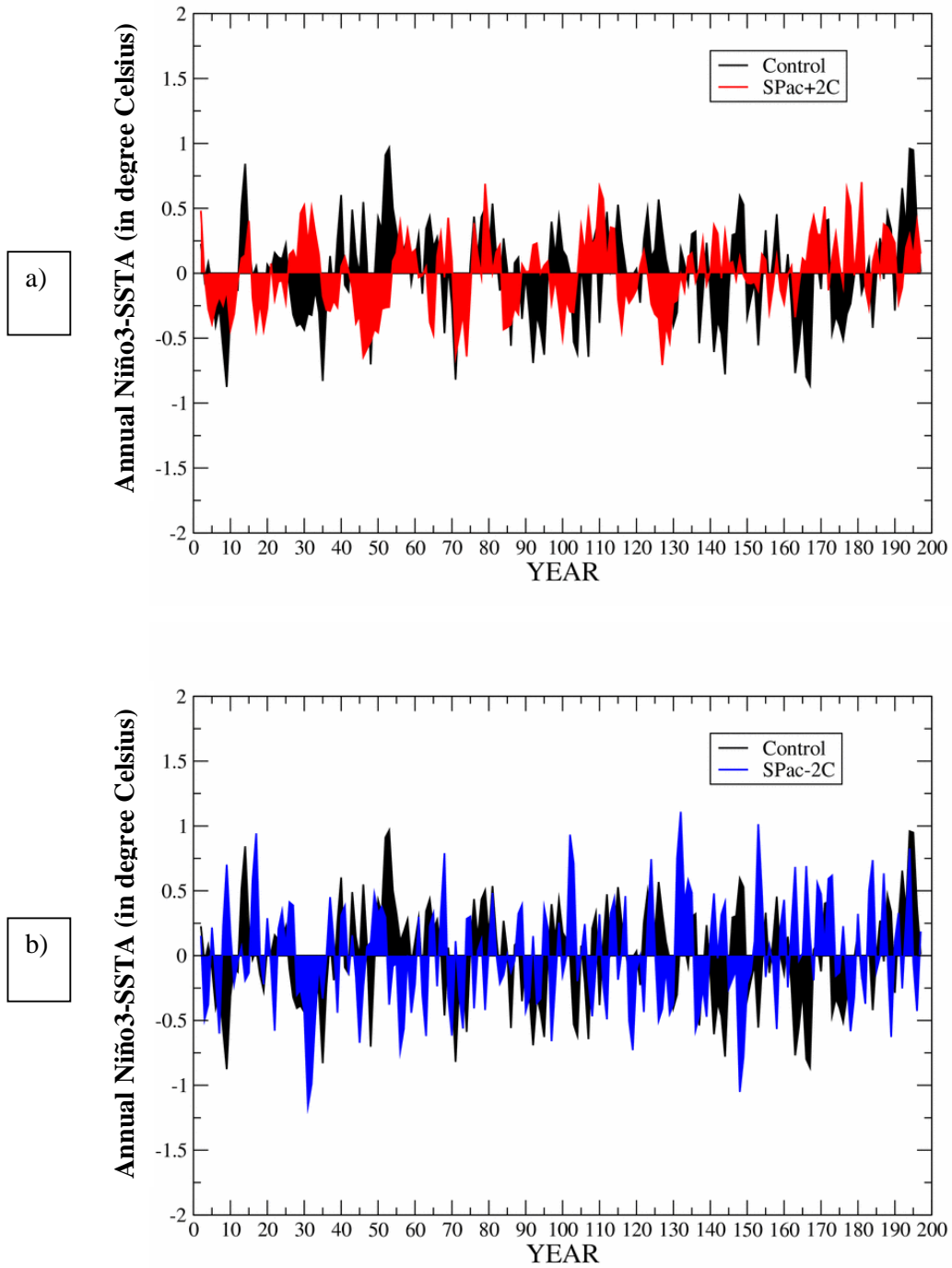
Figure 5.1 Time evolution of annual Niño3-SSTA (in °C) in **(a)** SPac+2°C (shaded red curve), and **(b)** SPac-2°C experiments (shaded blue curve). The shaded black curve represents the time evolution of Niño3-SSTA in the control integration. All plots are obtained applying a 5-yr running mean.

76
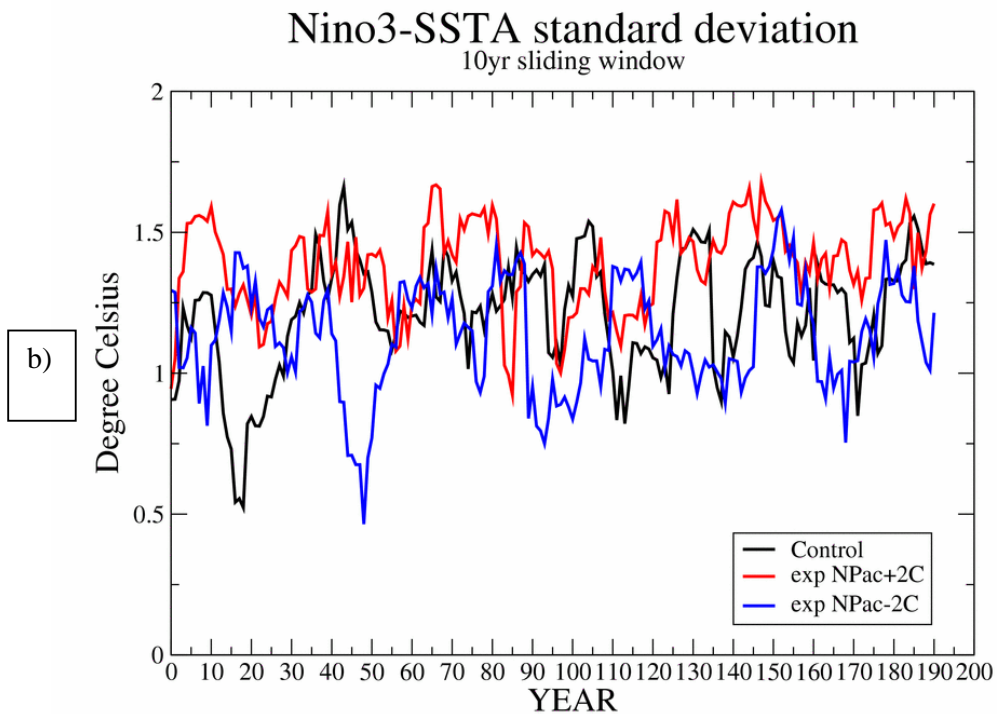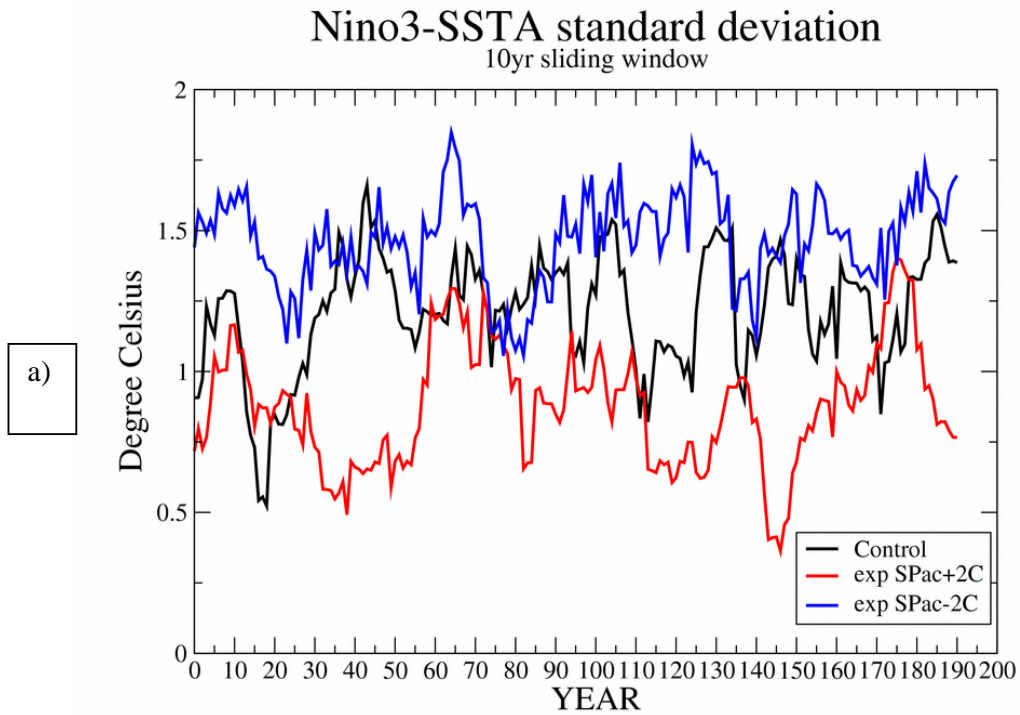
Figure 5.2 Standard deviation of Niño3-SSTA (in °C) as a function of time in **(a)** SPac±2°C, and **(b)** NPac±2°C experiments. A low-pass filter in the form of a sliding window 10 years wide was used to compute the standard deviations. Also shown here is the Niño3-SSTA standard deviation in the control integration (black curve). In both panels, the red curve (blue curve) represents the warming (cooling) experiment in the respective hemisphere.

al., 1993; Tett, 1995). ENSO period can also be changed: a broader meridional pattern of the anomalous zonal wind stress is associated with longer ENSO periods (Kirtmann, 1997; Capotondi et al., 2006). Merryfield (2006) linked changes in the sea surface temperature with changes in SST variability: higher mean SST or stronger SST difference between east and west equatorial Pacific intensify tropical SST variability.

For the beginning, we will check whether the changes in the background tropical climate in our sensitivity simulations have an effect on ENSO variability. We have found that the statistics of the ENSO present extensive changes in amplitude and frequency in response to the warming/cooling in the subtropical South Pacific. Relative to the control simulation, the time evolution of the annual SST anomaly in the Niño-3 region (150°W-90°W, 5°N-5°S) in the SPac+2°C shows a reduction in amplitude (see Figure 5.1a). On the contrary, the Niño-3 SST anomalies display an increase in amplitude as a response to the cooling in the subtropical South Pacific (see Figure 5.1b). The subtropical North Pacific has an opposite effect on ENSO comparing to the subtropical South Pacific: the subtropical North Pacific warming leads to increased ENSO amplitude, while the subtropical cooling leads to slightly decreased ENSO amplitude (not shown).

Figure 5.2 shows the standard deviation of the Niño-3 SST anomaly, computed using a 10-year sliding window, for the SPac+2°C and the NPac+2°C experiments. Looking at it we can now see even more clearly the stronger impact of the subtropical South Pacific on ENSO variability. A 2°C subtropical South Pacific SST warming can reduce the mean ENSO standard deviation by 28%, while a 2°C subtropical South Pacific SST cooling can increase the mean ENSO standard deviation by 21%. The impact of the subtropical North Pacific on ENSO interannual variability is opposite: a 14% increase in ENSO variability for the NPac+2°C experiment and a 6% decrease for the NPac-2°C experiment. In the following, we will focus on the ENSO variability changes in the South Pacific sensitivity experiments, since the impact of subtropical North Pacific on ENSO variability is much smaller in our model.

To investigate further the changes in ENSO statistics, we calculated the frequency distribution of annual Niño-3 SST anomalies. The frequency distribution for the SPac+2°C (red color) and the SPac-2°C (blue color) experiments are shown in Figure 5.3a, and Figure 5.3b, respectively. The control run frequency distribution is plotted with the black color in both histograms. The distribution obtained from the warming experiment in the South Pacific is narrower than the one obtained from the control run, in accordance with the decrease in interannual variability. For the SPac+2°C experiment the occurrence of weaker ENSO events

Histogram of Niño3-SSTA
annual values

a)

Histogram of Niño3-SSTA
annual values

b)
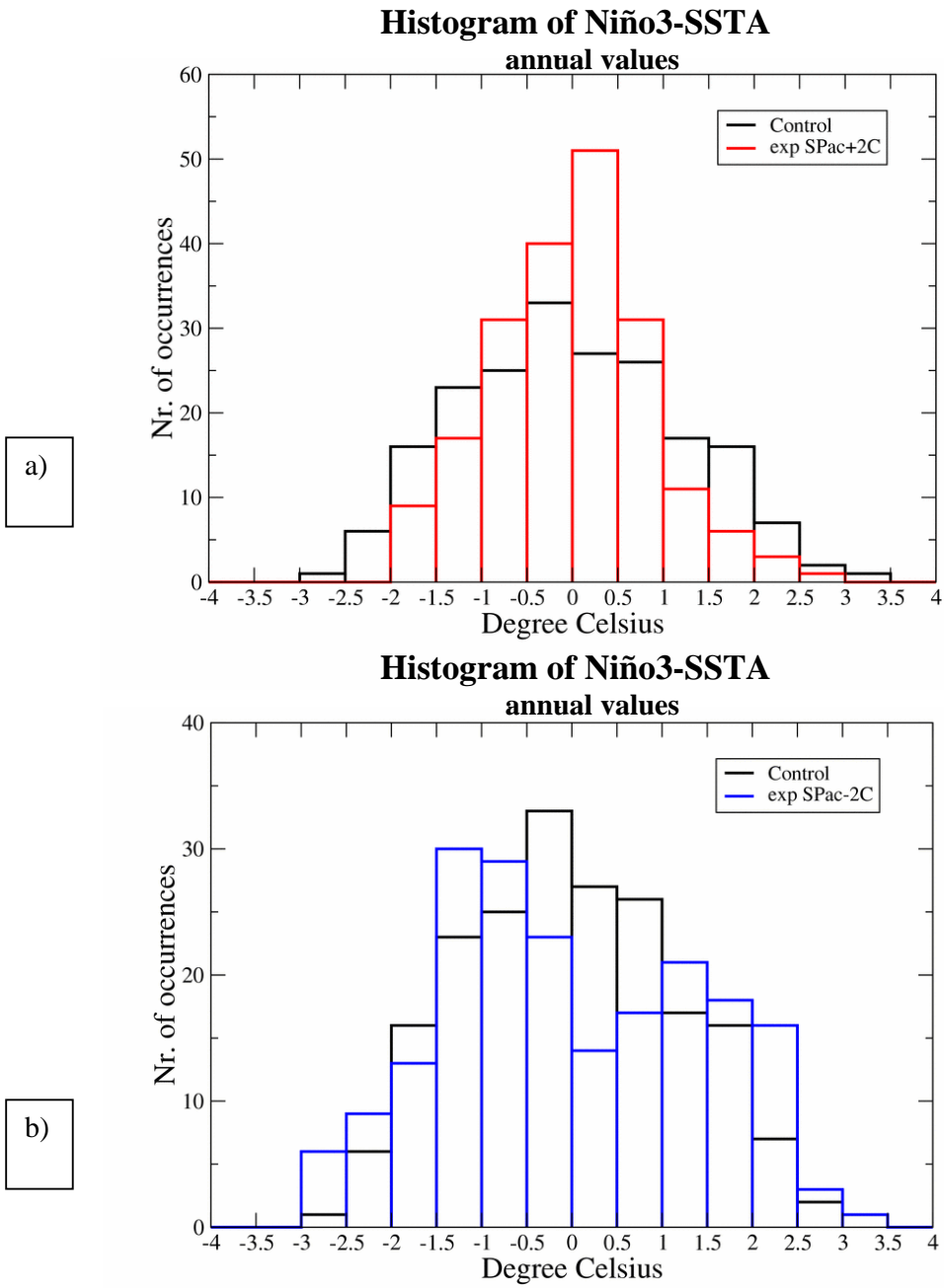
Figure 5.3 Frequency distribution of annual Niño3-SSTA during the **(a)** SPac+2°C (red), and **(b)** SPac-2°C experiments (blue). For comparison, we also show the frequency distribution of annual Niño3-SSTA during the control integration (black color).
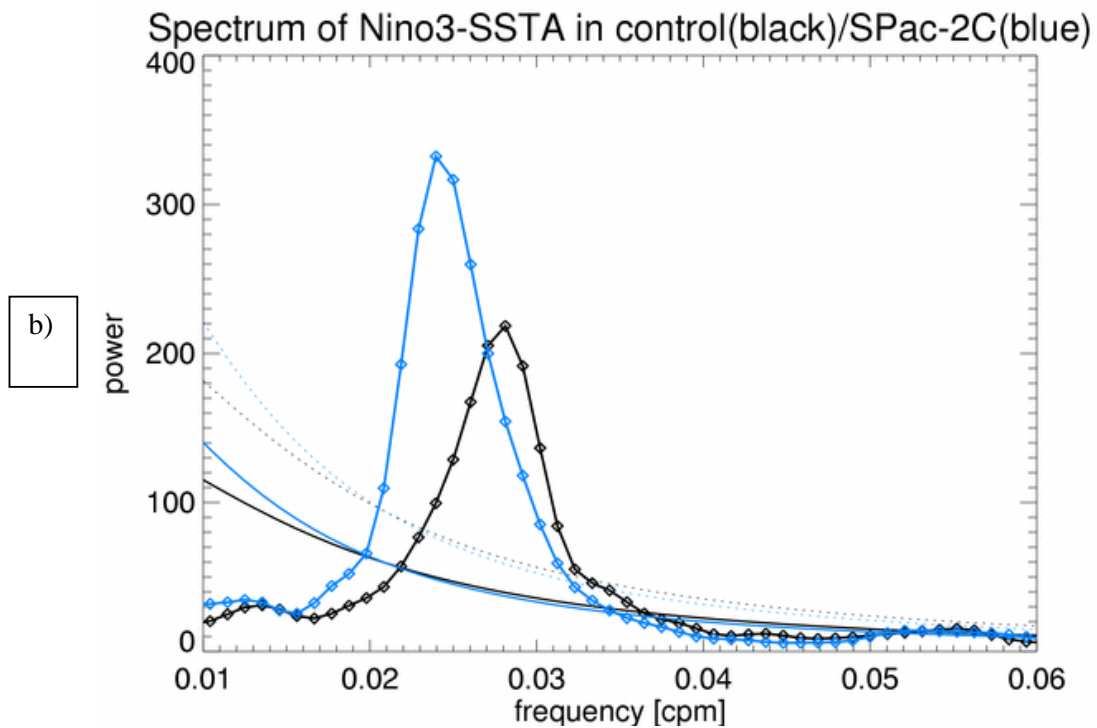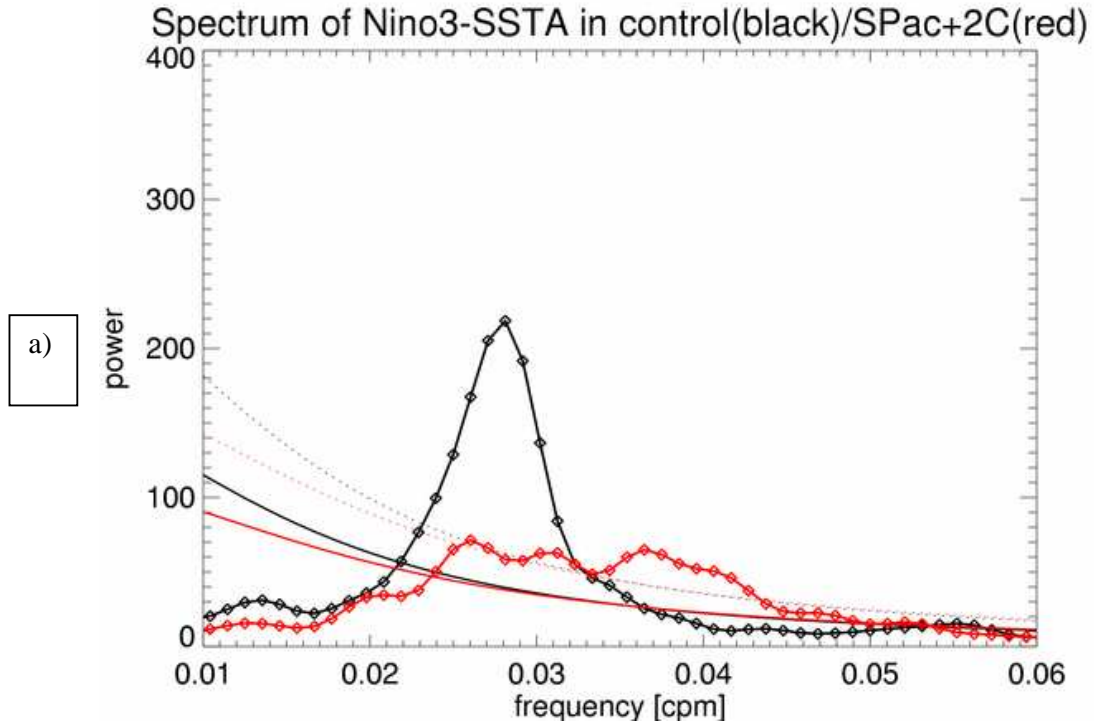
Figure 5.4 Power spectra of the simulated Niño3-SSTA in the **(a)** SPac+2°C (red line with diamonds), and **(b)** SPac-2°C experiments (blue line with diamonds). For comparison, the power spectra of Niño3-SSTA in the control integration is shown in black. The 95% confidence level is plotted as the dotted line, and the AR1 process fitted to the data as thin solid line.

increases and the occurrence of stronger ENSO events decreases. The opposite behavior is simulated for the cooling experiment in the South Pacific as a confirmation of the increased interannual variability, with less frequent weaker ENSO events and more frequent stronger ENSO events. In both South Pacific sensitivity experiments and in the control simulation, the distribution of Niño-3 SST anomalies is almost symmetrical. Therefore, there is no change in the skewness of ENSO in response to the subtropical South Pacific perturbations.

The remote modulation of the subtropical perturbations can also change the ENSO period. Figure 5.4 shows the power spectra of Niño-3 monthly SST anomaly associated with the subtropical South Pacific warming (red spectra in Figure 5.4a) and cooling (blue spectra in Figure 5.4b) experiments. For comparison, we have plotted with black color the power spectrum of Niño-3 SST anomaly in the control simulation. To compute the power spectra we have used the whole 200yr length of the sensitivity integrations. The monthly SST anomalies have the mean seasonal cycle removed. The 95% confidence level is plotted with a dotted line for each experiment, all the main peaks being located well above the confidence level. The above-mentioned significantly decreased/increased variability of ENSO in response to the subtropical warming/cooling is evident in the power spectrum plot. Figure 5.4b also suggests a shift to a longer period of the ENSO in the cooler climate of SPac-2°C experiment. The main peak in the ENSO spectrum is located at 42 months period for the SPac-2°C experiment and at 37 months period for the control simulation. In the warm climate of the SPac+2°C experiment, the power spectrum of Niño-3 SST anomaly exhibits a broadening with increased energy in the high frequency range (Figure 5.4a).

5.3 Background state changes associated with changes in ENSO

We will try now to identify the changes in the mean state that might lead to changes in the statistics of interannual variability for the South Pacific sensitivity experiments. The tropical Pacific interannual variability can be affected by changes in several factors: the mean state near the surface, the strength of the air-sea coupling, and the structure of the thermocline. Liu et al. (2002) proposed the annual cycle's interaction with ENSO through the nonlinear frequency entrainment process as another mechanism controlling the amplitude of ENSO.
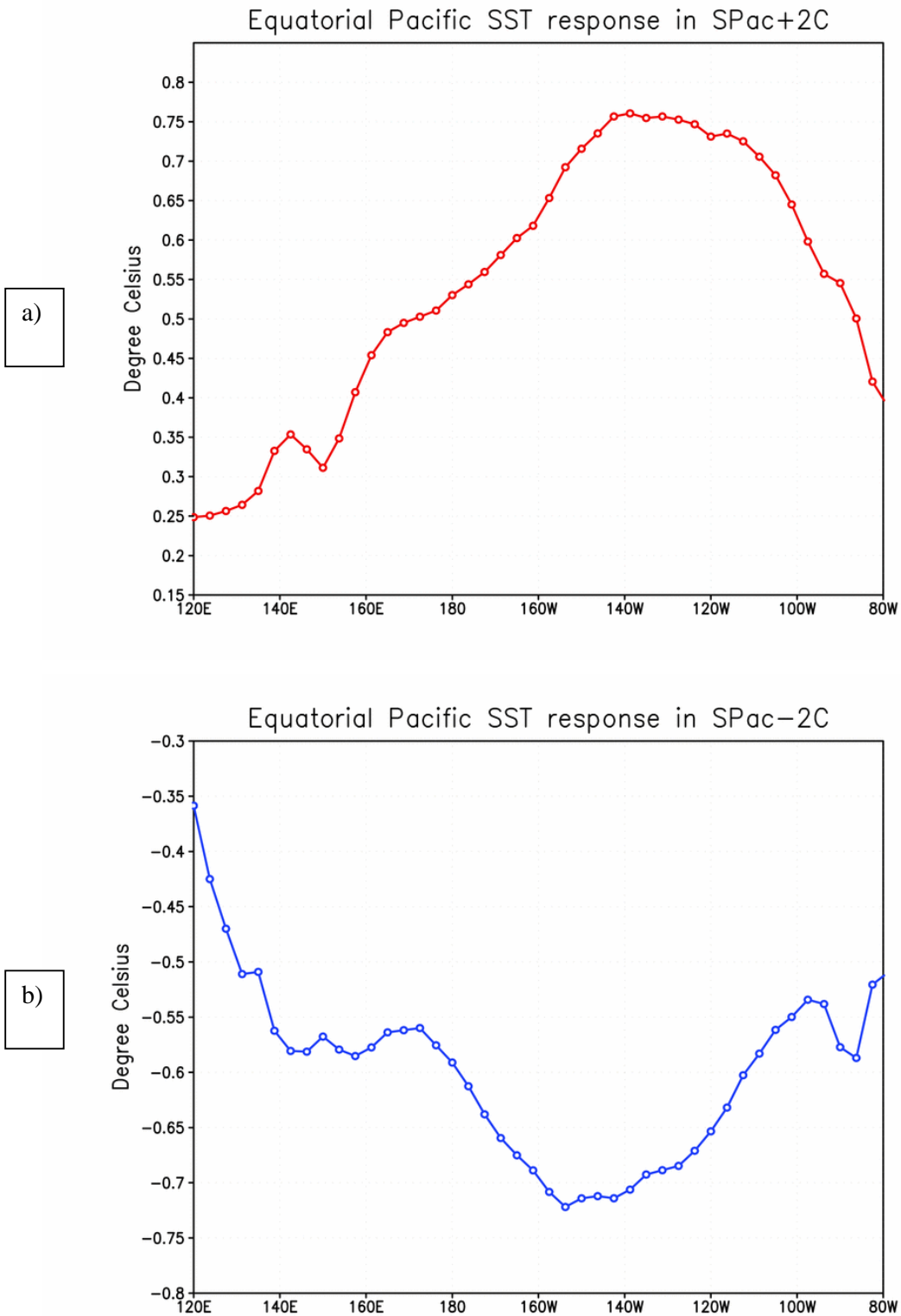
Figure 5.5 Anomalous sea surface temperature (in °C) in **(a)** the SPac+2°C (red curve), and **(b)** the SPac-2°C experiments (blue curve). The anomalies are computed as the spatial average between 5°S and 5°N.

Figure 5.5 shows the changes in the equatorial zonal SST contrast between the western and eastern Pacific for the South Pacific experiments. In response to an enhanced warming (cooling) in the subtropics of South Pacific, the zonal SST contrast has decreased (increased) by 0.55°C (0.4°C). A decrease in the zonal SST contrast between the warm pool and cold tongue area could favor a reduction in the variability of ENSO. Our findings are in accordance with Merryfield (2006) and Knutson et al (1997) that found a decrease in ENSO variability under the global warming conditions due to a reduced time-mean zonal SST gradient. A recent study by Sun et al. (2004) used a simplified ocean-atmosphere coupled model to study the effect of an enhanced subtropical surface cooling on ENSO. Their results suggest that an enhanced cooling in the subtropics results in a regime with stronger ENSO. Through the "ocean tunnel" (Gu and Philander, 1997), the stronger subtropical cooling decreases the temperature of the water feeding the equatorial undercurrent and therefore, results in a colder upwelling water in the eastern equatorial Pacific. The subsequent SST cooling in the eastern equatorial Pacific strengthens the equatorial zonal SST contrast, triggering a regime with stronger ENSO. In our SPac-2°C experiment, the change in the Hadley circulation determines the tropical wind change, which in turn changes the meridional overturning circulation in the upper Pacific. The spinning up of the STC in the South Pacific and the TC cells in both hemispheres will reduce the temperature of the upwelling water in the eastern equatorial Pacific (Kleeman et al., 1999), resulting in an increased zonal SST contrast and therefore, a stronger ENSO variability.

Changes in the mean equatorial trade winds can also produce changes in the equatorial thermocline structure that may alter the interannual variability. Figure 5.6 displays the thermocline depth and zonal wind stress anomalies associated with the SPac±2°C experiments, spatially averaged between 5°S and 5°N. The slackening/intensification of the equatorial trade winds in response to the warming/cooling in subtropical Pacific goes along with a shoaling/deepening of the thermocline in our experiments. The thermocline changes are mostly confined to western and central equatorial Pacific. According to the idealized modelling study of Fedorov and Philander (2001), an increase in the depth of the equatorial thermocline is stabilizing the tropical interannual variability. This is in contrast to our findings: the deepening of thermocline in SPac-2°C experiment is accompanied by an increased ENSO variability, while in the SPac+2°C experiment a shoaling of the thermocline goes along with a weakening of ENSO.
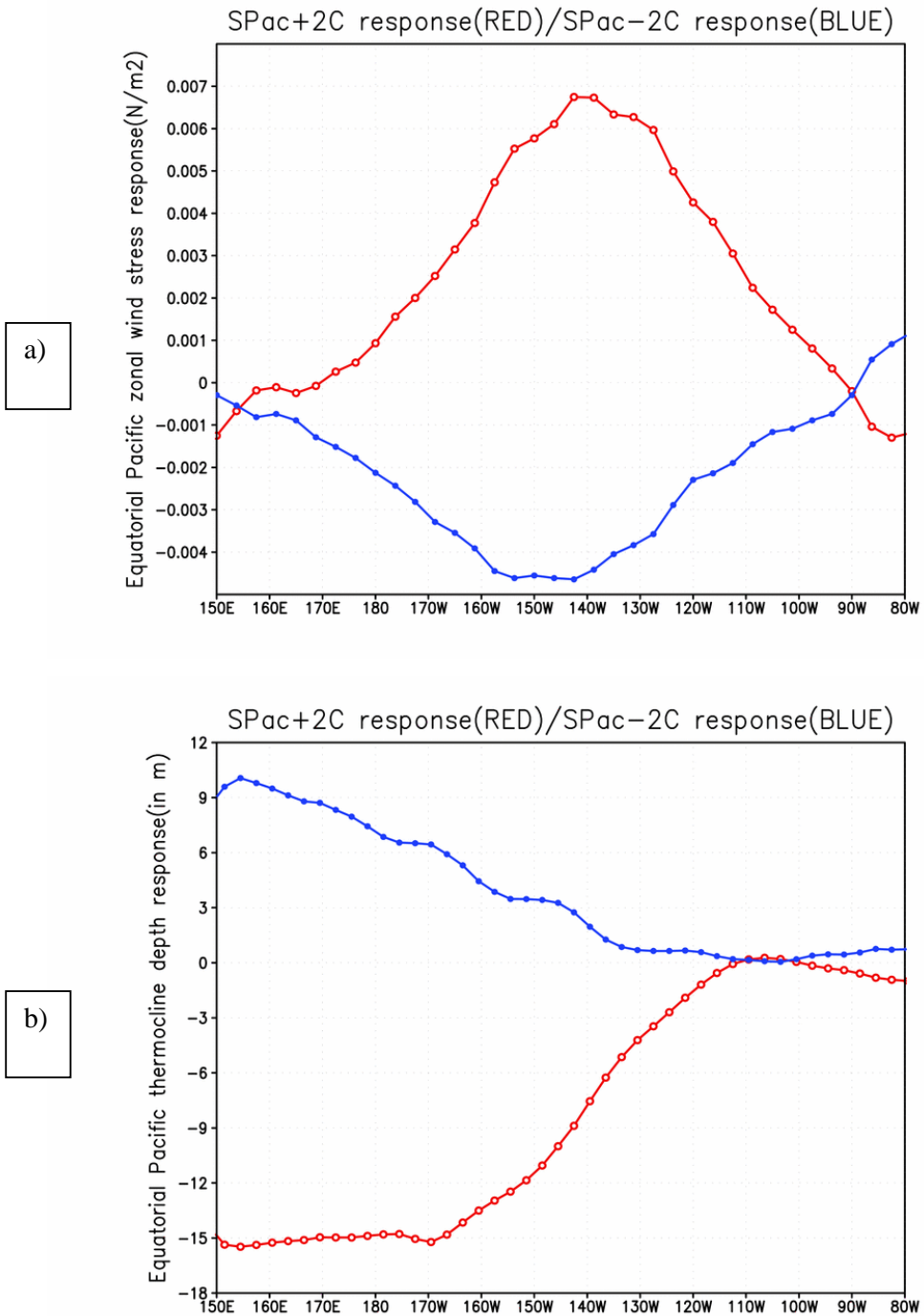
Figure 5.6 (a) Anomalous zonal wind stress (in N/m^2) in the SPac+2°C (red curve), and the SPac-2°C experiments (blue curve). **(b)** Anomalous depth of the thermocline (in m) in the SPac+2°C (red curve), and the SPac-2°C experiments (blue curve). The anomalies are computed as the spatial average between 5°S and 5°N.

The situation is further complicated by the fact that the depth and the sharpness of thermocline can change simultaneously with either reinforcing or counterbalancing effects on ENSO variability. A sharper thermocline with a weaker slope is stabilizing because it inhibits entrainment across the thermocline, and also because the vertical movements of thermocline are less effective (Fedorov and Philander, 2001). A sharper/less sharp and less steep/steeper equatorial thermocline in response to the subtropical South Pacific warming/cooling could lead to the reduced/enhance ENSO variability observed in our experiments (Figure 5.7). An explanation of simulated changes in ENSO period may be also obtained in the above-mentioned linear framework: a deepening of the thermocline, as observed in our SPac-2°C experiment, can suppress the high-frequency SST-mode in favor of a delayed oscillator mode, causing the period of ENSO to increase (Fedorov and Philander, 2001).

a)

b)
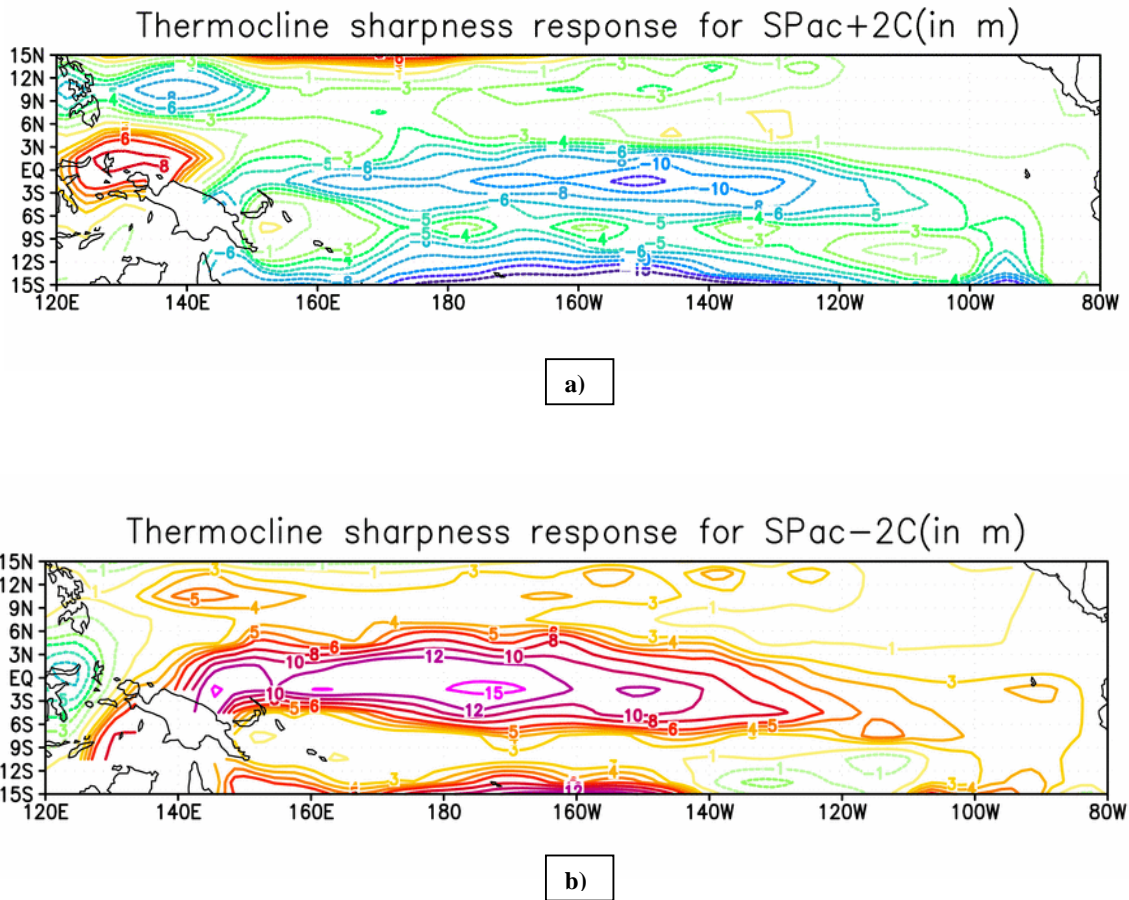
Figure 5.7 Anomalous sharpness of the thermocline (in m) in **(a)** the SPac+2°C, and **(b)** the SPac-2°C experiments. The sharpness of the thermocline is defined as the difference between the depth of the 16°C isotherm and the depth of the 22°C isotherm. The contour levels in **(a)** are ± 1, ± 2, ± 3, ± 4, ± 5, ± 6, ± 8, and ± 10 m. The contour levels in **(b)** are ± 1, ± 2, ± 3, ± 4, ± 5, ± 6, ± 8, ± 10, ± 12 and ± 15 m.

5.4 Explanation in terms of feedback changes

Changes in relevant positive/negative feedbacks generated by the change in the mean state will impact ENSO amplitude. We have estimated the strength of the atmosphere-ocean coupling using scatter plots and regression analysis of SST Niño-3 anomalies against zonal wind stress, thermocline depth, and net surface heat flux anomalies. One cause for the decrease in ENSO variability in response to an enhanced warming in subtropical South Pacific might be the reduction in central Pacific zonal wind stress sensitivity to eastern Pacific SST. As shown in Figure 5.8, the atmospheric sensitivity is reduced by about 10% in the SPac+2°C experiment. The atmospheric sensitivity has slightly increased in the case of SPac-2°C experiment (not shown). The SST-thermocline feedback is increased (decreased) by about 1-2 m/°C in the central-eastern Pacific for the SPac+2°C (SPac-2°C) experiment relative to the control integration (Figure 5.9) and thus, consistent with changes in the thermocline depth. For example, in the SPac+2°C experiment, the shallower equatorial thermocline will lead to an enhancement of the thermocline feedback, which in turn will increase ENSO variability – in contrast to our findings (Figure 5.2a). We have found no significant changes in the eastern SST-net surface heat flux feedback in both sensitivity experiments (not shown).

a)   b)
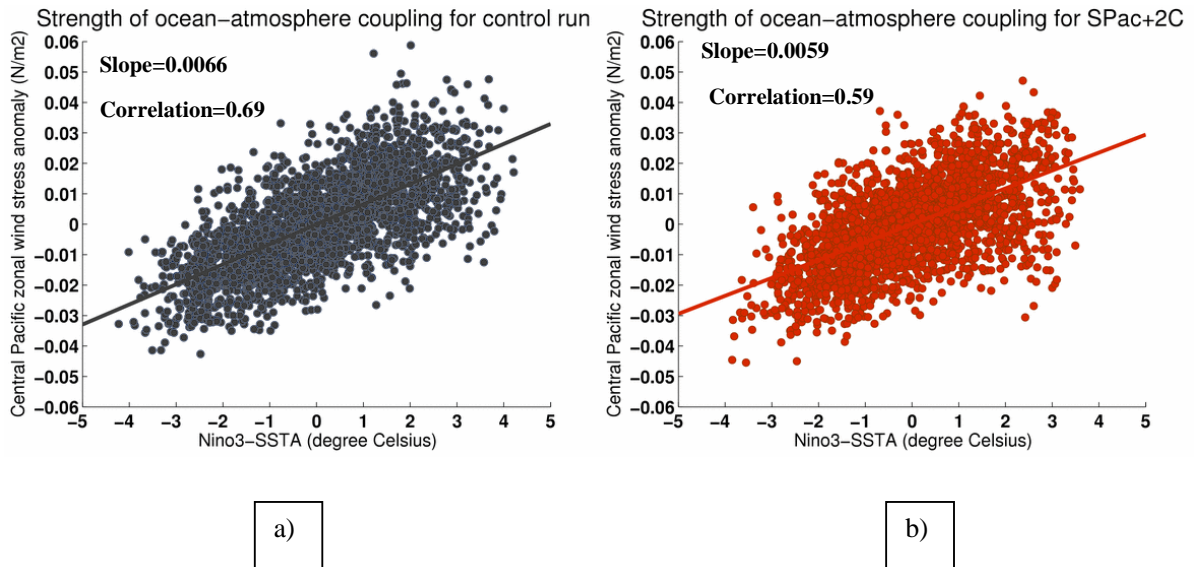
Figure 5.8 Scatter plot of Niño3-SSTA versus the wind stress anomalies over the central equatorial Pacific (120°E-150°W, 2°S-2°N) for **(a)** the control integration (black), and **(b)** the SPac+2°C experiment (red).

SPac+2°C

a)

SPac-2°C

b)
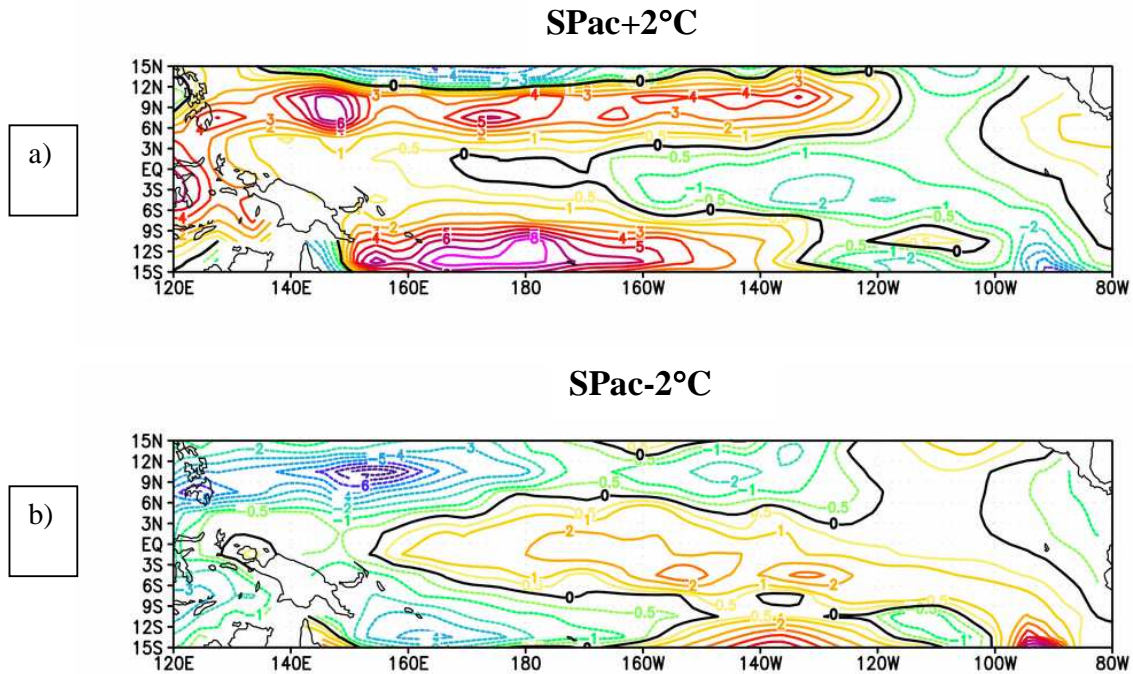
Figure 5.9 Linear regression of thermocline depth and sea surface temperature in **(a)** the SPac+2°C, and **(b)** the SPac-2°C experiments relative to the control integration. All values are in m/°C and represent the difference between the regression coefficient of the respective sensitivity experiment and the one in the control integration. The contour interval is 1 m/°C.

Although the changes in the atmospheric sensitivity contribute to the changes in ENSO variability, they cannot explain the magnitude of the variability changes observed in our sensitivity experiments. According to the linear theory framework (Fedorov and Philander, 2001), a relative shallow thermocline favors the high-frequency local modes (SST-mode) in which SST changes depend on wind-induced upwelling and advection. Since our model has a rather shallow zonal mean thermocline (103m), we suggest that the zonal temperature gradient changes are the main contributor to the modulation of ENSO variability in our South Pacific sensitivity experiments.

Our study shows that the SST perturbations in the subtropical South Pacific can modulate ENSO variability, the remote influence from the subtropical North Pacific being much weaker. The change in the background state of our model in response to an enhanced warming/cooling of subtropical South Pacific is El Niño/La Niña-like, and therefore, we can see this work also as a contribution to the study of changes in ENSO variability under the global warming scenario. Hence, we analyze the global warming experiment described in the subchapter 4.2 to see whether ENSO variability will change due to the greenhouse warming in

our model. Indeed, the trend in the Pacific sea surface temperature (Figure 5.10a) that decreases the zonal temperature contrast between the warm pool and the cold tongue areas is accompanied by a substantial reduction in ENSO variability (Figure 5.10b).

a)

SST trend in the global warming experiment

b)

Nino3-SSTA standard deviation
10yr sliding window
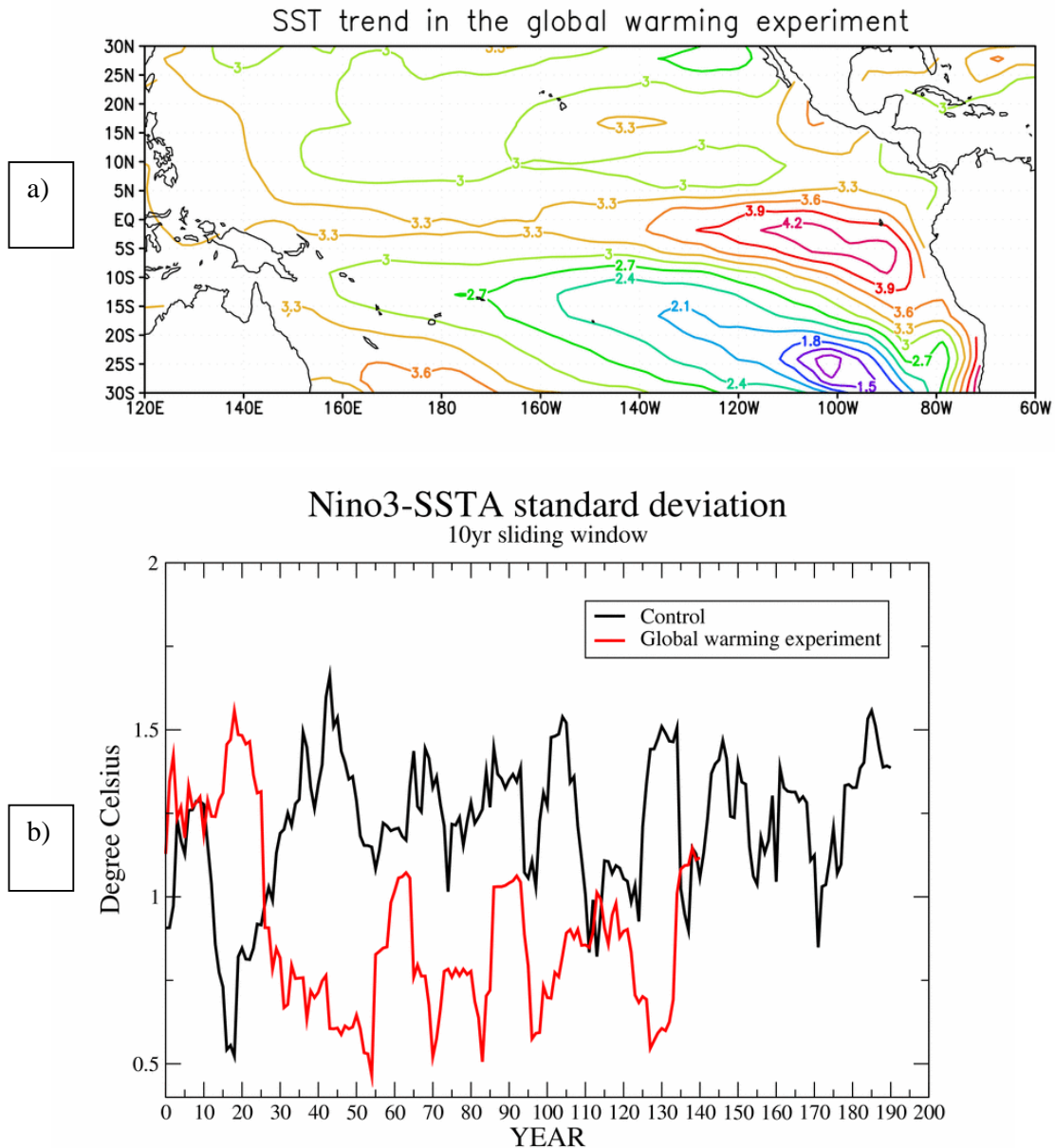
Figure 5.10 (a) The linear trend of anomalous sea surface anomalies (in °C) in the global warming experiment. **(b)** Standard deviation of Niño3-SSTA (in °C) as a function of time in the global warming experiment (red curve) and the control integration (black curve). A low-pass filter in the form of a sliding window 10 years wide was used to compute the standard deviations.

5.5 Changes in the annual cycle and their effect on ENSO

ENSO variability can be also influenced by the interaction with the equatorial Pacific annual cycle through the nonlinear frequency entrainment process (Liu, 2002; Timmermann et al., 2006). We will first check if there are any changes in the equatorial annual cycle in our SPac$\pm$2°C experiments. Then, we will investigate whether these annual cycle changes can help explaining the simulated changes in ENSO variability.

One important element for the generation of equatorial annual cycle is the northern location of the annual mean ITCZ and the associated meridional temperature asymmetry around the equator. Figure 5.11 shows the annual cycle of the sea surface temperature, wind stress and thermocline depth in the control integration and anomalous annual cycle for the SPac+2°C experiment. In the control integration, the thermocline anomalies are quite small (Figure 5.11a) and suggest that the annual cycle of SST in the eastern Pacific does not primarily involve thermocline dynamics (Xie, 1994). In response to an enhanced subtropical South Pacific warming, an intensification of the annual cycle is simulated (Figure 5.11b). The anomalous fall cooling around 135°W-115°W in the equatorial Pacific is a result of anomalous equatorial easterlies in August and September and will lead to a weak intensification of the annual cycle. The strong boreal summer warming around 125°W-100°W is also due to surface processes, specifically the weakening of equatorial easterly winds in late spring and early summer.

Several studies have produced observational and modeling evidence that the strength of ENSO can be anti-correlated with the strength of the annual cycle in eastern equatorial Pacific (Gu and Philander, 1995; Guilyardi, 2006). Liu (2002) used a conceptual model to study the effect of an external periodic forcing on the amplitude of ENSO and found that nonlinear frequency entrainment enables the external forcing, such as the annual forcing, to suppress ENSO significantly. For a weak annual cycle, ENSO will maintain its eigenfrequency; while for a very strong annual cycle, ENSO's frequency will be completely entrained into the forcing frequency and the interannual variability weakened. Our results are consistent with the above-mentioned theory: in response to an enhanced warming in the subtropical South Pacific, the annual cycle in the equatorial Pacific intensifies and therefore, leads to a weaker ENSO. The opposite is valid for the SPac-2°C experiment (not shown).
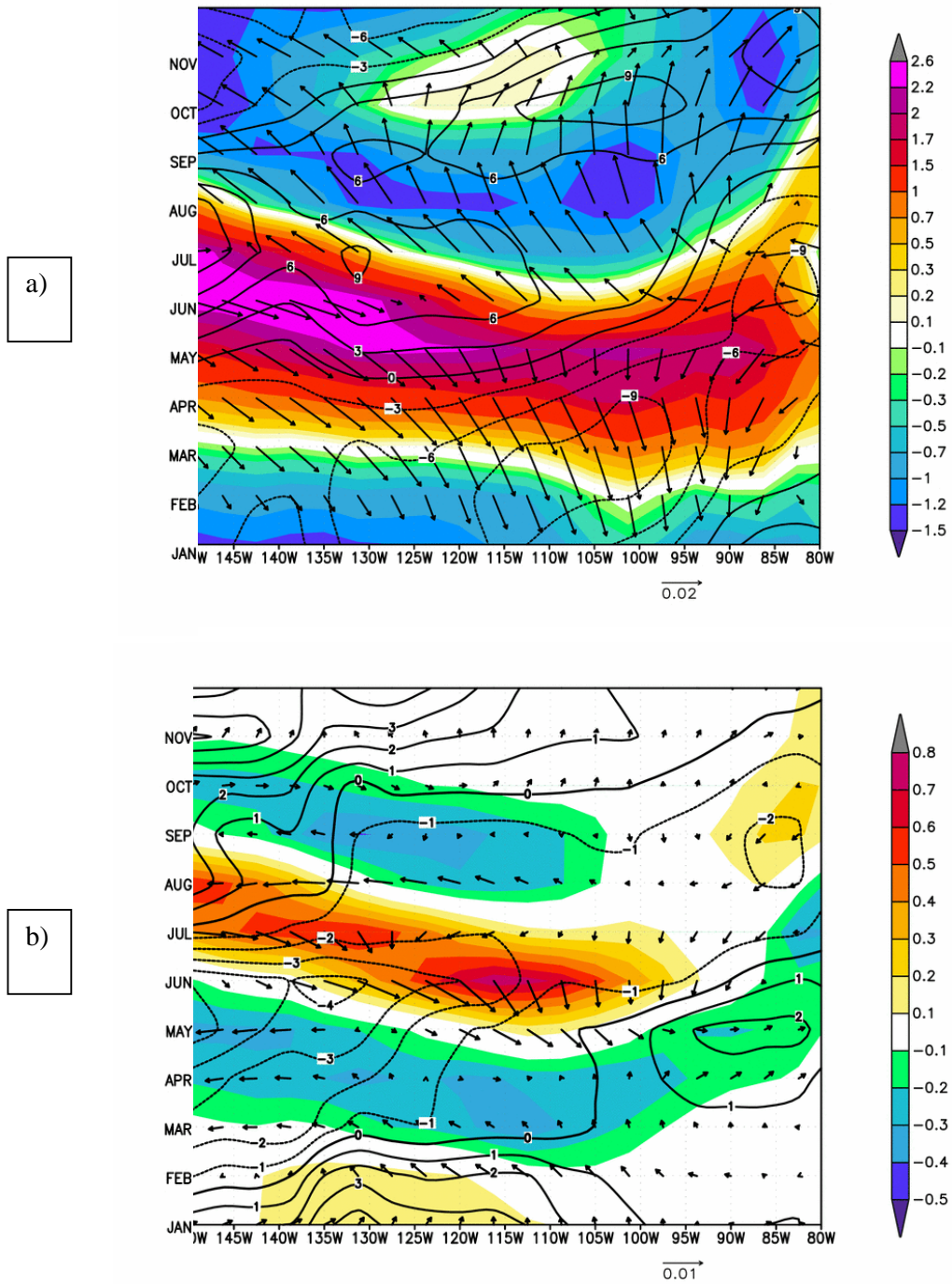
Figure 5.11 Hovmoller diagram of the seasonal cycle of Pacific equatorial sea surface temperature (shaded, in °C), wind stress (vectors, in N/m^2), and thermocline depth (contours, in m) climatologies in **(a)** the control integration and **(b)** the SPac+2°C experiment. The contour interval is 1m. The reference vector in **(b)** is 0.01 N/m^2.

6. Conclusions

In this study, connections between the tropical and subtropical Pacific on decadal timescales are investigated using an unforced integration and specifically designed experiments performed with the state-of-art ocean-atmosphere-sea ice coupled model ECHAM5/MPI-OM. The main findings are that subtropical South Pacific climate variations play a dominant role in tropical Pacific decadal variability and in the decadal modulation of ENSO activity. Since the available observational data is insufficient for these timescales, the research in this study focused on model analysis.

In Chapter 3, the origin of the tropical Pacific decadal climate variability was investigated by analyzing the output of an unforced integration of the coupled ECHAM5/MPI-OM ocean-atmosphere-sea ice model. The leading mode of decadal variability, isolated in the tropical cells index by means of SSA, has a period of about 17yr. The associated SST spatial structure is characterized by a horseshoe-like pattern with maximum explained variance in the central-western equatorial Pacific and off the equator, therefore resembling the signature of the observed decadal climate variability in the tropical Pacific. The mechanism for decadal variability in the model involves coupled ocean-atmosphere processes over the western tropical South Pacific, in the region of the SPCZ. It is as follows: anomalously strong tropical cells generate a cold SSTA over the western-central equatorial Pacific, due to increased equatorial upwelling. Through the atmospheric teleconnection from the central equatorial Pacific, an anomalous anticyclonic circulation is induced in the tropical South Pacific. The anomalous winds will lead to a southward shift in the SPCZ and thus, to a SE-NW tilted anomalous wind stress curl that favors Ekman downwelling. Due to the anomalous Ekman downwelling, the local thermocline deepens and a warm subsurface temperature anomaly is generated in the western tropical South Pacific along 10°S. The anomalous subsurface signal propagates westward and then equatorward. After reaching the equatorial Pacific, the positive subsurface temperature signal moves eastward along the equator, where via atmospheric response to SST changes weakens the tropical cells and complete the phase reversal. Lag-regression analysis between the ocean heat content and the decadal TC index suggests that the recharge-discharge mechanism proposed for ENSO (Jin, 1997) may also operate in the model at decadal timescales. It is interesting to note that

our coupled model results seem to reproduce the decadal variability characteristics described by the observational study of Luo and Yamagata (2001). However, the equatorward propagation of the South Pacific subsurface temperature signal in our model cannot be attributed to the mean flow advection or to the Rossby wave propagation as suggested by their study. Changes in ENSO characteristics associated with the decadal mode of the model were also investigated. Strong positive TCs are associated with periods of increased ENSO variability and vice versa, contributing to the decadal modulation of ENSO activity.

The impact of subtropical Pacific density perturbations (salinity and temperature) on the tropical Pacific mean climate was studied in Chapter 4 using idealized experiments performed with the coupled model ECHAM5/MPI-OM and with the stand-alone AGCM ECHAM5. The largest impact on tropical mean climate and variability was simulated in the SSTA experiments. Subtropical South Pacific thermal forcing had more impact on equatorial ocean sea surface temperature than the subtropical North Pacific. In response to a 2°C warming in the subtropical South Pacific (SPac+2°C), the equatorial Pacific SST increases by +0.58°C, being about 65% larger than the change in the North Pacific experiment (NPac+2°C). While the same fast "atmospheric bridge" seems to act in both South and North Pacific experiments, the amplitude and the spatial extension of the response differs: the thermal forcing of subtropical South Pacific has a maximum impact on eastern tropical Pacific climate, while the impact of subtropical North Pacific SST variations is mostly confined to the western tropical Pacific. A possible explanation for the weak impact of the subtropical North Pacific warming is the "thermodynamic thermostat" that may control the warm pool region and thus, prevent the amplification of SSTA through the local coupled ocean-atmosphere feedbacks in the western tropical Pacific.

The subtropical South and North Pacific SSTA have a completely different impact on the equatorial thermocline structure. The enhanced warming in the subtropical South Pacific forces a fast dynamical adjustment of the equatorial Pacific thermocline, through changes in the trade winds. As a result, the surface layer warming is accompanied by an anomalous cooling along the mean thermocline. The positive trend of the equatorial ocean heat content in the SPac+2°C experiment suggests that the "ocean bridge" plays also a role, albeit secondary, in the South Pacific subtropical-tropical connections at multi-decadal timescales. This oceanic connection is accomplished through both the delayed adjustment of the meridional overturning circulation in the upper Pacific, and the equatorward subduction along the mean pycnocline. On the contrary, the equatorial thermocline response in the NPac+2°C experiment is slow and exhibits an anomalous subsurface warming that penetrates till about 200m depth

and decreases upward towards the surface. We can conclude that the subtropics affect equatorial SST mainly through the „atmospheric bridge" for the SPac experiments and through the „oceanic bridge" for the NPac experiments. This explains the different timescale of the response in the two experiments.

In order to distinguish between the internal variability from externally forced climate variability, it is very important to understand the adjustment of climate system not only to global warming forcing, but also to global cooling forcing. This is why we also performed experiments in which the subtropics of both hemispheres are undergoing a 2°C cooling. Although the tropical Pacific surface response to an enhanced warming/cooling in the subtropics is to first order linear, we found that the negative thermal forcing has a stronger impact on the equatorial thermocline.

Similar sensitivity experiments conducted with the AGCM ECHAM5 shown that the role of air-sea interactions and ocean dynamics is crucial for the generation of simulated tropical climate response to the subtropical surface warming/cooling. Here, a surprising result is the much weaker atmospheric response to the thermal forcing in the subtropical North Pacific, compared to the one in the subtropical South Pacific.

In Chapter 5 we tried to answer the question: How do ENSO characteristics respond to an enhanced Pacific subtropical warming/cooling? We found that the statistics of ENSO exhibit significant changes in amplitude and frequency in response to a warming/cooling in the subtropical South Pacific: a 2°C subtropical South Pacific SST warming can reduce the mean ENSO standard deviation by 28%, while a 2°C subtropical South Pacific SST cooling can increase the mean ENSO standard deviation by 21%. Since our model has a rather shallow zonal mean thermocline, we suggest that the simulated changes in the equatorial zonal SST contrast between the eastern equatorial Pacific and the warm pool region are the main contributor to the modulation of ENSO variability in our South Pacific sensitivity experiments. ENSO variability can also be influenced by the interaction with the equatorial Pacific annual cycle through the nonlinear frequency entrainment process. Therefore, the simulated intensification/weakening of the annual cycle in response to an enhanced warming/cooling in subtropical South Pacific may also lead to a weaker/stronger ENSO. The subtropical North Pacific thermal forcing did not changed the statistical properties of ENSO.

7. Outlook

Results from earlier chapters underline the importance of subtropical-tropical South Pacific Ocean in the generation of low frequency climate variations in the tropical Pacific and in ENSO decadal modulation. However, further research is needed to fully determine the physical processes responsible for Tropical Pacific Decadal Variability (TPDV) and its sensitivity to external climate forcings such as greenhouse gases and natural/anthropogenic aerosols.

Here we focused on decadal climate variability that is internally generated in the Pacific Ocean and we did not take into consideration the possible interaction with decadal climate variability originating in other ocean basins. It will be interesting to study the possible connection between TPDV and Atlantic Multidecadal Oscillation (AMO; Kerr, 2000), which is thought to be related to the multi-decadal fluctuations of Atlantic Meridional Overturning Circulation (Delworth and Mann, 2000). On the one hand, TPDV can produce changes in the sea surface temperature and/or sea surface salinity of the tropical Atlantic, which may influence the North Atlantic climate via the atmospheric teleconnections or through changes in the ocean circulation. On the other hand, multi-decadal climate variations in the North Atlantic may also lead to low frequency climate variability in the tropical Pacific. For example, the study of Dong et al. (2006) presented evidence that variations in North Atlantic sea surface temperature associated with AMO can modulate ENSO activity at multi-decadal timescale.

The relative coarser horizontal resolution of our coupled model may introduce some limitations to our conclusions. Therefore, using a higher resolution AGCM to understand the different atmospheric response to SST variations in the subtropical North and South Pacific may be a further extension of the present study. A higher resolution ocean model may also help to distinguish between the contribution of western boundary and interior pycnocline flow to the ocean connection between subtropical and tropical Pacific.

Acknowledgements

References

Alexander, M.A., I. Blade, M. Newman, J.R. Lazarante, N.-C., Lau, and J.D. Scott, 2002: The atmospheric bridge: the influence of ENSO teleconnections on air-sea interaction over the global oceans. *Journal of Climate*, **15**, 2205-2231.

Arakawa, A. and V.R. Lamb, 1997: Computational design of the basic dynamical processes of the UCLA general circulation model. *Methods of Computational Physics*, **17**, 173-265.

Bader, J. and M. Latif, 2005: North Atlantic Oscillation Response to Anomalous Indian Ocean SST in a Coupled GCM. *Journal of Climate*, **18**, 5382-5389.

Barnett, T., D.W. Pierce, M. Latif, D. Dommenget, and R. Saravana, 1999: Interdecadal interactions between the tropics and the midlatitudes in the Pacific basin. *Geophysical Research Letters*, **26**, 615-618.

Bratcher, A. J. and B.S. Giese, 2002: Tropical Pacific decadal variability and global warming. *Geophysics Research Letter*s, **29**, 1918.

Broomhead, D.S., and G. King, 1986a: Extracting qualitative dynamics from experimental data. *Physica D*, **20**, 217-236.

Capotondi, A., and M.A. Alexander, 2001: Rossby wave maxima in the tropical North Pacific and their role in decadal thermocline variability. *Journal of Physical Oceanography*, **31**, 3496-3515.

Capotondi, A., M. A. Alexander, and C. Deser, 2003: Why are there Rossby wave maxima at 10°S and 13°N in the Pacific? *Journal Physical Oceanography*, **33**, 1549-1563.

Capotondi, A., M.A. Alexander, C. Deser, and M. McPhaden, 2005: Anatomy and Decadal Evolution of the Pacific Subtropical Cells. *Journal of Climate*, **18**, 3739-3758.

Capotondi, A. et al., 2006: Spatial and temporal structure of ENSO in the 20th century coupled simulations. Ocean Modelling (in press).

Cole J., 2001: A slow dance for El Niño. *Science*, **291**, 1496-1497.

Collins, M., 2000: The El Niño- Southern Oscillation in the second Hadley Center coupled model and its response to greenhouse warming. *Journal of Climate*, **13**, 1299-1312.

Colebrook, J.M., 1978: Continous plankton records-zooplankton and environment, northeast Atlantic and North Sea, 1948-1975**.** *Oceanology Acta*, **1**, 9-23.

Cubasch, U., G.C. Hegerl, R. Voss, J. Waszkewitz, and T.J. Crowley, 1997: Simulation with an OAGCM of the influence of varitions of the solar constant on the global climate. *Climate Dynamics*, **13**, 757-767.

D'Arrigo, R., E.R. Cook, R.J. Wilson, R. Allan, and M.E. Mann, 2005: On the variability of ENSO over the past six centuries. *Geophysics Research Letters*, **32**, L03711, doi: 10.1029/2004GL022055.

Delworth, T. and M. Mann, 2000: Observed and simulated multidecadal variability in the northern hemisphere. Climate Dynamics, 16, 661-676.

Deser, C., M.A. Alexander, and M.S. Timlin, 1996: Upper-ocean thermal variations in the North Pacific during 1970-1991. *Journal of Climate*, **9**, 1840-1855.

Deser, C., A. S. Phillips, and J.W. Hurrel, 2004: Pacific interdecadal climate variability: Linkage between the Tropics and the North Pacific during boreal winter since 1900. *Journal of Climate*, **17**, 3109-3124.

Dommenget, D., V. Semenov, and M. Latif, 2006: Impacts of the tropical Indian and Atlantic Oceans on ENSO. *Geophysical Research Letters*, **33**, doi: 10.1029/2006GL025871.

Dong, B.-W., R. Sutton, and A. Scaife, 2006: Multidecadal modulation of El Niño-Southern Oscillation (ENSO) variance by Atlantic Ocean sea surface temperatures. *Geophysical Research Letters*, **33,** L08705, doi: 10.1029/2006GL025766.

Fedorov, A. V. and S.G. Philander, 2000: Is El Niño changing? *Science*, **288**, 1997-202.

Fedorov, A. V. and S.G. Philander, 2001: A stability analysis of Tropical ocean-atmosphere interaction: bridging measurements and theory for El Niño. *Journal of Climate*, **14**, 3086-3101.

Garreaud, R. and D.S. Battisti, 1999: Interannual and interdecadal (ENSO-like) variability in the Southern Hemisphere tropospheric circulation. *Journal of Climate*, **12**, 2113-2123.

Giese, B.S., S.C. Urizar, and N.S. Fuckar, 2002: Southern hemisphere origins of the 1976 climate shift. Geophysical Research Letters, 29: 10.1029/2001GL013268.

Ghil, M., and R. Vautard, 1991: Interdecadal oscillations and the warming trend in global temperature time series. *Nature*, **350**, 324-327.

Ghil, M., M.R. Allen, M.D. Dettinger, K. Ide, D. Kondrashov, M.E. Mann, A.W. Robertson, A. Sounders, Y. Tian, F. Varadi, and P. Yiou, 2001: Advanced Spectral Methods for Climatic Time Series. *Review of Geophysics*, **40**, 1, 1-41.

Graham, N.E., 1994: Decadal-scale climate variability in the tropical and North-Pacific during the 1970's and 1980's: Observations and model results. *Climate Dynamics*, **10**, 135-162.

Gu, D., and S.G.H. Philander, 1997: Interdecadal climate fluctuations that depend on exchange between the Tropics and extratropics. *Science*, **275**, 805-807.

Guilyardi, E., 2006: El Niño-mean state–seasonal cycle interactions in a multi-model ensemble. *Climate Dynamics*, **26**, 329-348.

Hagemann, S. and L. Dümenil, 1998: A parameterisation of the lateral waterflow for the global scale. *Climate Dynamics*, **14**, 17-31.

Hagemann, S. and L. Dümenil-Gates, 2003: Improving a subgrid runoff parameterisation scheme for climate models by the use of high resolution data derived from satellite observations. *Climate Dynamics*, **21**, 349-359.

Hibler, W., 1979: A dynamic thermodynamic sea ice model. *Journal of Physical Oceanography*, **9**, 815-846.

Holland, C.L., R. Scott, S.-I. An, and F. W. Taylor, 2006: Propagating decadal sea surface temperature signal identified in the modern proxy records of the tropical Pacific. Climate Dynamics, 10.1007/s00382-006-0174-0.

Jin, F.-F., 1997: A theory of interdecadal climate variability of the North Pacific ocean-atmosphere system. *Journal of Climate*, **10**, 324-338.

Jin, F.-F., 2001: Low-frequenc modes of tropical ocean dynamics. *Journal of Climate*, **14**, 3874-3881.

Johnson, G.C. and M. J. McPhaden, 1999: Interior pycnocline flow from the subtropical to equatorial Pacific Ocean. *Journal of Physical Oceanography*, **29**, 3073-3089.

Kaplan, A., M.A. Cane, Y. Kushnir, A.C. Clement, M.B. Blumenthal, and B. Rajagopalan, 1998: Analyses of global sea surface temperature 1856-1991. *Journal of Geophysical Research*, **103**, 18 567-18 589.

Kerr, R., 2000: A North Atlantic climate pacemaker for the centuries. *Science*, **288**, 1984-1985.

Kerr, R.A., 2004: Three degrees of consensus. *Science*, **305**: 932-934.

Kirtman, B.P., 1997: Oceanic Rossby wave dynamics and the ENSO period in a coupled model. *Journal of Climate*, **10**, 1690-1704.

Kleeman, R., J.P.McCreary, and B.A.Klinger, 1999: A mechanism for generating ENSO decadal variability. *Geophysical Research Letters*, **26**, 1743-1746.

Klinger, B.A., J.P.McCreary, and R. Kleeman, 2002: The relationship between oscillating subtropical wind stress and equatorial temperature. *Journal of Physical Oceanography*, **32**, 1507-1521.

Knutson, T.R., S. Manabe, and D. Gu, 1997: Simulated ENSO in a global coupled ocean model: multidecadal amplitude modulation and CO2 sensitivity. *Journal of Climate*, **10**, 138-161.

Knudson, T.R., and S. Manabe, 1998: Model assessment of decadal variability and trends in the tropical Pacific Ocean. *Journal of Climate*, **11**,2273-2296.

Krishnamurthy, V. and B.N. Goswami, 2000: Indian Monsoon-ENSO relationship on Interdecadal Timescale. *Journal of Climate*, **13**, 579-595.

Kumar, K., B. Rajagopalan, and M.A. Cane, 1999: On the weakening relationship between the monsoon and ENSO. *Science*, **284**, 2156-2159.

Labitzke, K., 1987: Sunspots, the QBO, and the stratospheric temperature in the north polar region. *Geophysical Research Letters*, **14**, 535-537.

Latif, M., and T.P.Barnett, 1994: Causes of decadal climate variability over the North Pacific and North America. *Science*, **266**, 634-637.

Latif, M., and T.P.Barnett, 1996: Decadal climate variability over the North Pacific and North America: Dynamics and predictability. *Journal of Climate*, **9**, 2407-2423.

Latif, M., R. Kleeman, and C. Eckert, 1997: Greenhouse warming, decadal variability, or El Niño? An attempt to understand the anomalous 1990s. *Journal of Climate*, **10**, 2221-2239.

Latif, M. and Coauthors, 2001: ENSIP: The El Niño Simulation Intercomparison Project. *Climate Dynamics*, **18**, 255-276.

Lea, D.W., 2004: The 100,000-year cycle in tropical SST, greenhouse forcing, and climate sensitivity. *Journal of Climate*, **17**, 2170-2179.

Lean, J., J. Beer, and R. Bradley, 1995: Reconstruction of solar irradiance since 1600: Implications for climate change. *Geophysical Research Letters*, **22**, 3195-3198.

Legutke, S., E. Maier-Reimer, A. Stössel, and A. Hellbach, 1997: Ocean-sea ice coupling in a global ocean general circulation model. Annals of Glaciology, **25**, 116-120.

Lin, S.G. and R.B. Rood, 1996: Multidimensional flux-form semi-Lagrangian transport. *Monthly Weather Review*, **124**, 2046-2068.

Lindstrom, E.R., R. Lukas, R. Fine, E. Firing, S. Godfrey, G. Meyers, and M. Tsuchiya, 1987: The western equatorial Pacific Ocean circulation study. *Nature*, **330**, 533-537.

Liu, Z., S.G.H. Philander, and R. Pacanowski, 1994: A GCM study of tropical-subtropical upper ocean mass exchange. *Journal of Physical Oceanography*, 24, 2606-2623.

Liu, Z., J. Kutzbach, and L. Wu, 2000: Modeling climate shift of El Niño variability in the Holocene. *Geophysical Research Letters*, **27**, 2265-2268.

Liu, Z., 2002: A simple model study of the forced response of ENSO to an external periodic forcing. *Journal of Climate*, **15**, 1088-1098.

Lohmann, K. and M. Latif, 2005: Tropical Pacific Decadal Variability and the Subtropical-Tropical Cells. *Journal of Climate*, **18**, 5163-5178.

Lohmann, U. and E. Roeckner, 1996: Design and performance of a new cloud microphysics parameterization developed for the ECHAM4 general circulation model. *Climate Dynamics*, **12**, 557-572.

Lu, P., J. Mc Creary, and B. Klinger, 1998: Meridional circulation cells and the source waters of the Pacific Equatorial Undercurrent. *Journal of Physical Oceanography*, **28**, 62-84.

Luo, J.-J., and T. Yamagata, 2001: Long-term El Niño-Southern Oscillation (ENSO)-like variations with special emphasis on the South Pacific. *Journal of Geophysical Research*, **106**, 22 211-22 227.

Luo, J.-J., S. Mason, S. Behera, P. Delecluse, S. Gualdi, A. Novarra, and T. Yamagata, 2003: South Pacific origin of the decadal ENSO-like variation as simulated b a coupled GCM. *Geophysics Research Letters*, **30**, 2250, doi: 10.1029/2003GL018649.

Luo, Y., L.Rothstein, R.-H. Zhang, and A. Busalacchi, 2005: On the connection between South Pacific subtropical spiciness anomalies and decadal equatorial variability in an ocean general circulation model. *Journal of Geophysical Research*, **110**, C10002, doi: 10.1029/2004JC002655.

Lysne, J., P. Chang, and B. Giese, 1997: Impact of the extratropical equatorial variability. *Geophysical Research Letters*, **24**, 2589-2592.

Mantua, N.J., S.R. Hare, Y. Zhang, J.M. Wallace, and R.C. Francis, 1997: A Pacific interdecadal climate oscillation with impacts on salmon production. *Bulletin of the American Meteorological Society*, **78**, 1069-1079.

Marsland, S., H. Haak, J. Jungclaus, M. Latif, and F. Röske, 2003: The Max-Planck-Institute global ocean/sea ice model with orthogonal curvilinear coordinates. *Ocean Modelling*, **5,** 91-127.

Merryfield, W.J., 2006: Changes in ENSO under CO2 doubling in the IPCC AR4 coupled climate models. *Journal of Climate*, **19,** 4009–4027.

Merryfield, W. and G. Boer, 2005: variability of the upper Pacific Ocean overturning in a coupled climate model. *Journal of Climate*, **18,** 666-683.

McCreary, J. and P. Lu, 1994: Interactions between the subtropical and equatorial ocean circulations: the subtropical cell. *Journal of Physical Oceanography*, **24**, 466-497.

McPhaden, M. and D. Zhang, 2002: Slowdown of the meridional overturning circulation in the upper Pacific Ocean. *Nature*, **415,** 603-608.

McPhaden, M. and D. Zhang, 2004: Pacific Ocean circulation rebounds. *Geophysical Research Letters*, **31,** L18301, doi: 10.1029/2004GL020727**.**

Meehl, G.A., G.W. Branstator, and W.M. Washington, 1993: Tropical Pacific interannual variability and CO2 climate change. *Journal of Climate*, **6,** 42-63.

Meehl, G.A., P.R. Gent, J.M. Arblaster, B.L. Otto-Bliesner, E.C. Brady and A. Craig, 2001: Factors that affect the amplitude of El Nino in global coupled models. *Climate Dynamics*, **17,** 515-527.

Meehl, G.A. and A. Xu, 2006: Megadroughts in the Indian Monsoon Region and Southwest North America and a Mechanism for Associated Multidecadal Pacific Sea Surface Temperature Anomalies. *Journal of Climate*, **19**, 1605–1623.

Meehl, G.A., H. Teng, and G. Branstator, 2006b: Future changes of El Niño in two global coupled models. *Climate Dynamics*, **26,** 581-609.

Miller, A.J., M.A. Alexander, G.J. Boer, F. Chai, K. Denman, D.J. Erickson, R. Frouin, A.J. Gabric, E.A. Laws, M.R. Lewis, Z. Liu, R. Murtugudde, S. Nakamoto, D.J. Neilson, J R. Norris, J.C. Ohlmann, R.I. Perry, N. Schneider, K.M. Shell, and A. Timmermann, 2003: Potential feedbacks between Pacific Ocean ecosystems and interdecadal climate variations. *Bulletin of the American Meteoological Society,* **84 (5**), 617–633.

Nitta, T. and S. Yamada, 1989: Recent warming of tropical sea surface temperature and its relationship to the Northern Hemisphere Circulation. *Journal of the Meteorological Society of Japan*, **67**, 375-383.

Nonaka, M., and S.-P. Xie, 2000: Propagation of North Pacific interdecadal subsurface temperature anomalies in an ocean GCM. *Geophysical Research Letters*, **27**, 3747–3750.

Nonaka, M., S.-P. Xie, and J. McCreary, 2002: Decadal variations in the subtropical cells and equatorial Pacific SST. *Geophysical Research Letters*, **29**, 1116, doi: 10.1029/2001GL013717.

Pierce, D.W., T.P. Barnett, and M. Latif, 2000: Connections between the Pacific Ocean Tropics and midlatitudes on decadal timescales. *Journal of Climate*, **13,** 1173-1194.

Power, S., T. Casey, C. Folland, A. Colman, and V. Mehta, 1999: Interdecadal modulation of the impact of ENSO in Australia. *Climate Dynamics*, **15**, 319-324.

Power, S., M. Haylock, R. Colman, and X. Wang, 2006: The predictability of interdecadal change in ENSO activity and ENSO Teleconnections. *Journal of Climate*, **19,** 4755-4771.

Rasmusson, E.M., X. Wang, and C.F. Ropelewski, 1990: The biennial component of ENSO variability. *J. Mar. Syst.*, **1,** 71-96.

Robock, A.D. and J. Mao, 1995: The volcanic signal in the surface temperature observations. *Journal of Climate*, **8,** 1086-1103.

Roeckner, E., G. Bäuml, L. Bonaventura, R. Brokopf, M. Esch, M. Giorgetta, S. Hagemann, I. Kirckner, L. Kornblueh, E. Manzini, A. Rhodin, U. Schlese, U. Schulzweida, and A. Tompkins, 2003: The atmosphere general circulation model ECHAM5, part 1: Model description. *Max-Planck-Institute für Meteorologie*, **Report No. 349,** 127 pp.

Roeckner, E., R. Brokopf, M. Esch, M. Giorgetta, S. Hagemann, L. Kornblueh, E. Manzini, U. Schlese, and U. Schulzweida, 2006: Sensitivity of Simulated Climate to Horizontal and Vertical Resolution in the ECHAM5 Atmosphere Model. *Journal of Climate*, **19**, 3771-3791.

Rosenthal, Y. and A.J. Broccoli, 2004: In search of Paleo-ENSO. *Science*, **304,** 219-221.

Schneider, N., A. J. Miller, M.A. Alexander, and C. Deser, 1999: Subduction of decadal North Pacific temperature anomalies: observations and dynamics. *Journal of Physical Oceanography*, **29,** 1056-1070.

Schneider, N., S. Venzke, A.J. Miller, D.W. Pierce, T.P. Barnett, C. Deser, and M. Latif, 1999: Pacific thermocline bridge revisited. *Geophysical Research Letters*, **26,** 1329–1332.

Seager, R. and R. Mutugudde, 1997: Ocean dynamics, thermocline adjustment and regulation of tropical SST. *Journal of Climate*, **10**, 521-534.

Sun, D.-Z., T. Zhang, and S.-I. Shin, 2004: The effect of subtropical cooling on the amplitude of ENSO: a numerical study. *Journal of Climate*, **17**, 3786-3798.

V. Semenov and M. Latif, 2006: Impact of tropical Pacific variability on the mean state of the North Atlantic thermohaline circulation. *Geophysical Research Letters*, **33**, L16708, doi: 10.1029/2006GL026237.

Solomon, A., J.P. McCreary jr., R. Kleeman, and B.A. Klinger, 2003: Interannual and decadal variability in an intermediate coupled model of the Pacific region. *Journal of Climate*, **16,** 383-405.

Tett, S., 1995: Simulations of El Niño-Southern Oscillation-like variability in a global AOGCM and its response to CO2 increase. *Journal of Climate*, **8,** 1473-1502.

Timmermann, A., M. Latif, A. Bacher, J. Oberhuber, and E. Roeckner, 1999: Increased El Niño frequency in a climate model forced by future greenhouse warming. *Nature*, **398,** 694-696.

Timmermann, A., Y. Okumura, S.-I. An, A. Clement, B. Dong, E. Guilyardi, A. Hu, J. Jungclaus, U. Krebs, M. Renold, T.F. Stocker, R.J. Stouffer, R. Sutton, S.-P. Xie, and J. Yin,

2006: The influence of a weakening of the Atlantic meridional overturning circulation on ENSO. Submitted to *Journal of Climate*.

Tompkins, A.M., 2002: A prognostic parameterization for the sub-grid scale variability of water vapor and clouds in large-scale models and its use to diagnose cloud cover. *Journal of Atmospheric Science*, **59,** 1917-1942.

Trenberth, K.E., and J.W. Hurrell, 1994: Decadal atmosphere-ocean variations in the Pacific. *Climate Dynamics*, **9,** 3003-319.

Trenberth, K.E., G.W. Branstator, D. Karoly, A. Kumar, N.C. Lau, and C. Ropelewski, 1998: Progress during TOGA in understanding and modeling global teleconnections associated with tropical sea surface temperatures. *Journal of Geophysical Research*, **103**, 14291-14324.

Tudhope, A.W., et al., 2001: Variability in the El Niño-Southern Oscillation through a glacial-interglacial cycle. *Science*, **291,** 1511-1517.

Valcke, S., A. Caubel, D. Declat, and L. Terray, 2003: OASIS Ocean Atmosphere Sea Ice Soil user's guide. *CERFACS Technical Report* TR/CMGC/03/69**,** Toulouse, France, 85 pp.

Van Oldenborgh, G. J., S.Y. Philip, and M. Collins, 2005: El Niño in a changing climate: A multi-model study. *Ocean Science*, **1,** 81-95.

Venrick, E.L., J.A. McGowan, D.R. Cayan, and T.L. Hayward, 1987: Climate and Chlorophyll a: Long-term trends in the central North Pacific Ocean. *Science*, **238,** 70-72.

Vautard, R., and M. Ghil, 1989: Singular spectrum analysis in nonlinear dynamics, with applications to paleoclimatic time series. *Physica D*, **35**, 395-424.

Vautard, R., P. Yiou, and M. Ghil, 1992: Singular-spectrum analysis: A toolkit for short, noisy chaotic signals. *Physica D*, **58,** 95-126.

Zebiak, S.E. and M.A.Cane, 1987: A model of El Niño-Southern Oscillation. *Monthly Weather Review*, **115,** 2262-2278.

Zelle, H., G.J. van Oldenborgh, G. Burgers, and H.A. Dijkstra, 2005: El Niño and greenhouse warming: Results from ensemble simulations with the NCAR CCSM. *Journal of Climate*, **18,** 4669-4683.

White, W.B., Y. M. Tourre, M. Barlow, and M. Dettinger, 2003: A delayed action oscillator shared by biennal, interannual, and decadal signals in the Pacific basin. *Journal of Geophysical Research*, **108,** 3070, doi:10.1029/2002JC001490.

Wild, M. and E. Roeckner, 2006: Radiative Fluxes in the ECHAM5 General Circulation Model. *Journal of Climate*, **19,** 3792-3809.

Wolf, J.O., E. Maier-Reimer, and S. Legutke, 1997: The Hamburg Ocean Primitive Equation Model HOPE. *Technical Report*, **13,** German Climate Computer Center (DKRZ), Hamburg, Germany, 98 pp.

Wu, L., Z. Liu, C. Li, and Y. Sun, 2006: Extratropical control of recent tropical Pacific decadal climate variability: a relay teleconnection. *Climate Dynamics*, doi: 10.1007/s00382-006-0198-5.

Xie, S. –P., 1994: On the Genesis of the Equatorial Annual Cycle. *Journal of Climate*, **7,** 2008-2013.

Xie, S. –P. and S.G.H. Philander, 1994: A coupled ocean-atmosphere model of relevance to the ITCZ in the eastern Pacific. *Tellus*, **46A,** 340-350.

Yang, H. and Z. Liu, 2005: Tropical-extratropical climate interaction as revealed in idealized coupled climate model experiments. *Climate Dynamics*, doi: 10.1007/s00382-005-0021-8.

Yang, H., H. Jiang, and B. Tan, 2005: Asymmetric impact of the North and South Pacific on the equator in a coupled climate model. *Geophysical Research Letters*, **32,** doi: 10.1029/2004GL022195.

Yang, H., Z. Liu, and H. Wang (2004). Influence of Extratropical Thermal and Wind Forcing on Equatorial Thermocline in an Ocean GCM. *J. Physical Oceanography* **34(1),** p. 174-187.

Yeh, S.-W. and B.P. Kirtman, 2006: Origin of decadal El Niño-Southern Oscillation-like variability in a coupled general circulation model. *Journal of Geophysical Research*, **111,** C01009, doi:10.1029/2005JC002985.

Zhang, R.-H., T. Kagimoto, and S. Zebiak, 2001: Subduction of Decadal North Pacific Thermal Anomalies in An Ocean GCM. *Geophysical Research Letters*, **28**, 2449-2452.

Zhang, Y., J.M. Wallace, and D.S. Battisti, 1997: ENSO-like interdecadal variability: 1900-93. *Journal of Climate*, **10,** 1004-1020.

Publikationsreihe des MPI-M
„Berichte zur Erdsystemforschung" , *„Reports on Earth System Science*", ISSN 1614-1199
Sie enthält wissenschaftliche und technische Beiträge, inklusive Dissertationen.

Glacial and interglacial climate during the late
Quaternary: global circulation model simulations
and comparison with proxy data
Stephan J. Lorenz